
# A PARAMETRIC STUDY ON IBR SHEETING SUPPORTED BY PURLINS

**Marope Stella Mlasi**
Student number: 0412084R

**Supervisor: Prof A.A. Elvin**

A dissertation submitted to the
Faculty of Engineering and the Built Environment,
University of the Witwatersrand,
in fulfilment of the requirements for the degree of
Master of Science in Engineering

Johannesburg, 2016

# DECLARATION

I declare that this dissertation is my own unaided work. It is being submitted for the degree of Master of Science in Engineering to the University of the Witwatersrand, Johannesburg. It has not been submitted before for any degree or examination to any other University.

……..…

**Marope Stella Mlasi**

……day of May 2016

# ABSTRACT

This dissertation presents a parametric study conducted on the dimensions of an inverted box rib (IBR) sheet. The objectives of the study were (i) to obtain the optimum dimensions that would be used to simulate new IBR profiles made from standard sheet input coils whilst meeting the stiffness criterion; and (ii) to perform a cost analysis to determine the most economic simulated profile.

The dimensions which were varied in the parametric study were rib-height, rib-width, sheet thickness and the number of pans per 686 mm cover width of a single IBR 686 sheet. Numerical experiments were conducted using the Finite Elements Method and Abaqus/CAE software. The results were compared to the predictions obtained from Euler-Bernoulli beam theory. The outputs from the experiments were the sheet deflection from which stiffness was determined, and eigenvalues from which the profiles' stability and buckling modes were calculated.

This study found that sheet stiffness increased as the rib-height, sheet thickness and number of pans per 686 mm cover width increased. In contrast, the rib-width had little effect on the sheet stiffness. Hence, it was concluded that, for any IBR sheet profile, the rib-width should be kept at approximately 23 mm to avoid using more material in the sheet. The optimum dimensions found were rib-height of 34 mm, rib-width of 23 mm and four pans per 686 mm cover width. The commercially available IBR 686 sheet is made up of four pans and has a rib-height and a rib-width of 37 and 33 mm, respectively. It is manufactured from an input sheet coil of 925 mm. Reducing the rib-height from 37 mm to 34 mm and the rib-width from 33 mm to 23 mm resulted in increasing the cover width by 8 %.

The optimum dimensions were further used to simulate profiles made from the 925, 940, 1000, 1175, 1219, 1225, 1250 and 1320 mm standard sheet coils in order to find the most economic IBR profiles that met the stiffness criterion. The 1250 mm coil yielded the most economical IBR profile, which has six 97 mm wide pans, and a 996 mm cover width. This profile resulted in a 10 % cost saving compared with the next closest profile.

**KEYWORDS:**

Optimal IBR sheet profile
Parametric study of an IBR sheet profile
Z-section purlins
IBR sheet stiffness
IBR sheet buckling load

# ACKNOWLEDGEMENTS

I would like to thank:

- My supervisor, Prof. Alex Elvin, for the guidance and support received whilst working on this degree.
- The Southern African Institute of Steel Construction.
- University of South Africa for funding the first two years of my Master's degree and for purchasing the Abaqus/CAE software licences used in this study.
- My husband, Mr Bongani Mlasi, and our lovely son, Siyeza Olaninyi Mlasi, and daughter, Phetogo Titilayo Mlasi.
- Mrs Jeannette Menasce for assisting me to edit and correct this document.

# CONTENTS

# LIST OF FIGURES

# LIST OF TABLES

# LIST OF SYMBOLS

| | |
|---|---|
| $a$ | Bottom rib-width |
| $A$ | Cross-sectional area |
| $b$ | Rib-width in the IBR sheet |
| $B$ | Cover width of the sheet |
| $B'$ | Unfolded cover width of the sheet |
| $C_o$ | Topography factor |
| $C_{pe}$ | Coefficient of external pressure |
| $C_{pi}$ | Coefficient of internal pressure |
| $C_{prob}$ | Probability factor |
| $C_r$ | Roughness factor |
| $E$ | Elastic modulus |
| $EI$ | Sheet stiffness |
| $\sigma_y$ | Yield stress |
| $h$ | Rib-height in the IBR sheet |
| $H$ | Height of the building |
| $I$ | Second moment of area |
| $L$ | Sheet span between two adjacent supporting purlins (also called purlin spacing) |
| $L_u$ | Horizontal length of the upward wind slope |
| $M$ | Bending moment |
| $n$ | Number of pans per 686 mm cover width in a single IBR sheet |
| $P$ | Applied concentrated load on the sheet |
| $P_{cr}$ | Critical buckling concentrated load |
| $Q$ | Shear force |
| $q$ | Wind pressure |
| $R$ | External reaction force |
| $t$ | Thickness of the IBR sheet |
| $V$ | Wind speed |

| | |
|---|---|
| $W$ | Applied wind uplift loading on the sheet |
| $W_{cr}$ | Critical buckling wind uplift load |
| $X'$ | Pan width in the IBR sheet |
| $z$ | Height above the ground |
| $z_c$ | Minimum height below which no further reduction in wind speed is allowed |
| $z_g$ | Gradient height |
| $z_o$ | Height of reference plane |
| $\alpha$ | Roughness factor exponent |
| $\Delta$ | Total sheet deflection |
| $\varepsilon$ | Strain |
| $\lambda_i$ | The $i^{th}$ eigenvalue corresponding to the $i^{th}$ buckling mode |
| $\phi$ | Upward wind angle or slope |
| $\sigma$ | Direct bending stress |
| $\theta$ | Corrugation angle |
| $\rho$ | Density |
| $\nu$ | Poisson ratio |

# ABBREVIATIONS, ACRONYMS AND GLOSSARY

| | |
|---|---|
| **Abaqus/CAE** | Complete Abaqus Environment<br>(Dassault Systemes SIMULIA (2014)) |
| **ACO(s)** | Ant Colony Optimisation(s) |
| **ANSYS** | Finite Element Analysis Software |
| **FEA** | Finite Element Analysis |
| **FEM** | Finite Element Method / Finite Element Modelling |
| **GRS** | Global Roofing Solutions |
| **GUI** | Graphical User Interface |
| **IBR** | Inverted Box Rib |
| **MPC(s)** | Multi-Point Constraint(s) |
| **RP** | Reference Point |
| **SAISC** | Southern African Institute of Steel Construction |

# 1: INTRODUCTION

## 1.1 Background

Roof sheeting is popular in industrial and domestic buildings and warehouses. This is due to several reasons which include:

(1) the availability and wide range of cross-sectional shapes and sizes;

(2) thin-walled structure of the roof sheeting which reduces space consumption;

(3) longer life span due to coating;

(4) recyclability of materials;

(5) faster construction processes, and

(6) Light weight.

However, the quality of roof sheeting is not measured by its relatively low cost or the popularity of its manufacturer, but by considerations of each dimensional parameter of the sheet. The quality and dimensional parameters of sheeting as a roof-covering material are governed by durability, stiffness, cost, insulation and water-carrying capacity (Balex Metal, 2011).

Inverted Box Rib (IBR) sheeting has become one of the most popular profiles used in the construction of industrial buildings. An IBR sheet is defined as a "trapezoidal fluted profile sheet that is often adopted as roof-covering or side-cladding material" (Cousins Steel International, 2015). The IBR sheet profile is made up of flutes or corrugations known as "ribs" and the spaces between the ribs are known as "pans". The pans are measured from centre to centre of two adjacent ribs. There are different types of IBR sheeting, often named based on the cover width of a single sheet. Examples include IBR 686 and IBR 890 sheets, which have cover widths of 686 and 890 mm respectively (Southern African Institute of Steel Construction (SAISC), 2013). These sheets have well-established

dimensions and shapes and are available in different thicknesses (ranging from 0.3 to 0.8 mm), with galvanized zinc or Zincalume coating (SAISC, 2013).

In many IBR sheet profiles, the sizes of the dimensional parameters are known and established for several reasons (such as material and production cost, type of manufacturing process as well as the identification of the sheet itself). However, there is a deficiency in the current literature on the relationship between the dimensional parameters, sheet stiffness and stability of the IBR profiles (SANS 10162-1, 2011; Eurocode 3 – Part 1-3, 2005).

This research focuses on addressing the influence of the dimensional parameters of the IBR profiles on its stiffness, stability and material cost.

## 1.2 Introduction to roof components used in the research

### 1.2.1 Overview of what makes up a steel roof

A metal roof, particularly one made from structural steel, consists of rafters or trusses, purlins and roof sheeting which provides cover to the entire roof structure. The sheet is affixed to the purlins via screws; whilst the purlins are supported by rafters or trusses, which, in turn, are supported by the walls, beams or columns. Figure 1.1 shows a simple example of the components that make up a structural steel roof. For clarity, only three purlins are shown supporting three overlapped IBR 686 sheets. Usually the roof sheeting would cover the entire roof, making the structure waterproof.

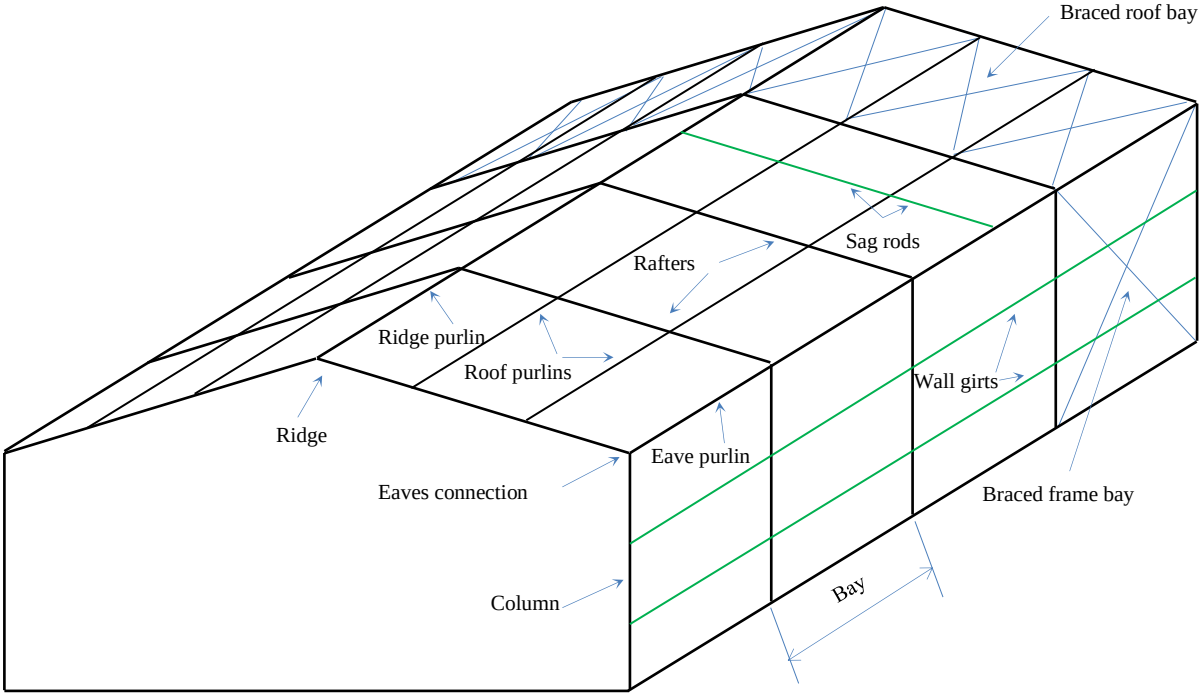


(a) General structure of a warehouse as a common example of a structural steel building

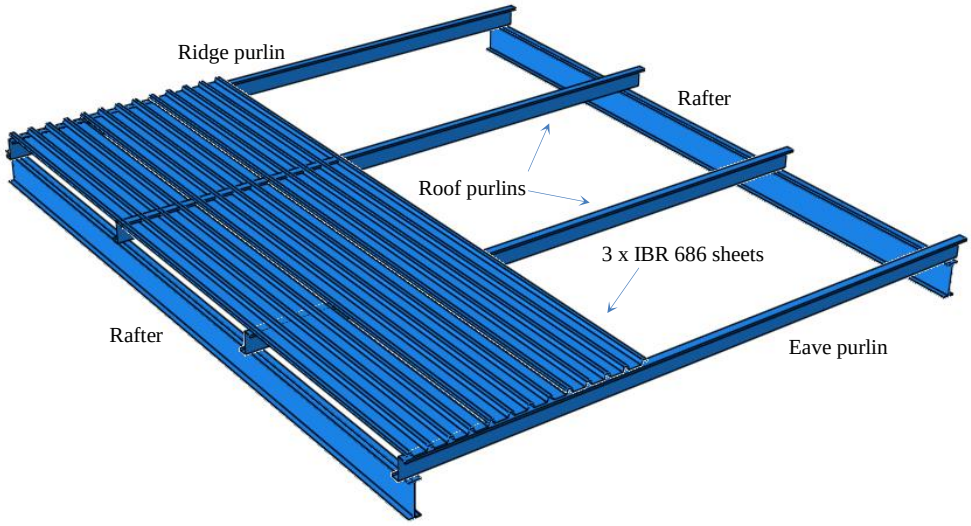


Eaves connection

Rafters: 305 x 102 x 25 mm I-section
Purlins: 200 x 75 x 20 x 3 mm Z-section

(b) Details of roof bay (sag rods and screws not shown)

**Figure 1.1: General components of a steel roof structure (not to scale)**

### 1.2.2 Description of a purlin

A purlin is a horizontal and longitudinal structural member in roofing that spans parallel to the eaves and is supported by rafters, walls or trusses. Purlins support the roof cladding or sheeting. Roof purlins in most steel-framed buildings are made from cold-formed, lipped open sections such as channels, angles and Z-sections. Generally, these cold-formed sections are lighter than hot-rolled sections and are, therefore, less expensive. The purlins can be designed to span up to 12 m but, for such long spans, the members should be designed in double span or continuous configurations in order to minimise deflections (SAISC, 2013). The thickness of the purlin section usually ranges from 2.0 to 4.5 mm (SAISC, 2013). According to SANS 10162: – Part 1, for commercial quality steel (such as a cold-formed section) the yield and ultimate tensile strength should be 200 and 365 MPa, respectively.

Unless stated otherwise, a 200 x 75 x 20 x 3 mm Z-section (shown in Figure 1.2) is used as a purlin in all cases in this research. The Z-section was chosen because it allows continuous span configurations through the overlaps over the supports, resulting in optimum adaptation of the cross-sections and an increased capacity to carry "hogging" moments (Robra & Luza, 2008; Metsec, 2016). Although the cross-section is not symmetrical, the shear centre coincides with the centroid, making the Z-section rotationally stiffer (Vlasov, 1959).

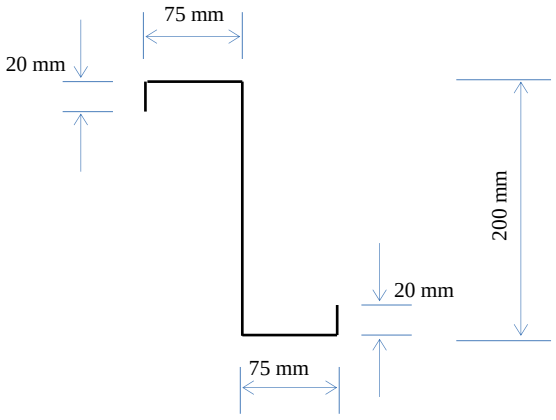


**Figure 1.2: A 200 x 75 x 20 x 3 mm Z-section purlin (not to scale)**

### 1.2.3 Description of an inverted box rib sheet (IBR)

An IBR sheet comes in different profiles and thicknesses. An example of an IBR 686 sheet is shown in Figure 1.3 with its cross-section shown in Figure 1.4. Sheet thickness (t) could range from 0.3 to 0.8 mm depending on the type, size and number of spans, type and purpose of the building and whether the sheet is used for side or roof cladding. An IBR 686 sheet is an IBR sheet with a cover width (B) of 686 mm (Figure 1.4). According to Global Roofing Solutions (2016), IBR sheeting offers the optimum strength, mass and load-span characteristics compared with other steel roofing profiles.

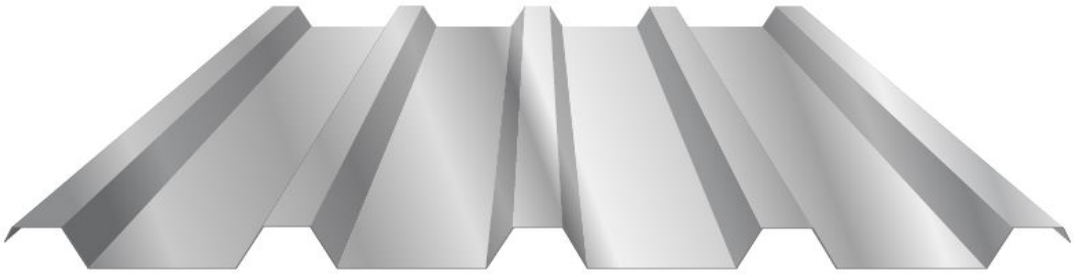

**Figure 1.3: Example of a typical IBR 686 sheet (TUFDEK IBR – see SAFINTRA, 2012)**

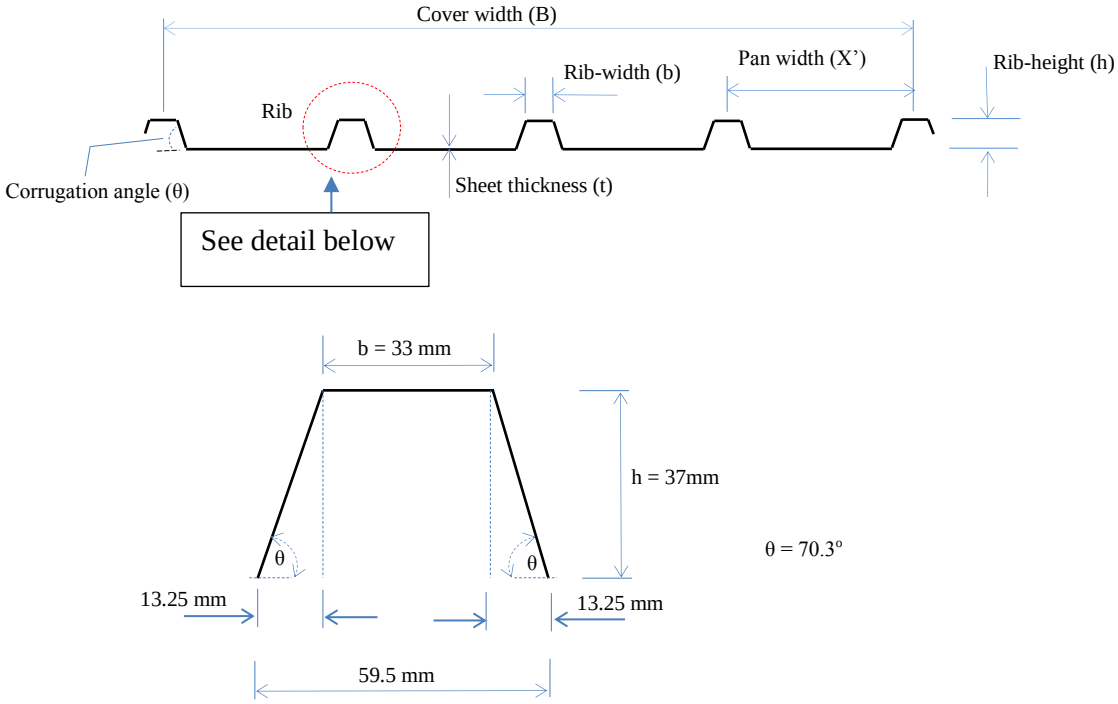


**Figure 1.4: A cross-section of a typical IBR sheet, including a depiction of the details of a rib (not to scale)**

### 1.2.4 Description of the fasteners

A corrugated sheet can be attached to the purlin with screws or bolts at alternating crests or troughs, or at intervals prescribed by the manufacturer. The type and spacing of the screws or bolts is usually determined by the type of loading and the sheet used. In practice Class 4.8 M16 bolts with Classes 8 and 5 nuts are adequate for purlin or girt connections in South Africa (SAISC, 2013). For more information on mechanical properties of Classes 8 and 5 nuts, reference may be made to SANS 1700:5-1. Class 4.8 M16 bolts have an ultimate tensile strength and yield stress of 400 and 320 MPa, respectively. Bolted connections should be designed in accordance with SANS 10162: Part 1 or Part 2, and should be fabricated and erected in accordance with SANS 10094. Self-tapping screws are used in fixing roof or side sheeting.

## 1.3 Statement of the problem

Failure modes of roof-sheet profiles are difficult to predict due to their complex behaviour when subject to different types of loading and other factors such as material, stiffness, handling during erection and support conditions; leading to high repair and maintenance cost. To reduce the chances of failure, manufactures produce coils of steel roof-sheet material in different grades of strength which usually range from 230 to 550 MPa depending on the thickness of the sheet coil (Arcelor Mittal, 2015). The thinner sheets are made from higher strength steel (550 MPa) and thicker sheets from a relatively lower strength (230 MPa) steel. The stiffness is governed by the dimensions, corrugation and the total cover width of the sheet profile. Excellent drainage pans and high production efficiency are desirable, but the most important aspect that will reduce the cycle of repair and maintenance is the sheet profile stiffness. Some manufactures incorporate rib stiffners in the pans in order to increase the stiffness of the profile and to prevent buckling on the pans.

## 1.4 Significance of the research

The significance of this research (conducted between 2013 and 2015) lies in both engineering and economics. Much research has been done on the subject of roof sheeting, covering the purlin and sheeting, environmental impacts, economic aspects and safety (SANS 10162-1, 2011; Eurocode 3 – Part 1-3, 2005). This research probes improved IBR sheet performance and cost.

## 1.5 Research objectives

The key objectives of this research are:

- to determine the optimum dimensional parameters of an IBR sheet profile, that would be used to simulate new and different IBR profiles made from standard commercially available input sheet coils whilst satisfying the stiffness criterion; and
- to perform a cost analysis in order to determine the most economic simulated profile.

## 1.6 Definitions of the terms used

In this dissertation:

- An "**optimal**" sheet is defined as one which satisfies the strength and stability criteria using the minimum material.
- The "**dimensional parameters**" are the geometrical characteristics of the sheet profile.
- The "**stiffness**" is defined as the force per unit deflection of an IBR sheet profile, or the extent to which it can resist deflection in response to the applied external loads.
- "**Material cost**" is the cost of input sheet coil from which the IBR sheet will be made.

## 1.7 Structure of the document

This document has the following structure: **Chapter 1** introduces the research topic and **Chapter 2** contains an overview of the literature. The methodology and structural theory underlying the modelling of purlin and sheeting, including material, characteristics, loading and design are presented in **Chapter 3**. **Chapter 4** discusses the selection of parameters and profiles used in the study. **Chapter 5** presents the results and discussion from the parametric study of the IBR sheet supported by the purlin, compared with the existing solutions in the literature and design codes in practice. **Chapter 6** presents overall conclusions on the research and discusses topics requiring future research. Thereafter, a comprehensive list of **References** is listed, followed by **Appendix A** and **Appendix B** which derive the applied loads and present the Euler-Bernoulli beam theory.

# 2 LITERATURE REVIEW

This chapter presents an overview of the literature available and research that has been done to date on different profile characteristics of corrugated or trapezoidal sheeting in general. It also presents a synopsis of different types of corrugated and trapezoidal metal roof sheeting and their importance and advantages as the preferred option over other types of roofing.

## 2.1 Reasons for using inverted box rib roof sheeting

Metal roof sheets are available in a wide variety of designs, sizes, textures and colours; and thus they are attractive and multipurpose (Yu & LaBoube, 2010). Metal roof sheeting is "durable" as it is resilient to cracking and corrosion, and can endure extreme cold and hot weather conditions. Thus it can last upwards of twenty years (Bergfelt, Edlund & Larsson, 1975). When it comes to constructability and installation, roof sheeting is relatively easy and quick to install compared with reinforced concrete slabs and tiling.

There are various types of metal roof sheeting: namely, the sinusoidal corrugated sheet, trapezoidal sheet, wide-span and IBR sheet (SAISC, 2013). The literature review revealed little work has been published that compares these sheets with one another. Rather, each type of sheet has been investigated separately by different researchers. IBR sheets have been proved by different researchers to have a good strength-to-weight ratio, better water-carrying capacity and are regarded as the most efficient sheet profile (Cousins Steel International, 2015; ArcelorMittal, 2015).

## 2.2 Overview of the parametric studies performed on roof sheeting

Of interest are design and dimension type parameters. "Designtype" parameters can include the material properties such as density, elastic modulus and weight. "Dimension type" parameters can include the size and shape of the cross-section of the sheet. Different authors followed different methods to study and investigate the parameters involved in the design, manufacturing, construction and performance of the IBR sheet (Lee, Mioduchowski & Faulkner, 1995; Chaudhary & Khan, 2015).

Most of the research done throughout the world is based on experiments and modelling using Finite Element Methods (Mezzomo *et al.*, 2010; Peng, Liew & Kitipornchai, 2006). Lee *et al*. (1995) followed numerical procedures to design appropriate profiles that would

satisfy the imposed dimensional constraints and minimise bending stresses in the trapezoidal sheet. Using the Finite Element Analysis software ANSYS, Mezzomo *et al*. (2010) investigated the mechanical behaviour of roof sheeting and discovered the sheet profile with the smallest displacement, high critical buckling load and maximum roof covering area. Peng *et al*. (2006) have investigated the design parameters of both corrugated and trapezoidal sheets, through studying the flexural properties in two perpendicular directions of the sheet.

It was observed from most of the literature reviewed that the objective of parametric studies is often to improve the load-carrying capacity of the profiled roof sheeting or to optimise the sheet profile (Morgan & Beck, 1976; Balázs, Melcher & Horáček, 2015; Balázs, Melcher & Horáček, 2012; Mezzomo *et al*., 2010). The cross-sectional shape of the sheet profile is the key element in enhancing its stiffness as it controls the local, distortional and global buckling modes (Sharafi, Teh & Muhammad, 2013). Sharafi *et al*. (2013) considered sheets of different grades and different thicknesses along with a range of wind speeds in order to optimize the dimensions of trapezoidal roof sheeting supporting solar panels. Sivachenko and Broacha (1982) invented an improved profile for a trapezoidal corrugated plate so as to optimize the moment of inertia and the section modulus utilizing a given material. In using metamodelling for shape optimization, Janushevskis, Melnikovs and Auzins (2015) obtained the cross-sectional shape of corrugated sheets by a global stochastic search procedure in order to minimise the displacement of the structure. Mahaarachchi and Mahendran (2009) investigated crest-fixed thin trapezoidal sheets with closely spaced ribs subject to wind uplift. Graph theory, combined with Ant Colony Optimization (ACO) algorithms, was used by Sharafi, Teh and Muhammad (2014) in open and closed thin-walled steel sections and trapezoidal roof sheeting with the objective of finding the optimum mass and stiffness.

However, in the results of the aforementioned research, a deficiency remains unanswered regarding the relationship between the dimensional parameters of an IBR sheet and its stiffness; thus prompting the research presented in this dissertation. Stiffness is an important aspect in the design and performance of any structure. Since it is the desire of every roof-sheeting manufacturer to reduce the input material cost, and hence the production cost yet offer the stiffest sheet, this research also focused on the material cost of IBR sheeting.

Having presented the literature review, the next chapter discusses the research methodology.

# 3 RESEARCH METHODOLOGY

## 3.1 Introduction

This chapter outlines the steps that were followed in modelling and simulation of the purlins, sheeting and screws. The Finite Element Method (FEM) as implemented in Abaqus/CAE (referring to **C**omplete **A**baqus **E**nvironment) (Dassault Systemes SIMULIA, 2014) [hereinafter referred to as "Abaqus/CAE" in this document] was used.

### 3.1.1 Abaqus/CAE overview

Many commercial Finite Element Analysis (FEA) software packages are available for analysis of roof structures. The FEA software, Abaqus/CAE (Dassault Systemes SIMULIA, 2014), was used in the simulations performed in this research. Abaqus/CAE is a well-known computer-aided engineering software used for the modelling and analysis of mechanical components and assemblies. It has become popular in research and academic institutions because of its large library of materials and elements and its ability to simulate multi-dimensional problems. With Abaqus/CAE the user is able to create any form of geometry using the graphical user interface (GUI), analyse and use the visualization options to view, interpret or communicate the results from the model.

## 3.2 Finite Element Model in Abaqus/CAE

Figure 3.1 shows a flow diagram summarising the logic that was followed when the model was developed in Abaqus/CAE.

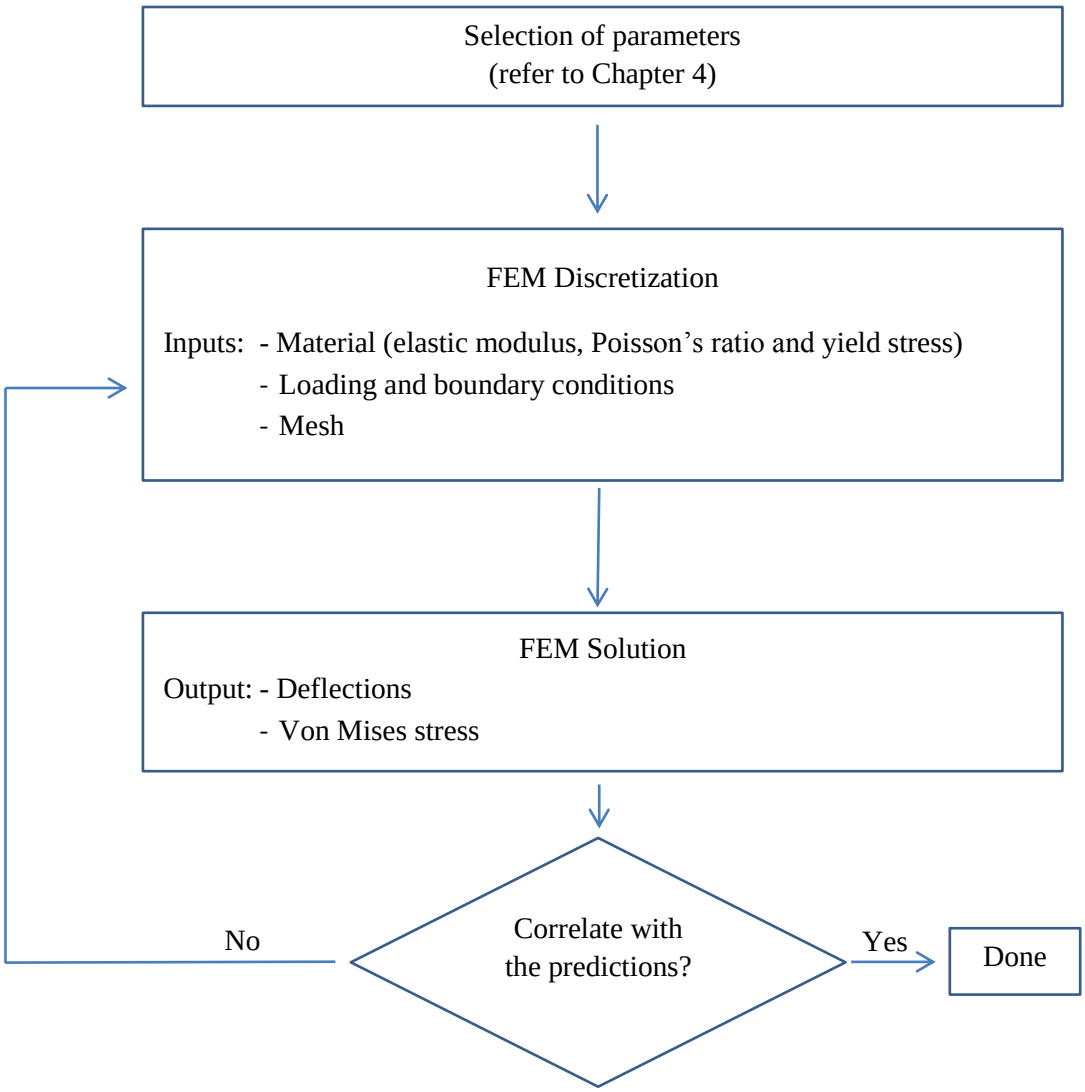


**Figure 3.1: Flow diagram of the development and application of the Abaqus/CAE model used in this research**

### 3.2.1 Abaqus/CAE experimental setup

The components of the steel roof structure used in the experimental setup were the two purlins, the IBR sheet with a constant 686 mm cover width and the screws. The purlins were assumed to be 200 x 75 x 20 x 3 mm lipped Z-sections and were not varied in this research. The purlins were spaced at 2200 mm since that is the recommended span for single span IBR 686 sheets with 0.8 mm thickness and a Grade of 230 MPa (SAISC, 2013). An allowable deflection of span/200 ratio (SAISC, 2013) was used.

The purlins were assumed to be simply supported by the rafters. The sheet was also assumed to be simply supported by the two purlins (Figure 3.2 (a)). In order to reduce the computational time and due to symmetry, half of the structure shown in Figure 3.2 (a) was modelled. This resulted in half the sheet span that equals 1100 mm and only one purlin having to be considered as shown in Figure 3.2 (b). A slider was inserted in order to allow for vertical movement but to prevent rotation and horizontal movement of the sheet at mid-span.

Steel roof sheeting can be subject to a few common types of loading. In this research only the wind uplift loading (W) on the IBR sheet will be considered as it is the most critical. To simplify the process and reduce the computational time, only one sheet of 686 mm cover width and a purlin span of 686 mm were used in the Abaqus/CAE experiments as shown in Figure 3.2 (c).

#### *3.2.1.1 Boundary conditions and coordinates system in Abaqus/CAE*

The side edges of the sheet were free in the z-axis and y-axis directions, and restrained in the x-axis direction to ensure that the cross-section maintained its shape during loading as shown in Figure 3.2 (c). At mid-span, the sheet was sectioned due to symmetry and supported with a vertical slider to allow for vertical movements in the y-axis and restrain the longitudinal movements in the z-axis direction as shown in Figure 3.2 (b).

**Coordinate system in Abaqus/CAE**

Origin of the global coordinate system:

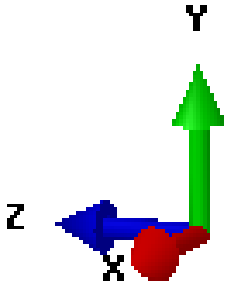


x: defined along the length of the purlin
(Deflection = $U_1$, Rotation about x-axis = $UR_1$)

y: defined along the height of the purlin and sheet
(Deflection = $U_2$, Rotation about y-axis = $UR_2$)

z: defined along the length of the sheet
(Deflection = $U_3$, Rotation about z-axis = $UR_3$)

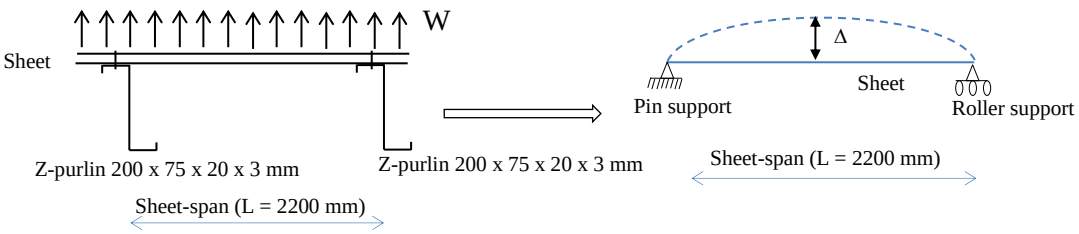


(a) A sheet supported by two purlins and modelled as a simply supported beam

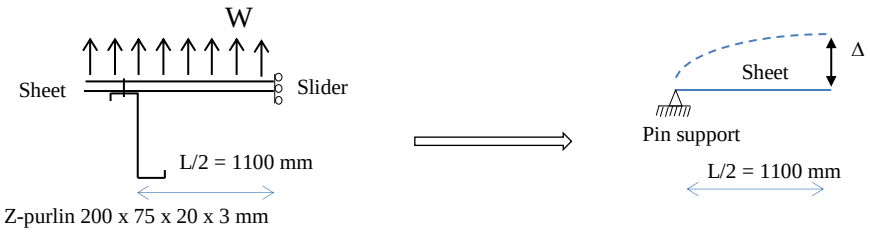


(b) One half of a sheet modelled as a simply supported beam due to symmetry

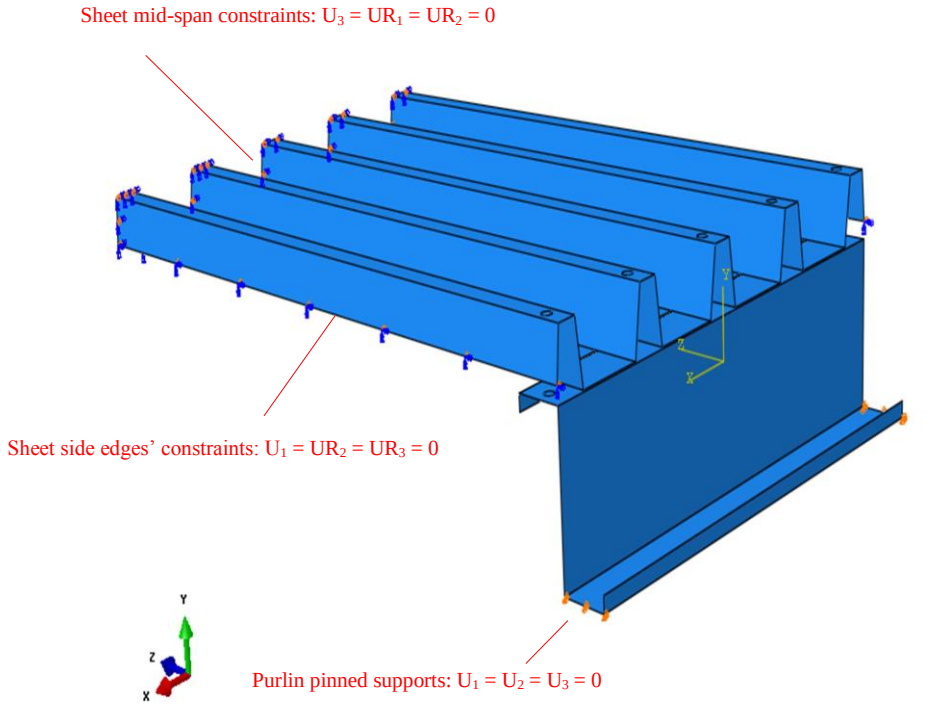


(c) Due to symmetry, one half of a sheet supported by a purlin was modelled in Abaqus/CAE

**Figure 3.2: Experimental setup of IBR sheet and a 200 x 75 x 20 x 3 mm Z-section purlin in Abaqus/CAE**

### 3.2.2 Creating purlin and sheet as parts in Abaqus/CAE

A Finite Element model for each IBR sheet profile (Chapter 4) was developed using Abaqus/CAE (Dassault Systemes SIMULIA, 2014). Both the purlin and sheet were created as separate parts and treated as three-dimensional deformable shell extrusions. A single sheet was used and attached to the purlin, which took the same length as the width of that single sheet. In all the models that were created, the sheet was connected to the purlin through crests or ribs. The units adopted in Abaqus/CAE for this research were millimetres (mm) and newtons (N).

### 3.2.3 Material and section properties

The material was assumed to have a tri-linear elastic-plastic behaviour, with elastic modulus (E) and Poisson ratio (ν) of $200 \times 10^3$ N/mm$^2$ and 0.3, respectively. The simplified stress-strain relationship adopted is shown in Figure 3.3 for material exhibiting linear elasticity and Von Mises (Liu, 2005) plasticity. The discrepancies in the yield strength – due to cold-forming and manufacturing of sheeting and purlins – were ignored. Homogeneous shell-sections were utilized for both the sheet and purlin using the Simpson's integration rule.

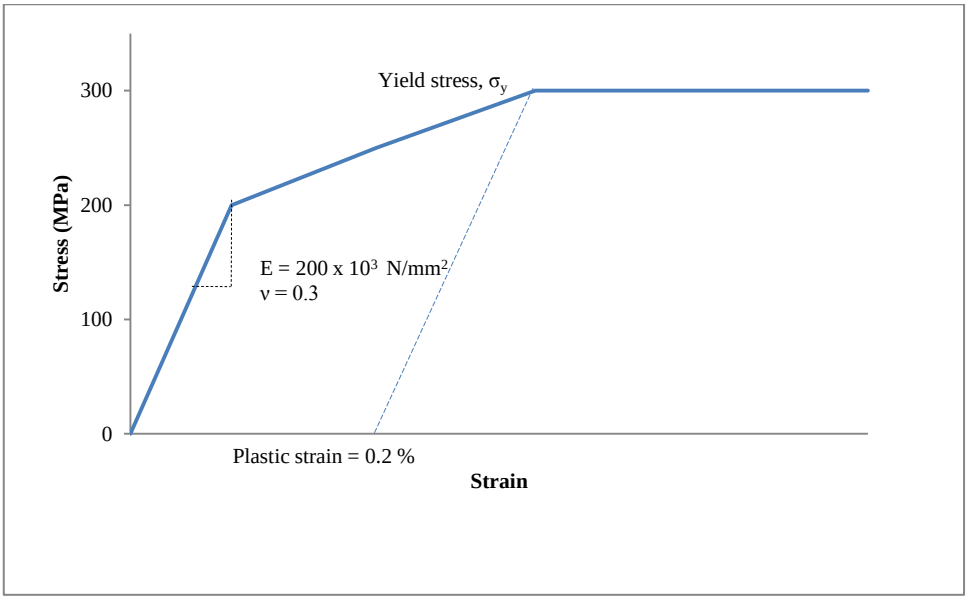


**Figure 3.3: Simplified stress-strain relationship for steel (after Case & Chilver, 1964; Case, Chilver & Ross, 1999)**

### 3.2.4 Fastenings

#### *3.2.4.1 Bolt heads and nuts*

Circular partitions of 16 mm diameter were made on the sheet to resemble the bolt or screw heads and on the top flange of the purlin to resemble the nuts as shown in Figure 3.4 (a) and (b). Partitioning in Abaqus/CAE is a tool that is used to divide parts into portions that can be treated separately. Kinematic couplings were created for all bolt heads and nuts, with the translational movements restrained and the rotational movement allowed. According to Abaqus/CAE, kinematic constraints are used when a large number of nodes (also referred to as the "coupling nodes") are constrained to rigid body motion of a single node and the degrees of freedom at that constraint are selected individually in a local coordinate system. In this case, the nodes in the bolt head and nut partitions were constrained to the rigid body motion of the nodes at reference points RP-3 and RP-6, respectively (Figure 3.4 (b)). A contact between the sheet and the purlin was created, assuming frictionless conditions.

#### *3.2.4.2 Bolts*

The bolt or screw was modelled by the multi-point constraints (MPCs) using rigid links. According to Abaqus/CAE, the MPCs are used to specify the linear and non-linear constraints; and can offer a multi-point constraint between two points. In this case, the MPCs are used as non-linear constraints between the reference points at the centres of the bolt head and nut (for example, the connecting line between RP-3 and RP-6 in Figure 3.4 (b)). The link provides a pinned but rigid connection between its two ends (which are at the centres of the bolt head and nut) to keep the distance between the nodes constant (this means that bolt length does not change).

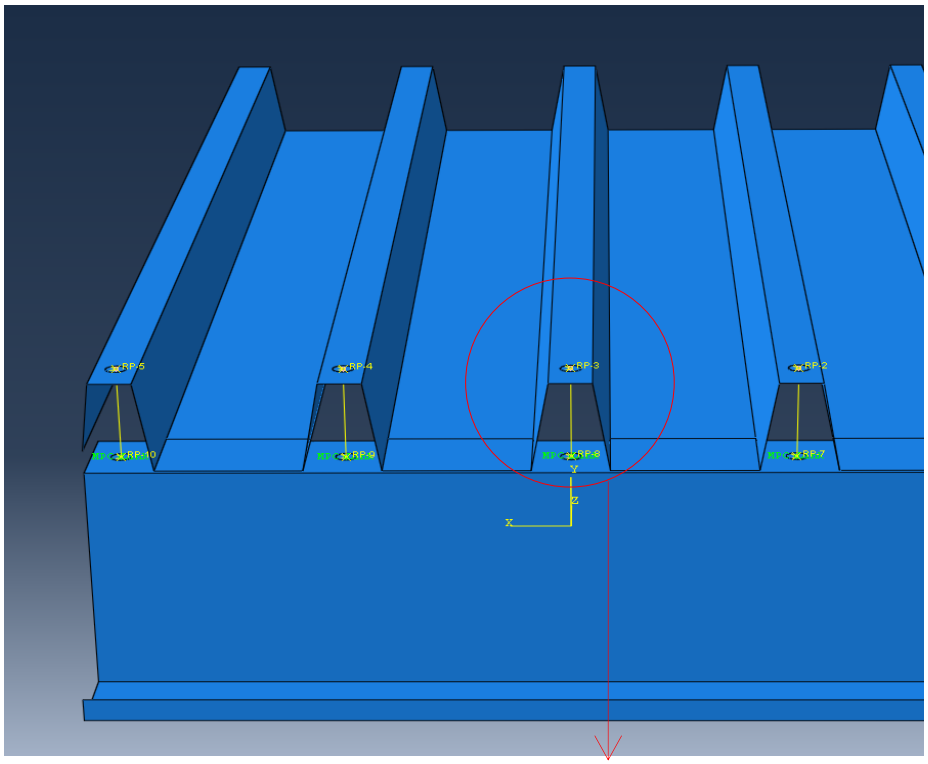


(a)

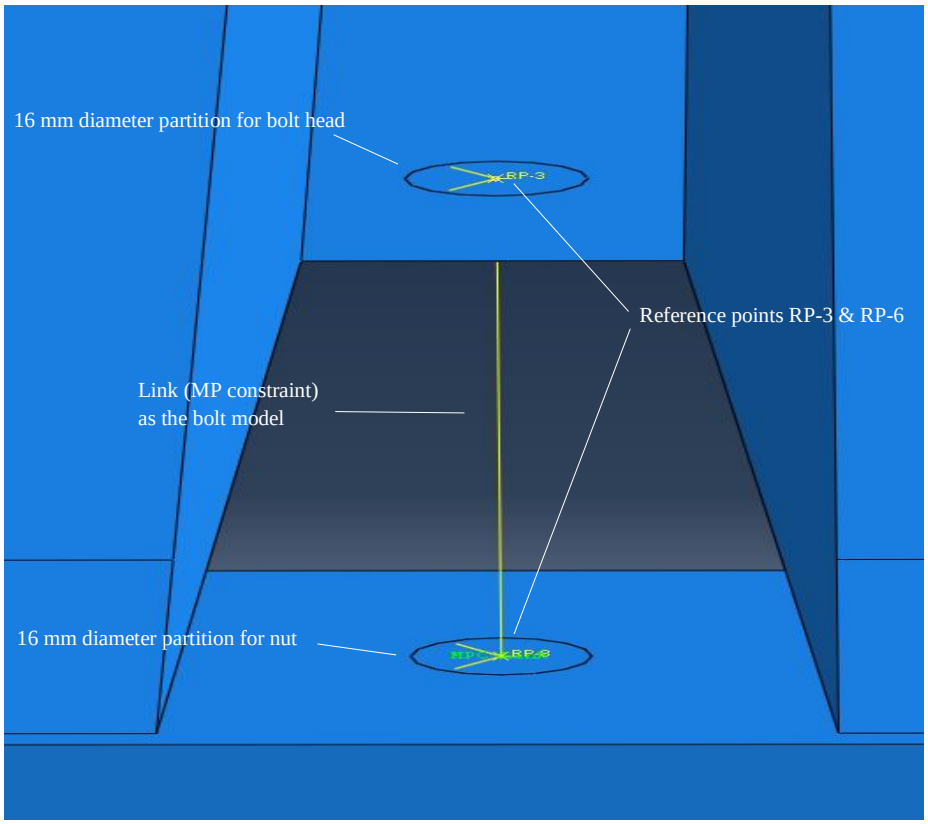


(b)

**Figure 3.4: Model for bolt heads, nuts and bolts**

### 3.2.5 Modelling the loads in Abaqus/CAE

#### *3.2.5.1 Wind uplift load*

Abaqus/CAE automatically creates an initial step under which the boundary conditions are defined. Next, the loading step is created in which the wind uplift load (W) is applied on the top surfaces of the sheet as shown in Figure 3.5. The step is quasi-static with no time effects. The non-linear geometric analysis option is chosen, and the increment step size is set automatically. The computed uniform uplift pressure load is applied as a ramp until the specified pressure is reached. During the parametric study (presented in Chapters 4 and 5), the applied wind uplift load (W) is kept at a magnitude of 0.0016 N/mm$^2$ in all the experiments conducted. The calculation of the estimated wind uplift loading is presented in Appendix A.

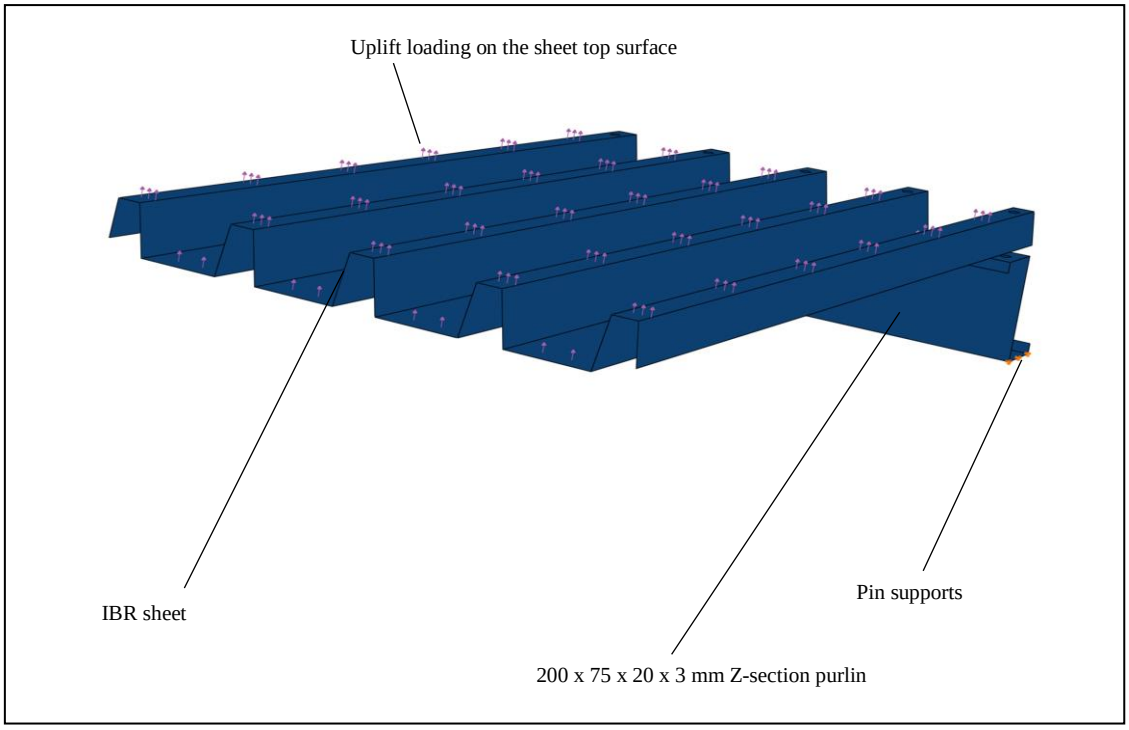


**Figure 3.5: Wind uplift loading on the sheet**

### *3.2.5.2 Buckling load*

Stability is an important aspect in the design and analysis of many structures including shells. In this investigation, both the IBR sheet and purlin were modelled as 3-dimensional shell structures, and it was necessary to perform a buckling strength assessment, especially to determine the stability of the ribs of the IBR sheet.

The whole sheet was subject to a wind uplift loading (Figure 3.5), and the sheet experienced a bending moment and thus a compression at the lower surfaces of the cross-section. A stability study was conducted on the whole sheet, using eigenvalue buckling analysis. Eigenvalue buckling analysis is a method used to estimate the critical load at which the response of a structure will bifurcate (Dassault Systemes, 2014). The analysis is based on the assumption that the response and behaviour of the structure before bifurcation is linear; therefore, eigenvalue buckling analysis is useful for structures that undergo small elastic deformations before buckling.

The linear perturbation step was created, during which a wind uplift load (W) of 0.0016 N/mm$^2$ and a concentrated load of 834 N (the equivalent mass of a human weighing 85 kg, but SANS 10237 specifies 900 N) were applied to the sheet. The Lanczos eigensolver in Abaqus/CAE was used and ten eigenvalues were requested in order to reduce computational time.

**Buckling due to (1) wind uplift loading and (2) concentrated load**

Equations 3.1 and 3.2 were used to estimate the critical buckling loads, $W_{cr}$ and $P_{cr}$, due to wind uplift and concentrated load acting on the IBR sheet, respectively:

$$W_{cr} = \lambda_i W \qquad 3.1$$

$$P_{cr} = \lambda_i P \qquad 3.2$$

where:

$W =$ The wind uplift load applied to the sheet during the linear perturbation step

$P =$ The concentrated load applied to the sheet during the linear perturbation step

$\lambda_i =$ The $i^{th}$ eigenvalue corresponding to the $i^{th}$ buckling failure mode

Note that if:

$\lambda > 1$ $W_{cr} > W$ or $P_{cr} > P$; Buckling is not predicted

$\lambda = 1$ $W_{cr} = W$ or $P_{cr} = P$; Buckling is predicted

$0 < \lambda < 1$ $W_{cr} < W$ or $P_{cr} < P$; Buckling will occur

$-1 < \lambda < 0$ Buckling is predicted if the load acts in the opposite direction

$\lambda < -1$ Buckling is not predicted.

For the detailed derivation of equations 3.1 and 3.2, the reader is referred to Abaqus/CAE Documentation (Dassault Systemes, 2014).

Figure 3.6 shows the point of application of the concentrated load (P) acting on the middle rib at mid-span of the IBR sheet.

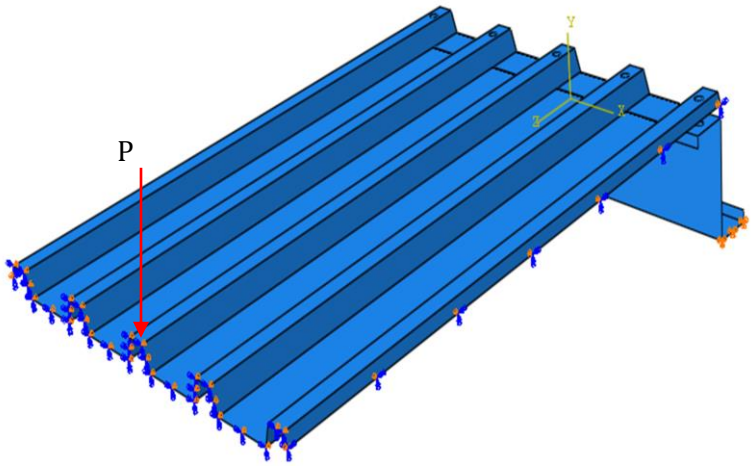


**Figure 3.6: A schematic representation of the IBR sheet used in the buckling analysis**

The objective of the eigenvalue buckling analysis in this investigation was to:

- predict the critical buckling load as a function of the rib-height (h) of an IBR sheet with four pans, 33 mm rib-width (b) and 0.8 mm thickness.
- establish the buckled mode shape of an IRB sheet with large values of rib-height (h).

### 3.2.6 Meshing technique

Since steel roof sheeting is thin, it is likely to experience large deformation and localized yielding around the areas that are highly stressed. In order to account for this, a geometric and material non-linear static analysis was carried out. The quadrilateral shell element with six degrees of freedom at each node, S4R was chosen as the meshing element for the sheet and the purlin as shown in Figure 3.7 (a) and (b). The element size was set to 10 mm after a numerical convergence study was carried out. The element sizes considered in order to reach convergence were 150 mm, 80 mm, 40 mm, 20 mm, 10 mm and 5 mm. The reduced integration option was chosen in order to reduce the computation time and to improve the accuracy of the results. The results of the convergence study are discussed and analysed in Chapter 5.

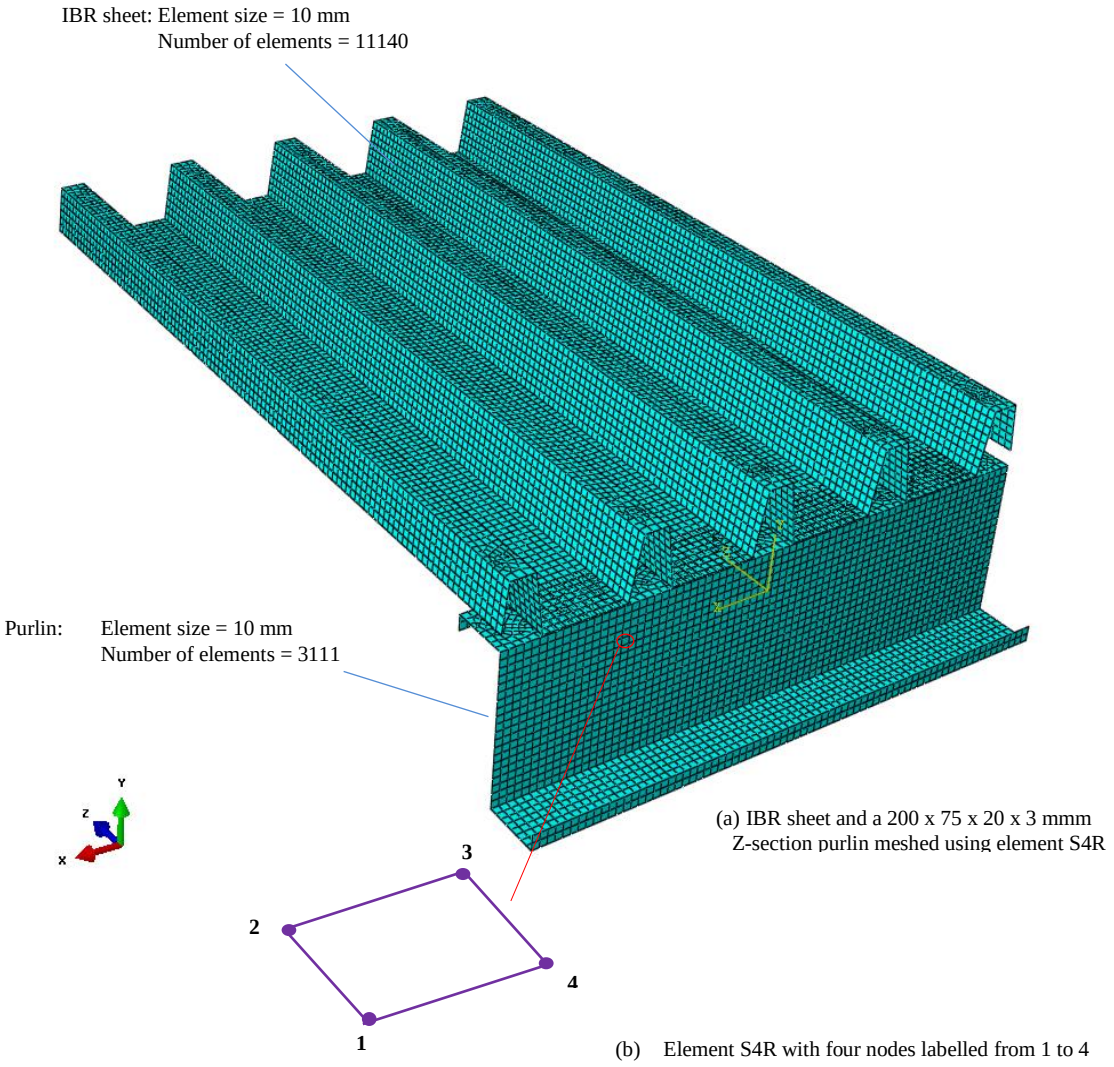


**Figure 3.7: Element S4R and typical mesh of the sheet and purlin**

### 3.2.7 Data analysis and convergence study

#### *3.2.7.1 Incrementation in Abaqus/CAE*

The total time period for the step analysis in Abaqus/CAE is assumed to be 1 unit. Abaqus/CAE divides this total time period into increments. For the general static step in Abaqus/CAE the following options were considered:

- An automatic time increment option was chosen, which means Abaqus/CAE will start the incrementation using the value chosen and entered as the 'initial increment size'. The sizes of the increments to follow are then chosen automatically by Abaqus/CAE based on how fast the model converges.
- The initial time increment size was taken as 0.05 (5 % of the total step).
- The minimum time increment size was taken as $1 \times 10^{-5}$.
- The maximum time increment size was assumed to be equal to 1.

#### *3.2.7.2 Deflection outputs*

In every simulation that was performed, the deflections of the nodes at sheet mid-span were recorded. The deflections were $U_1$ in the x-direction, $U_2$ in the y-direction and $U_3$ in the z-direction (Section 3.2.1.1).

## 3.3 Euler-Bernoulli beam theory

The Euler-Bernoulli beam theory, also called "classical" or "engineer's" beam theory is one of the simplest and most useful theories that provides a way of calculating the load-carrying capacity and the deflection of the beam (Case *et al*., 1999). (For a derivation of the Euler-Bernoulli beam theory, refer to Appendix B.) Although beams are generally three-dimensional bodies, the Euler-Bernoulli theory presents a two-dimensional beam model.

The Euler-Bernoulli beam theory (Case *et al*., 1999) was used to estimate the deflections in order to validate the results from Abaqus/CAE. The Euler-Bernoulli beam theory was chosen over other methods of calculating beam deflection because:

- An IBR sheet supported by multiple purlins would behave as a 2-dimensional beam on continuous supports, hence the beam theory was applied to solve for the deflection of the IBR sheet.
- In the Euler-Bernoulli beam theory, the internal energy is due to bending deformation only, whilst Timoshenko's (1953) beam theory considers the contributions of the shear deformation (Beer *et al*., 2012). In this research only bending deformation of the IBR sheet is considered.
- The Euler-Bernoulli beam theory gives good results for normal or direct stresses because of its capability to produce the bending-dominated deformations (Beer *et al*., 2012).

Equation 3.3 is used to estimate the deflection ($v_c$) of the sheet at mid-span (L/2) supported by two purlins and subject to uplift wind loading.

$$\text{Maximum deflection} = v_C\left(x = \frac{L}{2}\right) = \frac{5WL^4}{384EI} \qquad 3.3$$

Where

$W =$ Applied wind uplift

$L =$ Sheet span between adjacent purlins

$I =$ Second moment of area of cross-section of the IBR sheet profile (Appendix B)

$E =$ Elastic modulus

The methodology for this research was discussed in detail in this chapter. Selection of the parameters researched is given in Chapter 4.

# 4 SELECTION OF PARAMETERS

## 4.1 Introduction

The influence of the profile parameters and thickness of a corrugated sheet on its overall behaviour and performance is not well understood by designers and manufacturers. "Corrugation", which is the main source of sheet "stiffness", is formed by the rises in heights (called "ribs"), spaces in between the ribs (called "pans") and the inclination angle of the ribs' vertical walls which is usually less than $90^{o}$. The design shape and sizes of each profile parameter in any corrugated or trapezoidal sheet govern its failure modes and overall performance.

This chapter selects the dimensional parameters that were used in the parametric study conducted on an IBR corrugated sheet. This was achieved by first identifying the key profile parameters to be varied, defining the range for each parameter, specifying the constraints and then analysing and discussing the results of each parameter variation.

## 4.2 Key parameters

Figure 4.1 shows the cross-section of a typical IBR sheet. The profile parameters that were varied were rib-height (h), rib-width (b), sheet thickness (t) and number of pans (n) per 686 mm cover width measured from centre to centre of each rib.

Other parameters which were studied but not shown in Figure 4.1 are the unfolded cover width or the width when the ribs are flattened (B') and the span ( $L$) of the sheet.

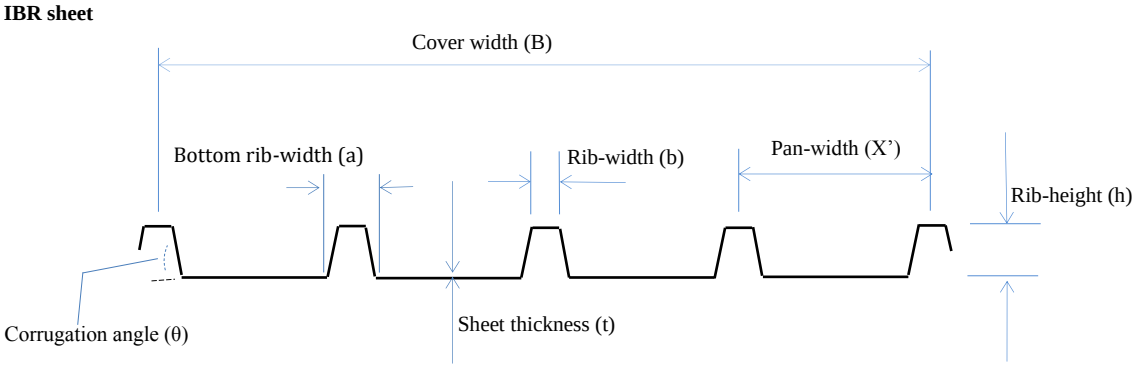


**Figure 4.1: Cross-section of a typical IBR sheet (not drawn to scale)**

**Reasons for deciding on the key parameters**

It should be noted from Equation 3.3 that the sheet deflection is inversely proportional to the second moment of area (I). The formula for calculating the second moment of area is presented in Appendix B. The second moment of area (I) of the cross-section of the IBR sheet is affected by the dimensional parameters: rib-height (h), rib-width (b), number of pans (n) per 686 mm cover width, sheet thickness (t) and the corrugation angle (θ). The rib-height (h) and rib-width (b) are affected by the corrugation angle (θ) and thus the corrugation angle (θ) is not an independent parameter and that is why it was not selected as a key parameter to be varied. The pan-width (X') was not varied because it depends on the number of pans fitted in the cover-width. The bottom rib-width (a), which affects the stability of the rib, was kept constant at a value of 59.5 mm in order reduce the number of varying parameters in a rib during the analysis.

### 4.2.1 Variation of rib-height

The rib-height (h) was varied from 34 to 80 mm while keeping the rib-width (b), sheet thickness (t) and number of pans (n) per 686 mm cover width constant at 33 mm, 0.8 mm and four, respectively, as shown in Figure 4.2. A minimum rib-height (h) of 34 mm was chosen to prevent the allowable sheet deflection from being exceeded, whilst the maximum rib-height (h) of 80 mm was chosen in order to ensure that the required sheet width falls within the sizes of the 925 mm input coil.

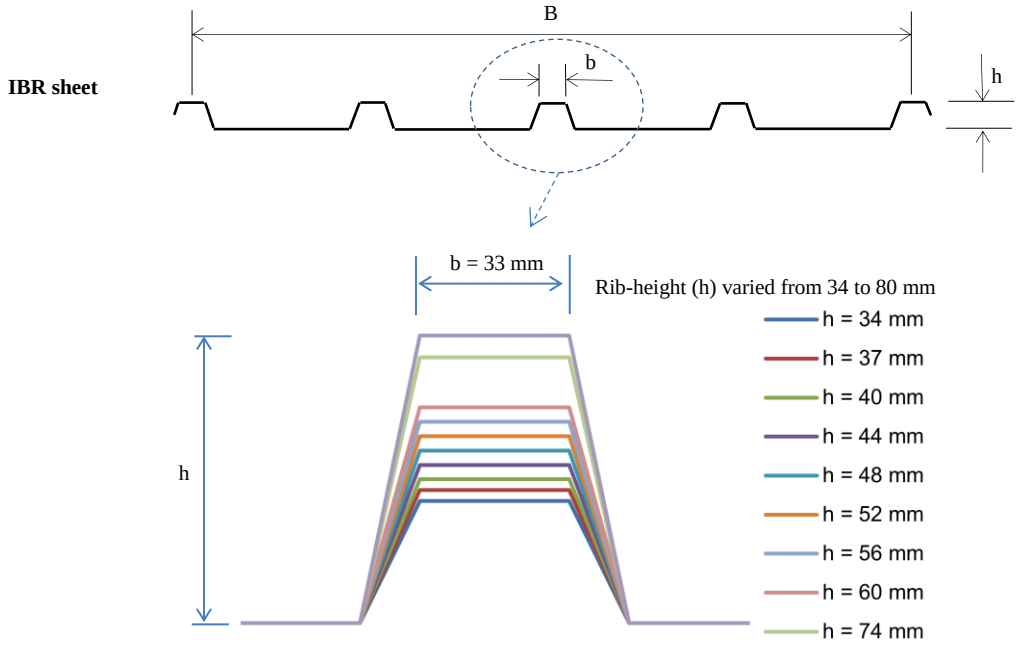


**Figure 4.2: Rib-height varying from 34 to 80 mm**

### 4.2.2 Variation of rib-width

The rib-width (b) was varied from 20 mm to 59.5 mm, whilst keeping the rib-height (h), sheet thickness (t) and number of pans (n) per 686 mm cover width constant at 37 mm, 0.8 mm and four, respectively. Choosing a minimum rib-width (b) of 20 mm was to ensure that the area around the bolt on the sheet is not too small; otherwise the top corners of the rib will be under high stresses and might be susceptible to local buckling. A maximum rib-width (b) of 59.5 mm was chosen so that the inclination angle of the rib does not exceed 90°. Figure 4.3 shows a single rib of different widths used in the analysis.

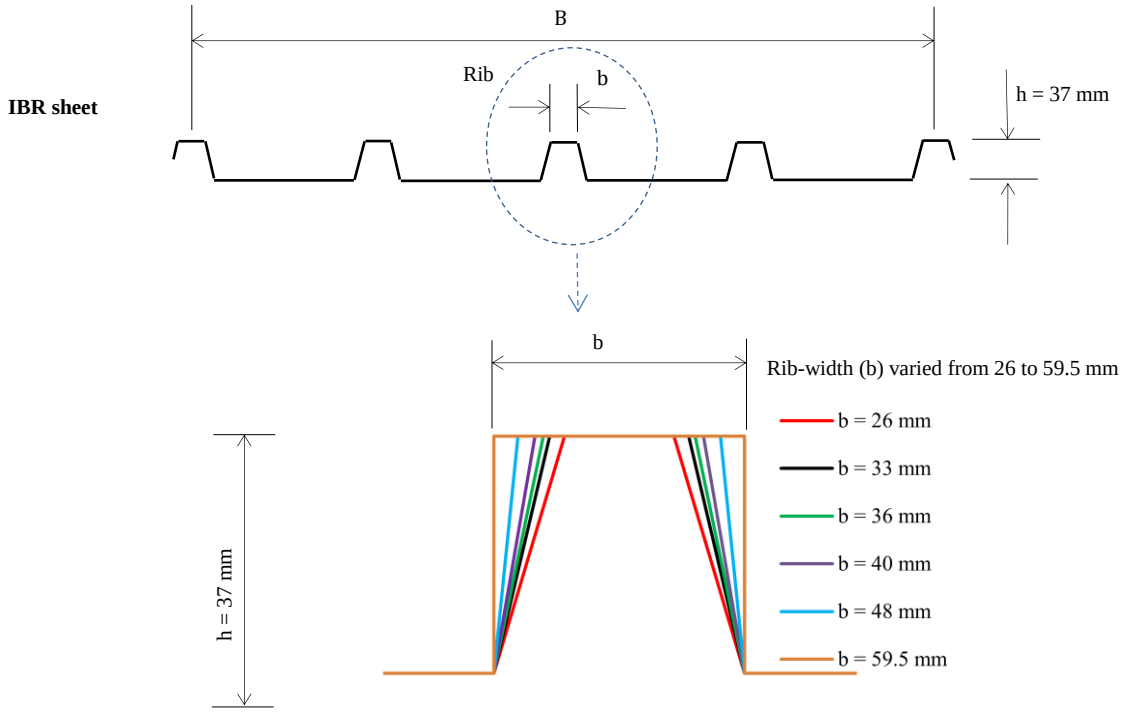


**Figure 4.3: Rib-widths varying from 26 to 59.5 mm**

### 4.2.3 Variation of sheet thickness

The sheet thickness (t) was varied from 0.3 mm to 0.8 mm whilst keeping the rib-height (h), rib-width (b) and number of pans (n) per 686 mm constant at 37 mm, 33 mm and four, respectively. According to the SAISC Handbook (2013), the IBR sheet thickness often varies from 0.3 mm for light industrial and residential buildings to 0.8 mm for heavy industrial buildings.

### 4.2.4 Variation of number of pans

The number of pans (n) per 686 mm cover width in the single sheet was varied from three to eight, while keeping the rib-height (h), rib-width (b) and sheet thickness (t) constant at 37 mm, 33 mm and 0.8 mm, respectively. The minimum number of pans (n) per 686 mm cover width was chosen to be three in order to avoid excessive deflections in the sheet, while the maximum number of pans (n) per 686 mm cover width was chosen to be eight in order to have a minimum space between the ribs. Figure 4.4 shows the four profiles to demonstrate the number of pans and sizes in each profile. B' is the unfolded cover width of the sheet also used as a measure of cost. It should be noted that the profile with the number of pans n = 4, is the standard IBR 686 sheet.

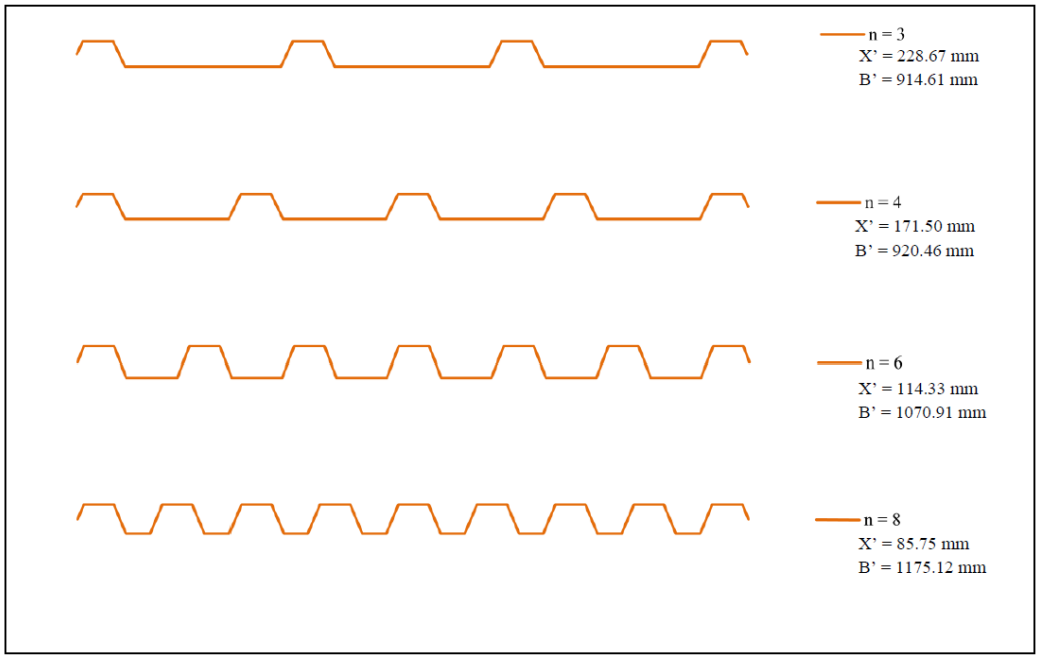


**Figure 4.4: Different IBR sheet profiles with three, four, six and eight pans**

### 4.2.5 Simultaneous variation of rib-height and rib-width

The rib-heights (h) and rib-widths (b) were simultaneously varied from 34 mm to 80 mm and 20 mm to 59.5 mm, respectively. This was done in a single sheet whilst keeping the

sheet thickness (t) and number of pans (n) per 686 mm cover width constant at 0.8 mm and four, respectively. For every rib-width of 20 mm, 40 mm and 59.5 mm, the rib-height was varied from 34 mm to 80 mm. Figure 4.5 presents an IBR sheet with a 20 mm rib-width and the rib-height varying from 34 mm to 80 mm. Figure 4.6 shows an IBR sheet with rib-width of 48 mm and the rib-height varying from 34 mm to 80 mm. The IBR sheet with rib-width of 59.5 mm and the rib-height varying from 34 mm to 80 mm is shown in Figure 4.7.

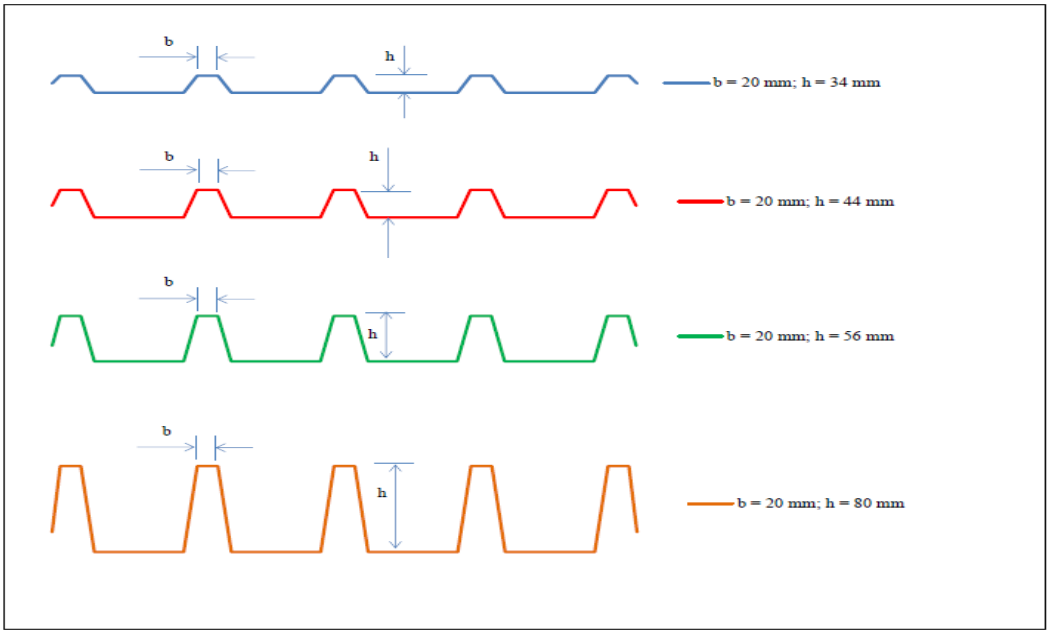


**Figure 4.5: IBR sheet profiles with 20 mm rib-width and rib-height varying from 34 to 80 mm**

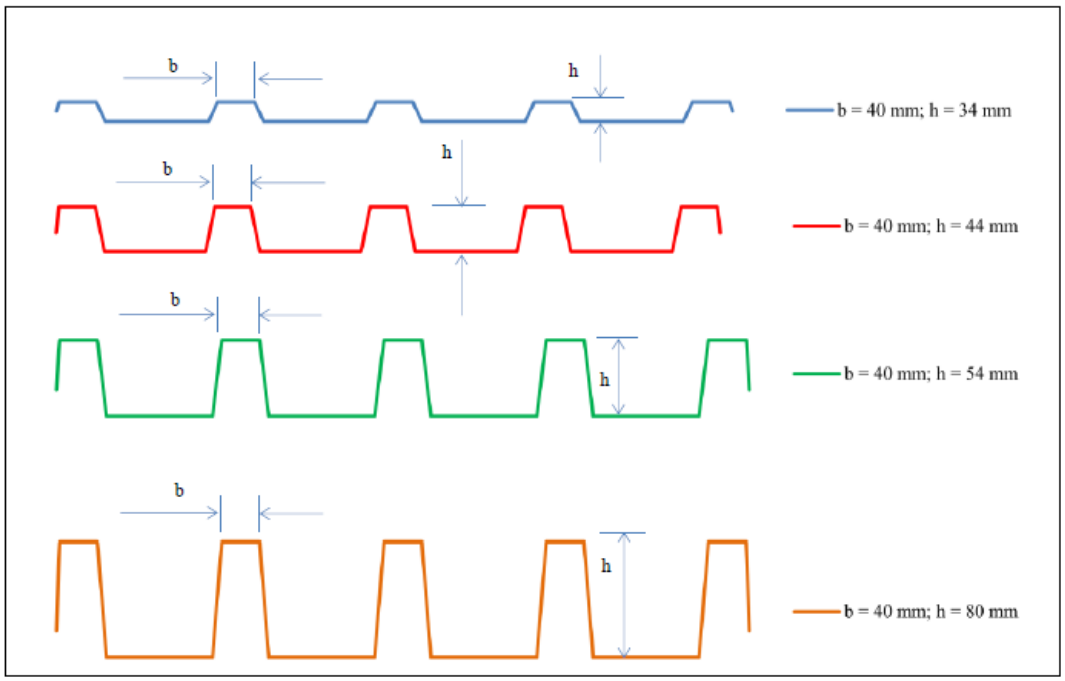


**Figure 4.6:** **IBR sheet profiles with 40 mm rib-width and rib-height varying from 34 to 80 mm**

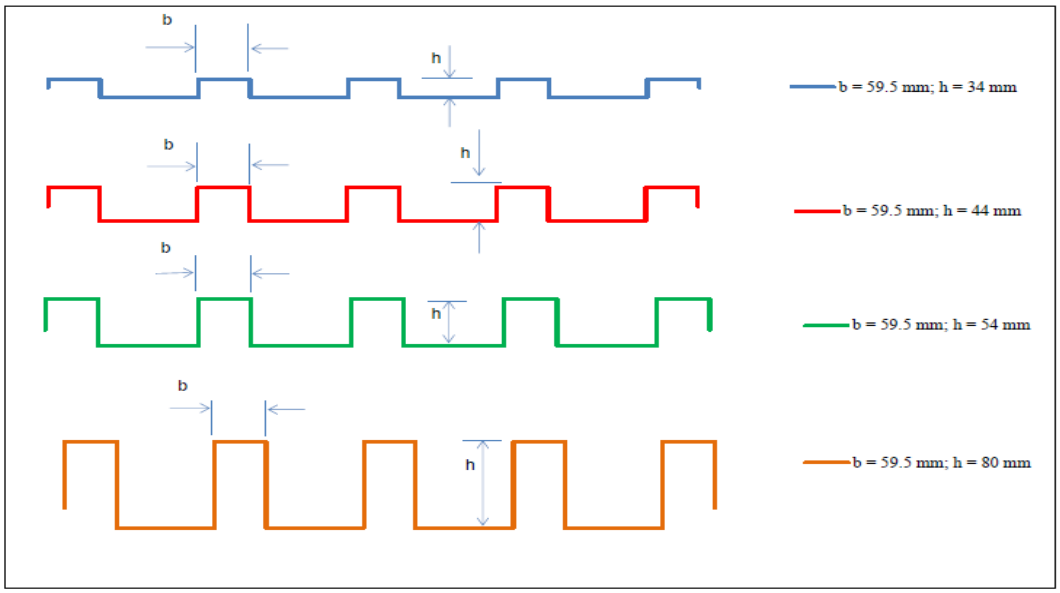


**Figure 4.7:** **IBR sheet profiles with 59.5 mm rib-width and rib-height varying from 34 to 80 mm**

### 4.2.6 Simultaneous variation of rib-height and number of pans

The rib-height (h) and number of pans (n) per 686 mm were simultaneously varied from 34 mm to 80 mm and three to eight, respectively. This was done whilst keeping rib-width (b) and sheet thickness (t) constant at 33 mm and 0.8 mm, respectively. For every number of pans (n) per 686 mm from three to eight, the rib-height was varied from 34 mm to 80 mm as shown in Figures 4.8 to 4.11.

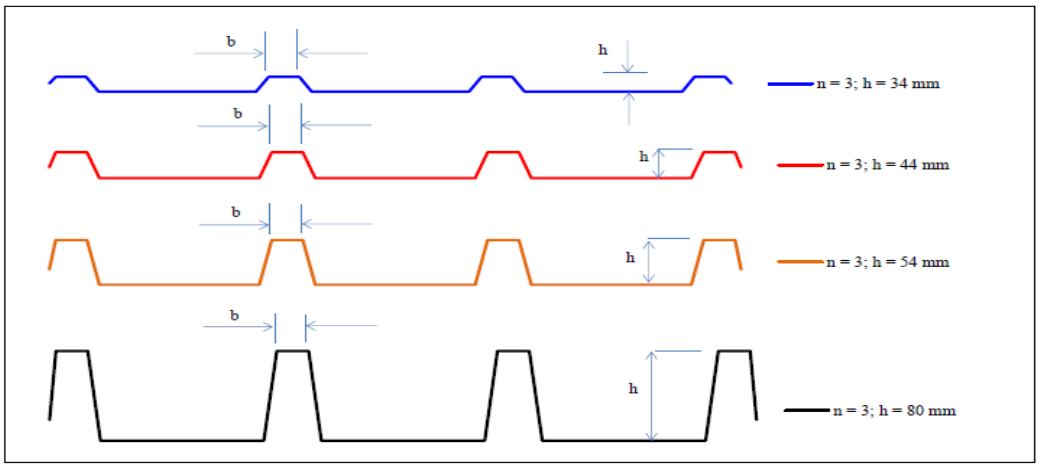


**Figure 4.8: Sheet profiles with three pans and rib-height varying from 34 to 80 mm**

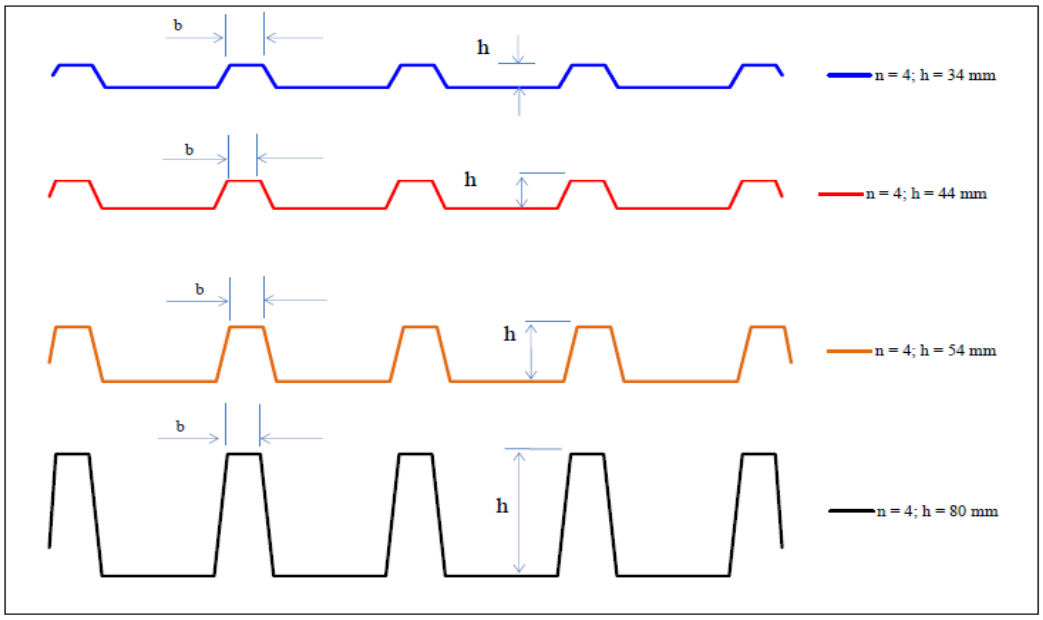


**Figure 4.9: Sheet profiles with four pans and rib-height varying from 34 to 80 mm**

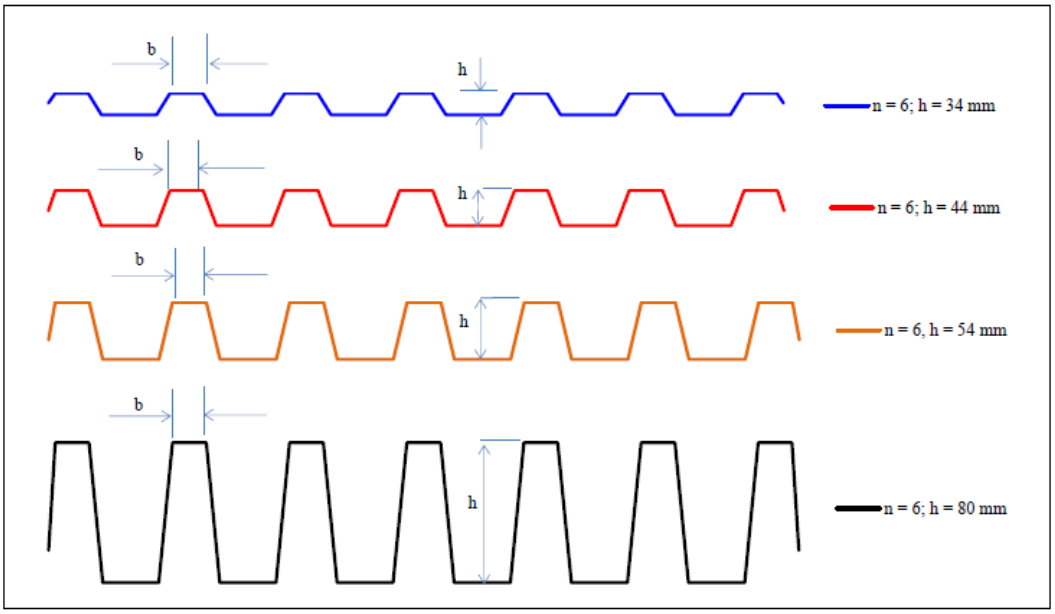


**Figure 4.10: Sheet profiles with six pans and rib-height varying from 34 to 80 mm**

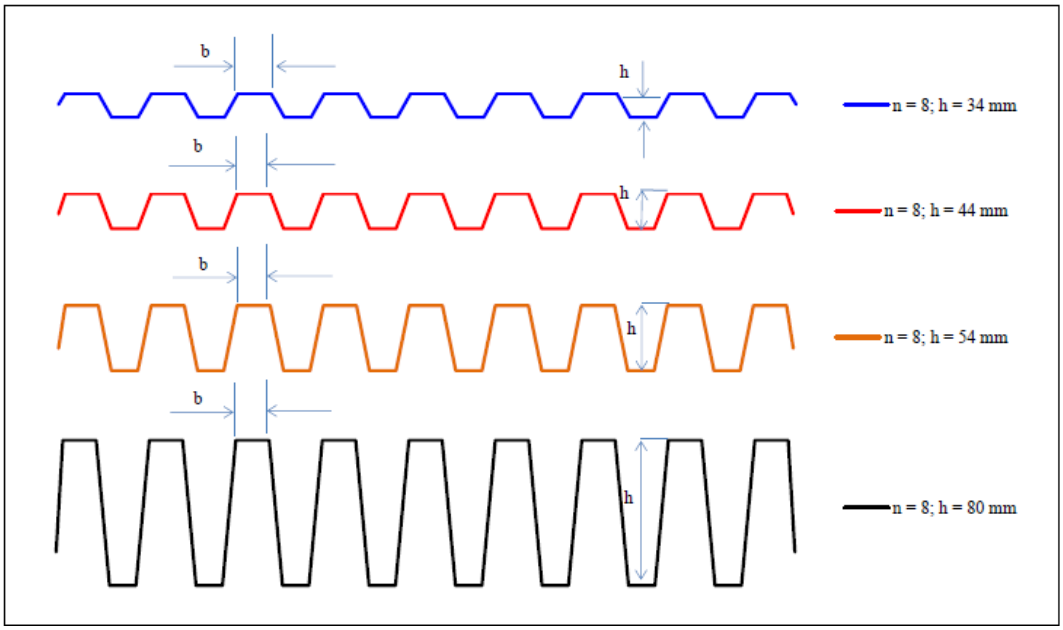


**Figure 4.11: Sheet profiles with eight pans and rib-height varying from 34 to 80 mm**

### 4.2.7 Simultaneous variation of rib-width and number of pans

Lastly, the rib-width (b) and number of pans (n) per 686 mm were varied simultaneously from 20 mm to 59.5 mm and three to eight, respectively. This variation was performed whilst keeping the rib-height (h) and sheet thickness (t) constant at 37 mm and 0.8 mm, respectively. For every number of pans (n) per 686 mm from three to eight, the rib-width (b) was varied from 20 mm to 59.5 mm as shown in Figures 4.12 to 4.16.

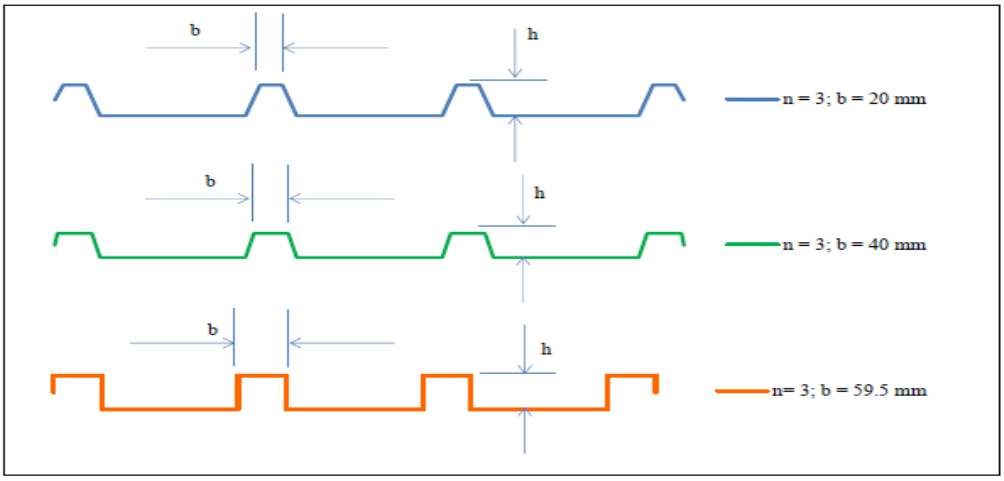


**Figure 4.12: Sheet profiles with three pans and rib-width varying from 20 to 59.5 mm**

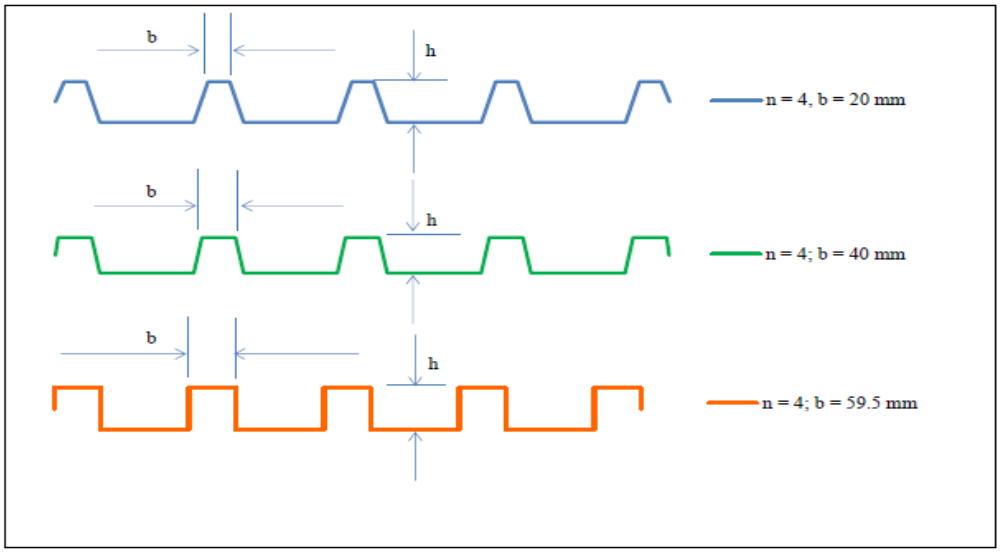


**Figure 4.13: Sheet profiles with four pans and rib-width varying from 20 to 59.5 mm**

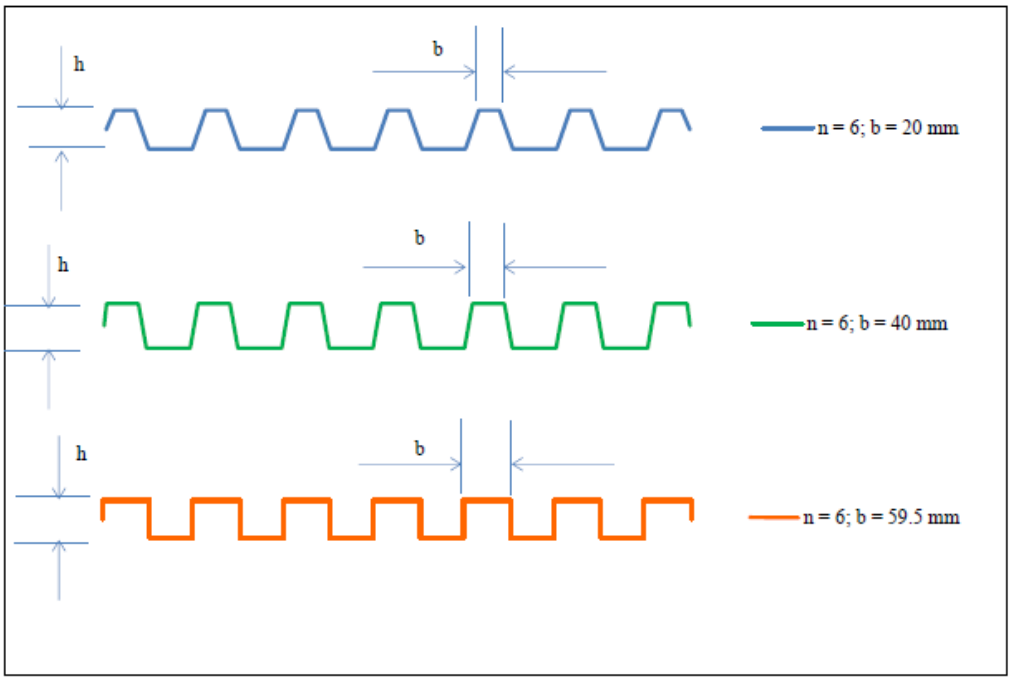


**Figure 4.14: Sheet profiles with six pans and rib-width varying from 20 to 59.5 mm**

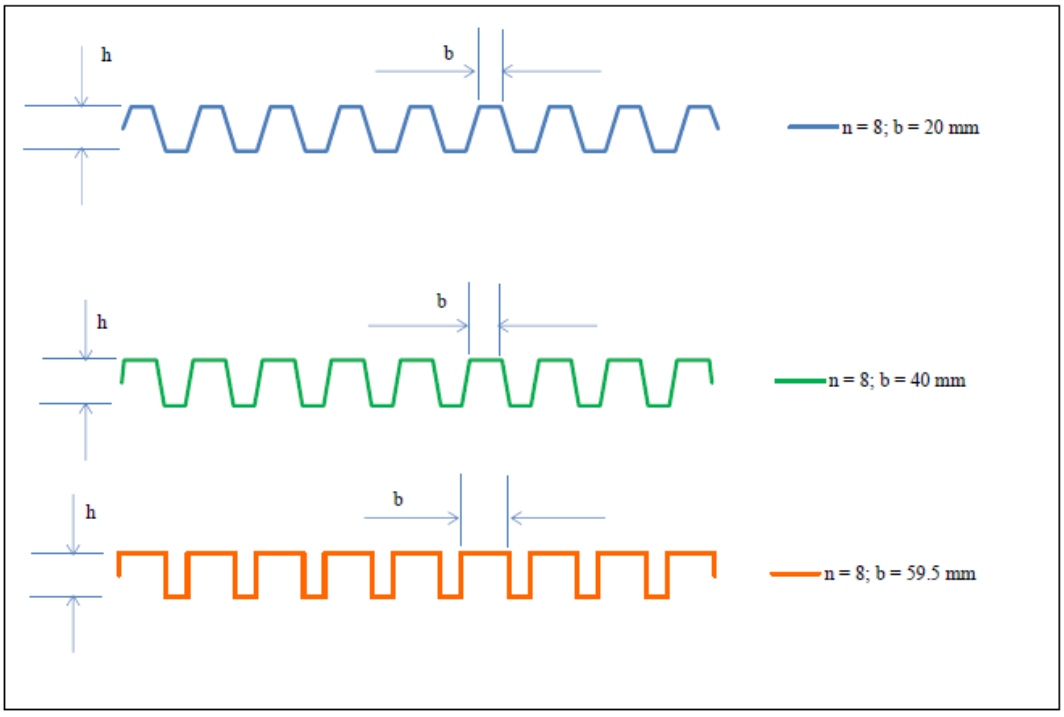


**Figure 4.15: Sheet profiles with eight pans and rib-width varying from 20 to 59.5 mm**

In this chapter the parameters selected for variation were shown. The results, discussion and analysis from the parametric variations are presented in Chapter 5.

# 5 DISCUSSION AND ANALYSIS OF PARAMETRIC VARIATION RESULTS

## 5.1 Introduction

In this chapter, the results of the parametric study are discussed and analysed. The effects of the rib-height (h), rib-width (b), sheet thickness (t) and number of pans (n) per 686 mm cover width on the deflection and performance of the IBR sheet are evaluated and assessed. The combined effects of the parameters including the rib-height (h) and the rib-width (b); the rib-height (h) and the number of pans (n), and the rib-width (b) and the number of pans (n) are also evaluated and assessed.

## 5.2 Result implications of the convergence study

In order to determine the correct element size for meshing, a convergence study was carried out. Figure 5.1 plots the deflection versus the number of elements in a typical model. The standard IBR 686 sheet with rib-height of 37 mm, rib-width of 33 mm, thickness of 0.8 mm and four pans was used to produce the plots shown in Figure 5.1. The characteristic element sizes considered were 150, 80, 40, 20, 10 and 5 mm. Both the sheet and the purlin were meshed using an S4R four-node quadrilateral linear element. At the bolt-head and nut areas, the linear S3 triangular linear elements were used. The number of elements plotted in Figure 5.1 refers to the total number of elements including both the S4R and S3.

Convergence started to occur when the element size was 20 mm and the total number of elements was 4,948. The 10 mm sized elements were used in this research, and resulted in a mesh with 46,775 elements. Elements that were smaller than 10 mm gave slightly more accurate results but the computational time increased significantly. An example is the 5 mm element which improved the deflection accuracy by 0.003 mm or 0.2 %, but the computational time increased by approximately three minutes or 19 %.

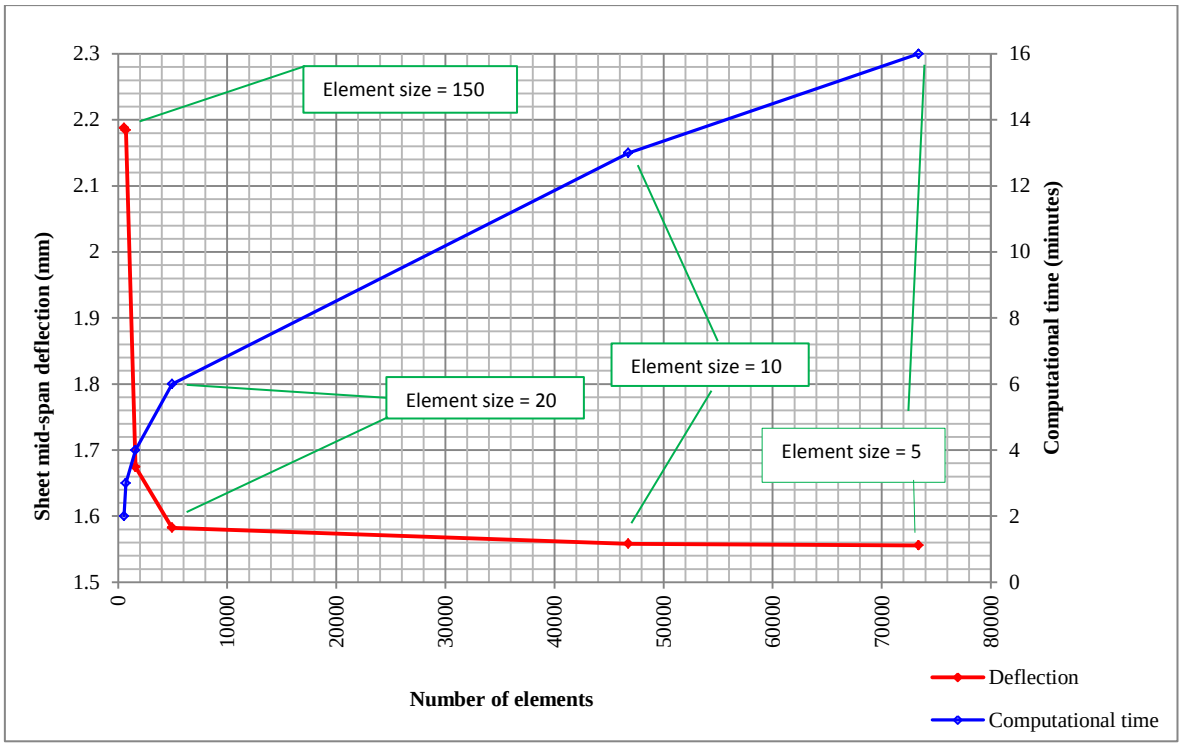


**Figure 5.1: Convergence study of the Finite Element mesh**

The convergence study was also performed on a standard IBR 686 sheet to determine the element size at which buckling will occur under wind uplift and concentrated load cases. The characteristic element sizes considered were 50, 20, 10 and 5 mm. Results of the convergence study are presented in Figure 5.2 for the wind uplift loading and Figure 5.3 for the concentrated load. The graphs in Figure 5.2 and Figure 5.3 plot the smallest eigenvalues obtained versus the number of elements in the mesh.

Convergence started to occur at the 20 mm sized element, and the 10 mm sized elements were used in the model. The total number of elements in the mesh was also affected by the variation of the rib-height in each case. The eigenvalues ($\lambda$) obtained from the convergence study are shown in Tables 5.1 and 5.2. The percentage error in Tables 5.1 and 5.2 indicates how close the deflection value is to correct deflection value, which was the deflection when the element was 5 mm in the mesh.

**Table 5.1: Eigenvalues calculated when rib-height and element sizes were varied with the sheet subject to wind uplift**

| h (mm) | 50 mm Element | | 20 mm Element | | 10 mm Element | | 5 mm Element |
|---|---|---|---|---|---|---|---|
| | λ | % Error | λ | % Error | λ | % Error | λ |
| 37 | 2.95 | 60 | 1.23 | 3 | 1.2 | 1 | 1.19 |
| 40 | 3.11 | 59 | 1.31 | 2 | 1.29 | 1 | 1.28 |
| 50 | 3.63 | 56 | 1.68 | 4 | 1.62 | 1 | 1.61 |
| 60 | 4.13 | 52 | 2.05 | 3 | 2 | 1 | 1.98 |
| 74 | 5.33 | 52 | 2.68 | 4 | 2.59 | 1 | 2.56 |
| 80 | 5.89 | 52 | 2.96 | 4 | 2.86 | 1 | 2.83 |

**Table 5.2: Eigenvalues calculated when rib-height and element sizes were varied with the sheet subject to a concentrated load**

| h (mm) | 50 mm Element | | 20 mm Element | | 10 mm Element | | 5 mm Element |
|---|---|---|---|---|---|---|---|
| | λ | % Error | λ | % Error | λ | % Error | λ |
| 37 | 5.76 | 74 | 2.91 | 48 | 1.75 | 14 | 1.51 |
| 40 | 6.68 | 76 | 3.08 | 47 | 1.87 | 13 | 1.62 |
| 50 | 10.42 | 82 | 2.91 | 35 | 2.12 | 10 | 1.9 |
| 60 | 11.46 | 82 | 2.93 | 31 | 2.18 | 8 | 2.01 |
| 74 | 6.91 | 71 | 2.5 | 21 | 2.08 | 5 | 1.98 |
| 80 | 6.81 | 71 | 2.46 | 21 | 2.05 | 5 | 1.95 |

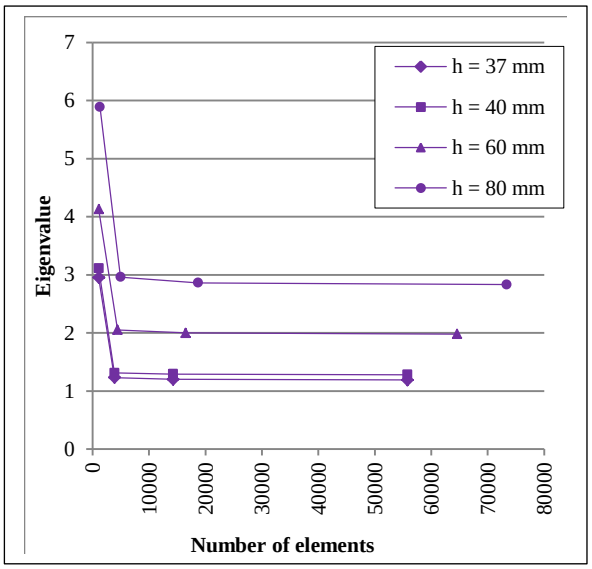


**Figure 5.2: Convergence study for buckling under wind uplift**

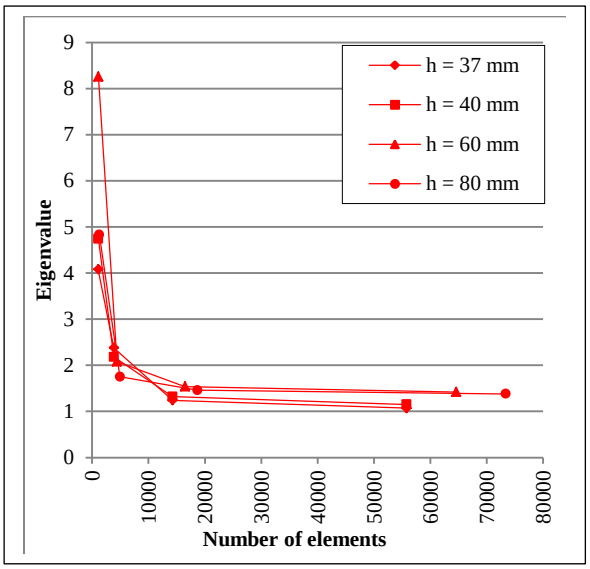


**Figure 5.3: Convergence study for buckling under concentrated load**

## 5.3 Effect of variation of rib-height

Figure 5.4 plots the sheet mid-span deflection versus the rib-height (h). The results are in agreement with the predictions of Euler-Bernoulli beam theory. The difference in the results from the two methods was 3 % on average and 7 % maximum. The results from Finite Elements model are expected to be more accurate since the model is 3-dimensional. The average discrepancy in the deflections is approximately 1 mm. The sheet mid-span deflection decreased as the rib-height increased. The dashed line gives the allowable sheet deflection, which is independent of the rib-height but depends on the sheet span, which was taken as 2200 mm for a single-span sheet of thickness 0.8 mm (SAISC, 2013).

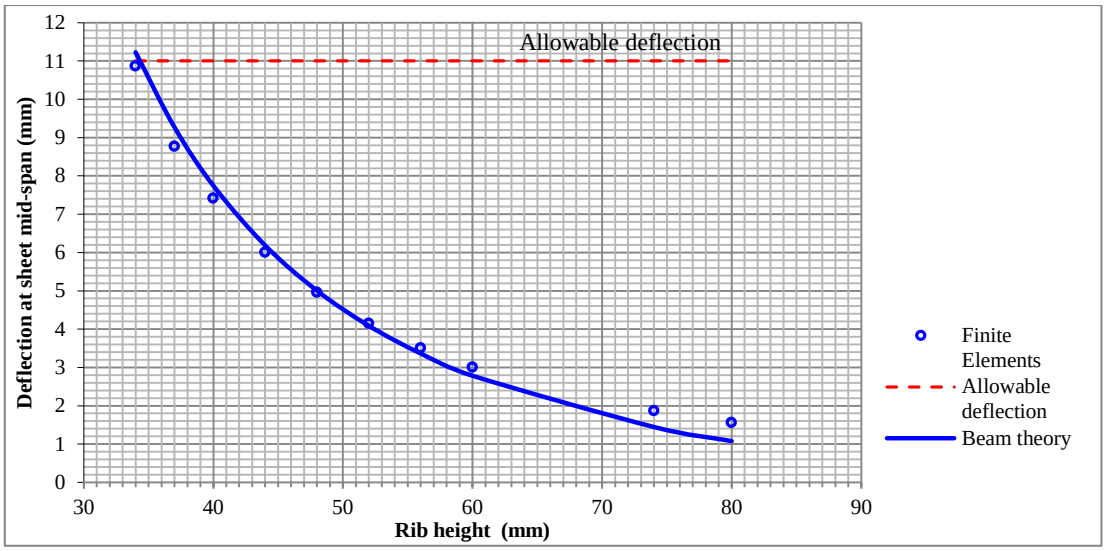


**Figure 5.4: Graph of sheet deflections versus rib-heights**

From Figure 5.4 both the Finite Elements results and Euler-Bernoulli beam theory decreased as the rib-height increased. This implies that as the rib-height increased the sheet became stiffer, and since the load remained constant there was a decrease in the deflection. Thus the profile with the highest rib-height had the greatest stiffness and experienced the lowest deflections under a constant load. However, such profiles will be more expensive since more material is used.

Table 5.3 presents a comparison between the performance of the profiles made from rib-heights (h) of 37 mm and 74 mm.

**Table 5.3: Effects on the deflection when the rib-height is doubled**

| Rib-height (h) (mm) | Sheet deflection (Δ) from Finite Elements (mm) | Percentage smaller than allowable deflection = 11 mm (%) | Unfolded cover width of the profile (mm) |
|---|---|---|---|
| 37 | 8.8 | 20 | 921 |
| 74 | 1.9 | 83 | 1 254 |

If the rib-height (h) was doubled from 37 mm to 74 mm, the deflection (Δ) decreased by 6.9 mm, which is approximately 80 %; the unfolded cover width of the respective profiles increases by 287 mm, which represents an approximate 30 % increase in material.

When the rib-height was 74 mm to 80 mm, the discrepancies between the Finite Elements and Euler-Bernoulli theory increased. It was assumed in Appendix B.2 that, according to Euler-Bernoulli beam theory, plane sections originally normal to the longitudinal axis of the beam before bending remain plane and normal to the longitudinal axis of the beam after bending; and thus the internal strain energy of the beam is due to bending only. According to Vlasov (1959) if the cross-section of a thin-walled beam is not rigid, internal stresses are directly proportional to the internal strains. Vlasov's (1959) criteria for thin-walled beams are:

$$\frac{\text{Thickness of the crosssection}}{\text{Depth of the crosssection}} \leq 0.1 \qquad \text{and} \qquad \frac{\text{Depth of the crosssection}}{\text{Length of the beam member}} \leq 0.1$$

In this case, the sheet is 0.8 mm thick, 80 mm deep and 2200 mm in length:

$$\frac{0.8}{80} = 0.01 < 0.1 \qquad \text{and} \qquad \frac{80}{2200} = 0.04 < 0.1$$

When the beam (or sheet in this case) satisfies the abovementioned criteria, it is regarded as a "thin-walled beam". For thin-walled beams, the Euler-Bernoulli assumption about plane sections remaining plane and normal to the neutral axis does not hold according to Vlasov (1959). Thin-walled beams experience distortion of the plane cross-section caused by longitudinal displacements. It was also observed from Finite Elements outputs, that the displacements in the longitudinal direction of the sheet were not zero and this was true at all values of the rib-heights. The Euler-Bernoulli beam theory does not account for the longitudinal displacements of the thin-walled beam section, hence the small discrepancy in the results.

### 5.3.1 Buckling strength of the web

A buckling analysis was performed on the IBR sheet that had four pans (n = 4), a rib-width (b) of 33 mm, thickness (t) of 0.8 mm and rib-height (h) of 37, 40, 50, 60, 74 and 80 mm.

Figure 5.5 plots the estimated critical buckling load as a function of the rib-height (h). When the sheet was subjected to wind uplift, the buckling load was directly proportional to the rib-height. However, when the sheet was subjected to the concentrated load, the buckling load increased when the rib-height was between 37 and 60 mm and started decreasing thereafter. This means that the critical buckling concentrated load reached its maximum possible value when the rib-height equalled 60 mm. The profile that has a rib-height of 37 mm (equivalent to IBR 686) will start to buckle at a wind uplift of 0.0019 N/mm$^2$ and a concentrated load of 1460 N.

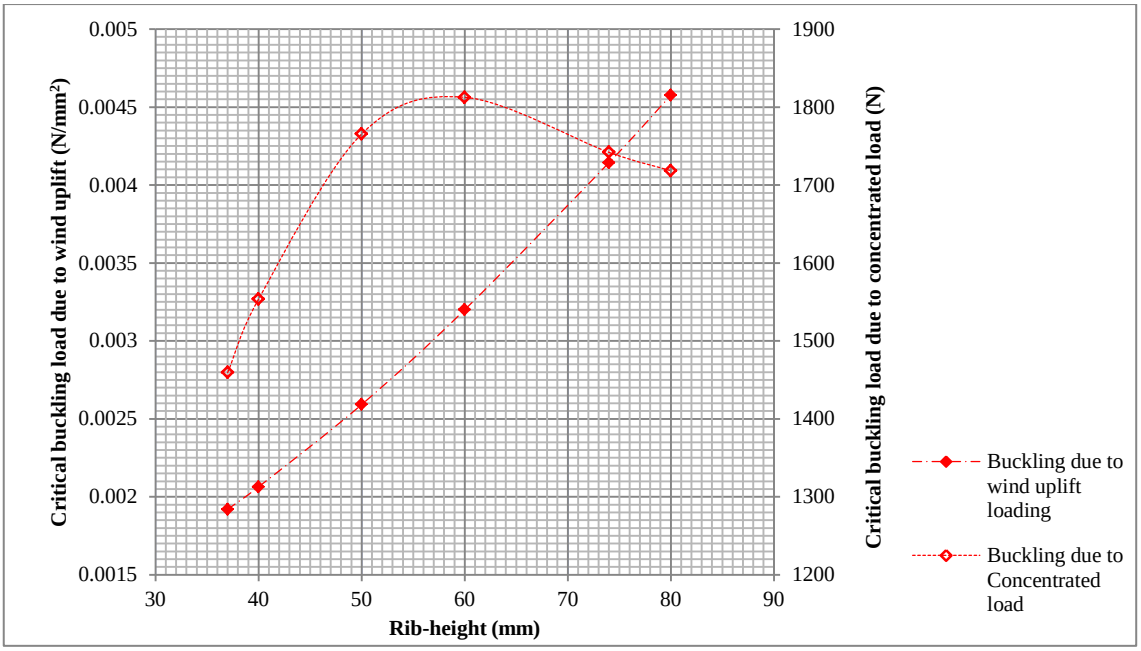


**Figure 5.5: Graph of critical buckling load of the sheet versus rib-heights**

Figure 5.6 (a) shows the standard IBR 686 sheet profile as one of the profiles that was assessed for buckling, and was meshed with the 10 mm element. When the sheet was subjected to wind uplift, the first buckling mode that corresponds with the smallest positive eigenvalue ($\lambda = 1.2$) is shown in Figure 5.6 (b); and the predicted buckling load ($W_{cr}$) was 0.0019 N/mm$^2$. When the sheet was subjected to the concentrated load, the 37$^{th}$ buckling mode that corresponds with the smallest positive eigenvalue ($\lambda = 1.75$) is shown in Figure 5.6 (c), and the predicted concentrated buckling load ($P_{cr}$) was 1460 N.

When the sheet was subjected to wind uplift, the bottom parts were in compression and therefore buckling occurred in the pans. When the profile was subjected to the concentrated load, buckling occurred on the rib but only around the area of load application.

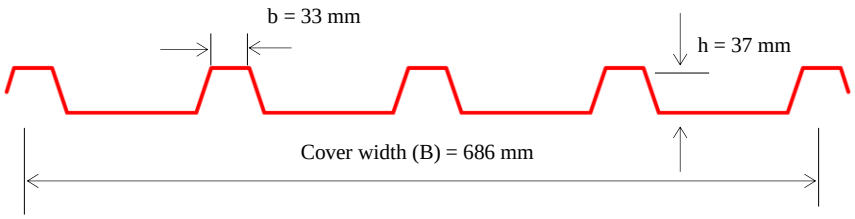


(a) A profile that was assessed for buckling

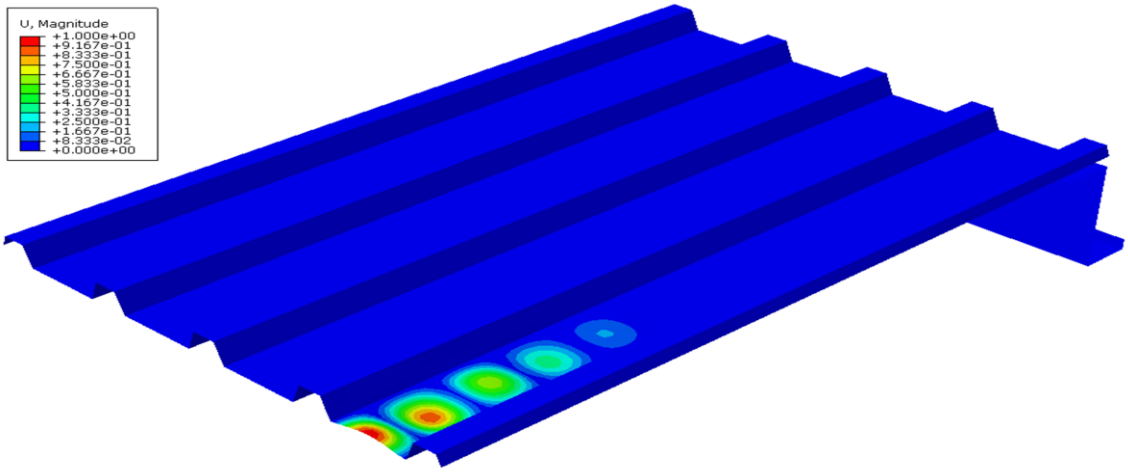


(b) First buckling mode of the profile shown in (a) subject to wind uplift

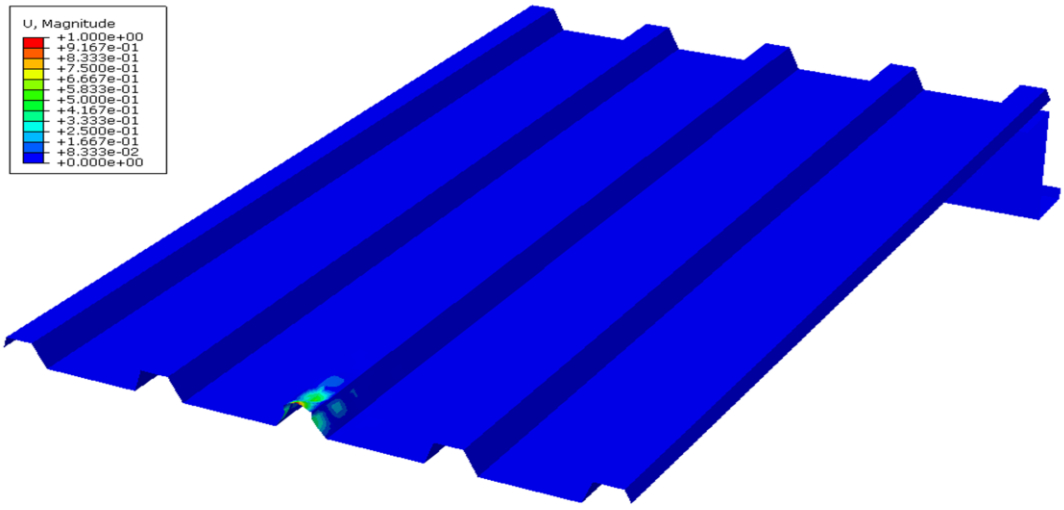


(c) The 37$^{th}$ buckling mode of the profile shown in (a) subject to a concentrated load

**Figure 5.6: Buckling modes of an IBR sheet subject to wind uplift and a concentrated load**

It should be noted that obtaining accuracy and performing checks on the numerical experiment such as in Abaqus/CAE is difficult and confidence is based on good modelling techniques and software outputs, such as choosing the correct element size and type for meshing and deciding on the suitable boundary condition. It was presented in Tables 5.1 and 5.2 that the accuracy of the results increased with a finer mesh. The estimated buckling loads from this investigation are theoretical and non-conservative because, in reality, the erected IBR sheet's buckling load is also influenced by its geometric and mechanical imperfections, which often exhibit non-linear behaviour.

According to Sun and Spencer (2005), the buckling failure modes of a stiffened panel can be categorised into three levels: local face/web plate buckling; unit corrugation buckling, and entire/global corrugation buckling. At higher values of the rib-height (h), the profile might experience local face/web buckling since the web becomes too slender.

## 5.4 Effect of variation of rib-width

Figure 5.7 plots the sheet mid-span deflection versus the rib-width (b). The profiles were formed from the IBR sheet with the rib-width (b) varying from 20 mm to 59.5 mm. The Finite Elements results follow a similar trend to the Euler-Bernoulli beam theory.

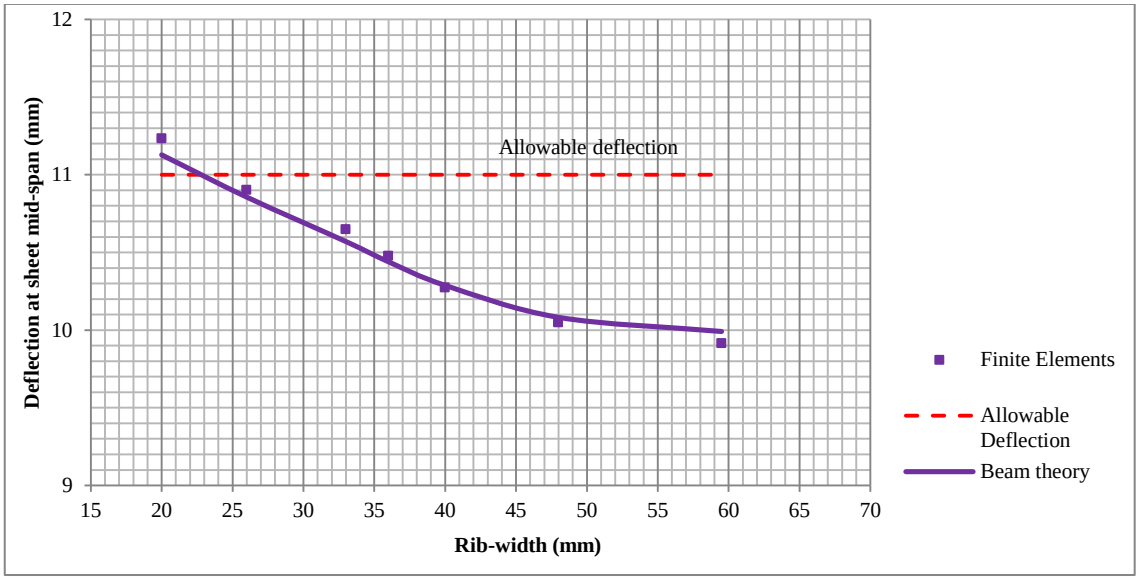


**Figure 5.7: Graph of sheet mid-span deflection versus rib-width**

The difference in the results from the Finite Elements and Euler-Bernoulli beam theory was 0.5 % on average and 0.9 maximum. It was observed that the rib-width (b) had a small effect on the sheet deflection. A sheet profile with a rib-width (b) of 26 mm experienced a deflection of 11.2 mm, whilst the same profile – but with a rib-width of 52 mm – experienced a deflection of 10.1 mm. This implies that doubling the size of the rib-width produces a decrease of 1.1 mm or 9 % in the sheet deflection. For an IBR sheet with four pans per 686 mm (n = 4), an increase of 26 mm in each rib-width (b) would lead to an overall increase in the unfolded cover width of the sheet of approximately 112 mm, which is approximately a 12 % increase in material. It is, therefore, recommended not to increase the rib-width, but rather to keep it at a minimum because it has less impact on the deflection but increases the material of the sheet substantially. The Finite Elements and the allowable deflection graphs intersect when the rib-width, b = 23 mm, which is the minimum rib-width one should choose for the profile subjected to 0.0016 N/mm$^2$ used in this study.

## 5.5 Effect of variation of sheet thickness

Figure 5.8 plots the sheet mid-span deflection versus the sheet thickness (t). The sheet thickness (t) was varied from 0.3 mm to 0.8 mm. It was observed that the Finite Elements results are in good agreement with the Euler-Bernoulli beam theory. The difference in the Finite Elements and beam theory results was 15 % on average and 28 % maximum. The graph illustrates that, at higher values of sheet thicknesses, the deflections are lower. The thickest profile experienced the lowest deflections under the same load. The thicker the sheet, the heavier it is, and the higher the cost of the input material required.

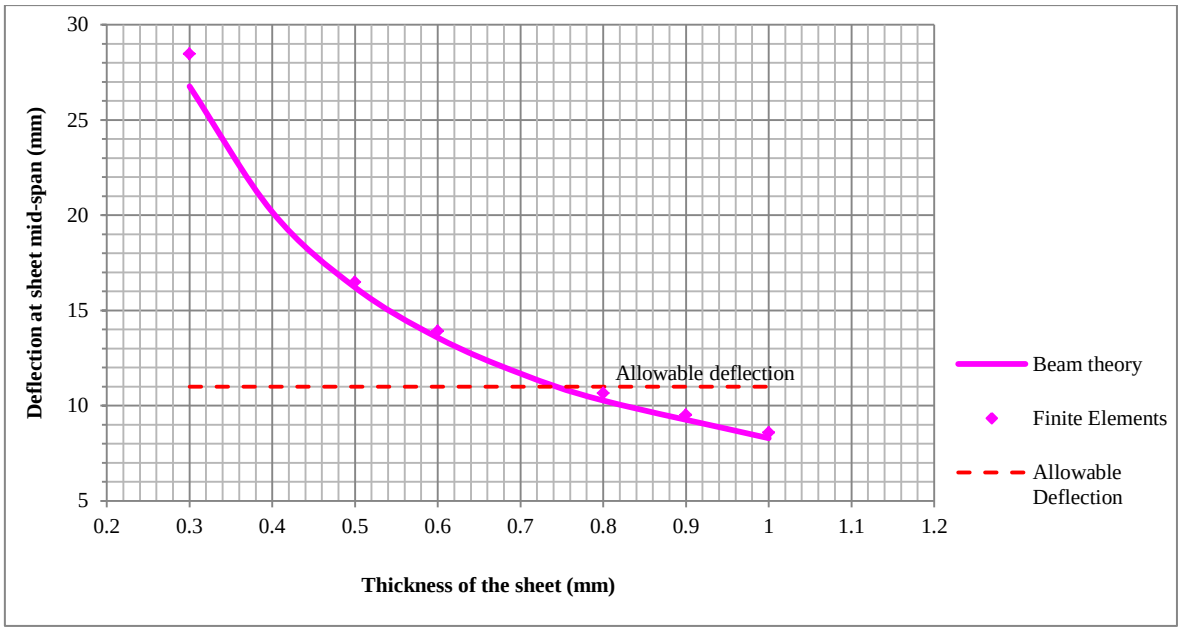


**Figure 5.8: Graph of sheet mid-span deflection versus sheet thickness**

## 5.6 Effect of variation of number of pans in a single sheet

Figure 5.9 plots the sheet mid-span deflection versus the number of pans (n) per 686 mm (or per single sheet). The profiles were formed using an IBR sheet with the number of pans (n) per 686 mm sheet width varying from three to eight.

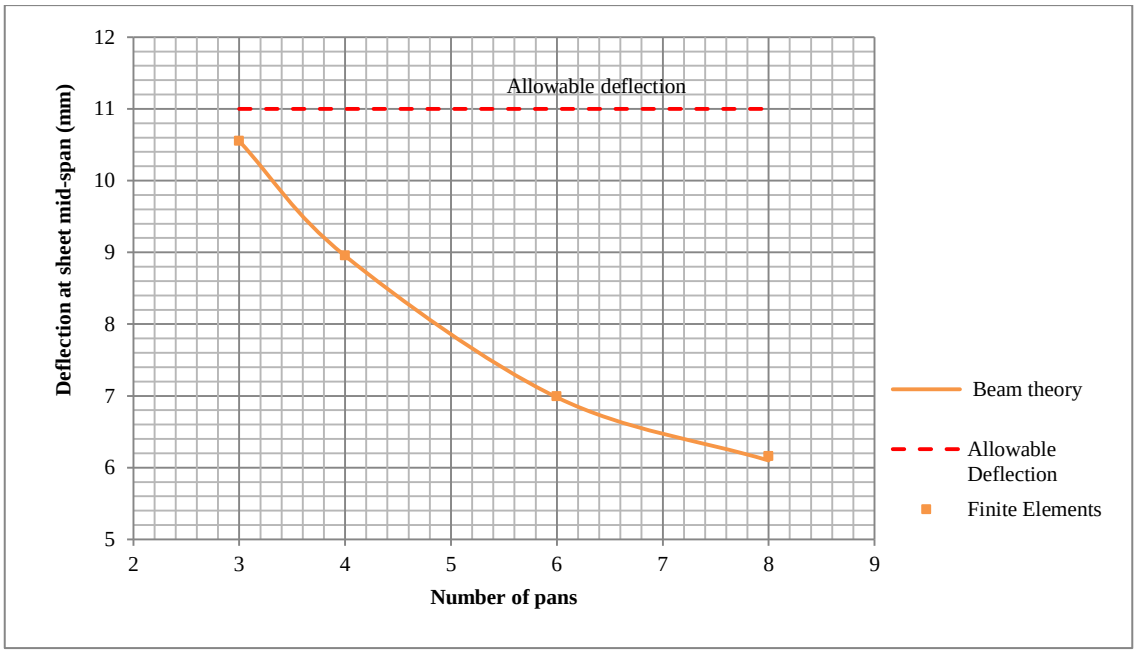


**Figure 5.9: Graph of sheet mid-span deflection versus number of pans in a single sheet**

The Finite Elements results are in good agreement with the Euler-Bernoulli beam theory as shown in Figure 5.9. The difference in the results from the Finite Elements and beam theory was 0.3 % and 0.9 % maximum. The profile with eight pans (n = 8) was the stiffest. In order to increase the number of pans (n) per 686 mm from four to eight, the unfolded cover width (B') of the sheet must be increased by 254.7 mm, which is an approximately 22 % increase in material. The sheet with four pans (n = 4) per 686 mm experienced a deflection of 9 mm, whilst the sheet with eight pans (n = 8) per 686 mm experienced a 6.2 mm deflection, which is approximately a 31 % difference. It is thus advantageous to have more ribs in a single sheet since this will reduce deflection although there will be a substantial increase in material and production cost.

## 5.7 Effects of simultaneous variation of rib-height and rib-width

Figure 5.10 plots the sheet mid-span deflection versus the rib-height (h) at different values of rib-width (b). The profiles were formed using an IBR sheet with rib-height (h) and rib-width (b) simultaneously varied from 34 to 80 mm and 20 to 59.5 mm. The Finite Elements results agreed with the predictions from the Euler-Bernoulli beam theory.

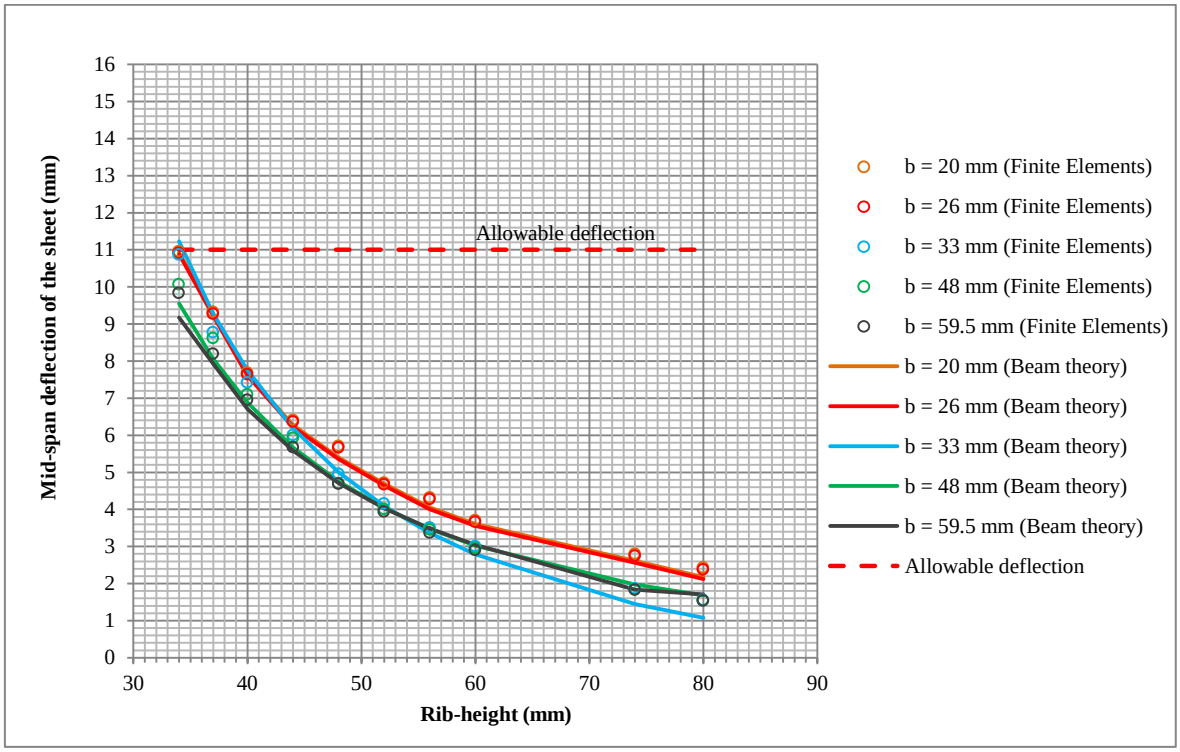


**Figure 5.10: Graph of sheet mid-span deflection versus rib-height at different rib-widths**

It was observed from Figure 5.10 that an increase of 40 mm in the rib-width (b) will increase the profile's stiffness by approximately 12 % and the material used by 19 %. This further shows that the rib-width (b) has only a small influence on the sheet stiffness.

Eight sheet profiles from Figure 5.10 – and presented in Table 5.4 – were compared in terms of deflection and the unfolded cover width (B'). The profiles had rib-widths of 20, 33, 48 and 59.5 mm, and a rib-height (h) of 37 and 74 mm. Listed on the far right-hand side of Table 5.4 are the differences in savings or excess of materials which were obtained by comparing the unfolded cover width (B') with the standard width of 925 mm for the input sheet coil. A positive number indicates the amount of material one would save when manufacturing the corresponding profile from a 925 mm coil; whilst a negative number indicates the amount of material that will be needed in addition to 925 mm to manufacture the corresponding coil. There are only two positive numbers, which are +6 and +2, and they indicate the savings in material if the rib-height (h) is kept constant at 37 mm and the rib-width (b) equals 20 mm and 33 mm.

**Table 5.4: Comparison of profiles with the rib-height and rib-width varied simultaneously**

| Rib-width (b) (mm) | Rib-height (h) (mm) | Unfolded cover width (B') of the profile (mm) | Mid-span sheet deflections (Δ) (mm) | | Savings (+) or Excess (-) in material relative to the 925 mm standard input sheet coils (%) |
|---|---|---|---|---|---|
| | | | Finite Elements (mm) | Euler-Bernoulli's theory (mm) | |
| **20** | 37 | 886 | 9.3 | 9.3 | **+ 6** |
| | 74 | 1 173 | 2.8 | 2.6 | **- 25** |
| **33** | 37 | 921 | 8.8 | 9.3 | **+ 2** |
| | 74 | 1 208 | 1.9 | 1.6 | **- 28** |
| **48** | 37 | 996 | 8.6 | 8.1 | **- 6** |
| | 74 | 128 | 1.8 | 2.0 | **- 36** |
| **59.5** | 37 | 1 078 | 8.2 | 7.9 | **- 17** |
| | 74 | 1 340 | 1.8 | 1.8 | **- 43** |

## 5.8 Effects of simultaneous variation of rib-height and number of pans

Figure 5.11 plots the sheet mid-span deflection versus the rib-height (h) at different number of pans (n) per 686 mm cover width. The profiles were formed from an IBR sheet with the rib-height (h) varied from 34 to 80 mm and the number of pans (n) from three to eight.

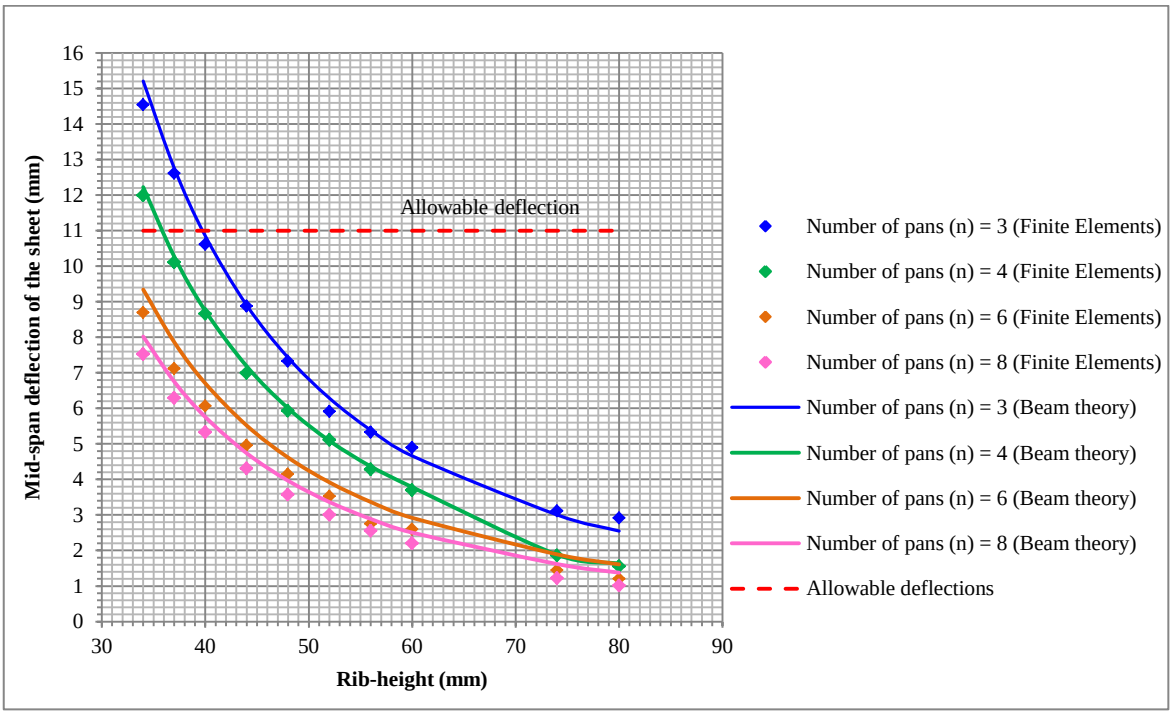


**Figure 5.11: Graph of sheet mid-span deflection versus rib-height at three, four, six and eight pans in a single sheet**

From Figure 5.11, eight sheet profiles were compared in terms of deflection and unfolded width (B'). The profiles had a rib-height (h) of 37 mm and 74 mm and the number of pans (n) varied from three to eight, as shown in Table 5.5. Out of the eight sheet profiles that were compared, only two resulted in savings even though they have relatively higher deflections. That is, the profiles with three pans and rib-height of 37 mm would save 3 % of material if manufactured from a 925 mm coil; and doubling the rib-height would require 30 % of material in addition to 925 mm.

**Table 5.5: Comparison of profiles with varying rib-height and number of pans**

| Number of pans (n) | Rib-height (h) (mm) | Unfolded cover width (B') of the profile (mm) | Mid-span sheet deflections (Δ) (mm) | | Savings (+) or Excess (-) in material relative to the 925 mm standard input sheet coils (%) |
|---|---|---|---|---|---|
| | | | Finite Elements (mm) | Euler-Bernoulli's theory (mm) | |
| **3** | 37 | 915 | 12.6 | 12.8 | **+ 3** |
| | 74 | 1 202 | 3.1 | 3.0 | **- 30** |
| **4** | 37 | 921 | 8.8 | 9.3 | **+ 2** |
| | 74 | 1 208 | 1.9 | 1.6 | **- 36** |
| **6** | 37 | 1 071 | 7.1 | 7.9 | **- 14** |
| | 74 | 1 574 | 1.5 | 1.2 | **- 67** |
| **8** | 37 | 1 175 | 6.3 | 6.8 | **- 25** |
| | 74 | 1 822 | 1.2 | 1.01 | **- 94** |

## 5.9 Effects of simultaneous variation of rib-width and number of pans

Figure 5.12 plots sheet mid-span deflection versus number of pans (n) per 686 mm cover width at different rib-widths (b). The profiles were formed from an IBR sheet with the rib-width (b) and number of pans (n) per 686 mm cover width varied simultaneously from 20 to 59.5 mm and three to eight, respectively.

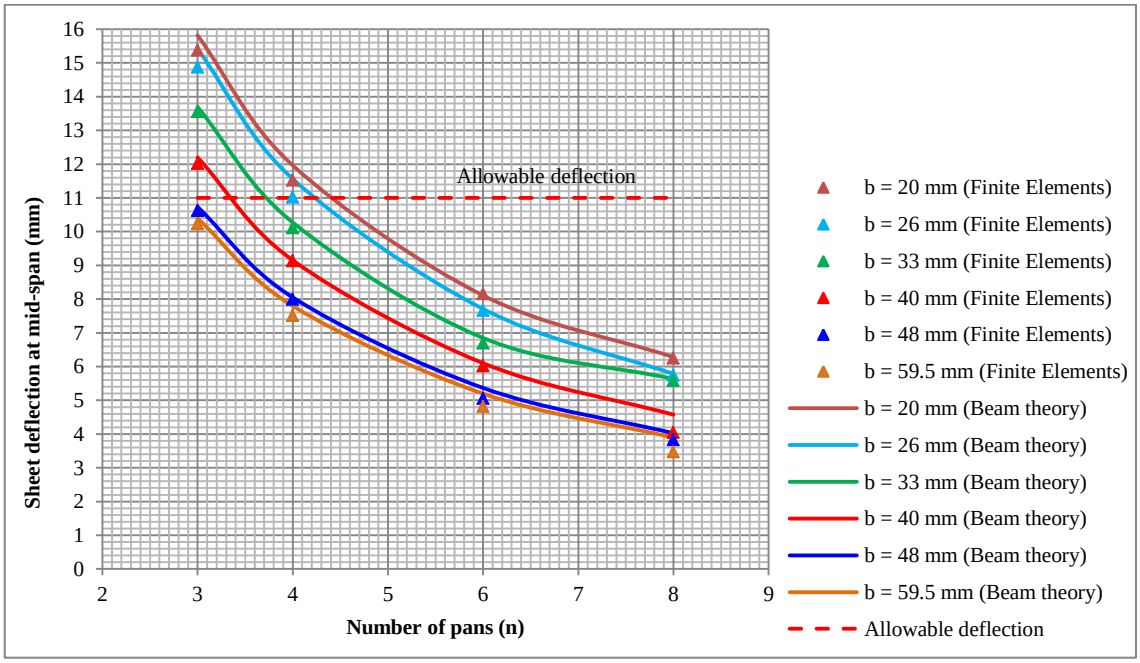


**Figure 5.12: Graph of sheet mid-span deflection versus number of pans at different rib-widths**

From Figure 5.12, sixteen sheet profiles presented in Table 5.6 were compared in terms of deflection and unfolded cover width (B'). The profiles had a rib-width (b) of 20, 33, 48 and 59.5 mm and the number of pans (n) varied from three to eight. It was observed from the right-hand side column of Table 5.6 that only four profiles showed savings in material. By reducing the rib-width (b) to 20 mm and keeping the rib-height (h) constant at 37 mm, one would save 11 % and 6 % in materials from the profiles with three and four pans, respectively. As was discussed in the previous sections, increasing the rib-width (b) will result in more material being used with a relatively small increase in stiffness.

Of major interest is the sheet profile made up of four pans (n = 4), with a rib-width (b) of 23 mm which was found to be the 'optimal' IBR sheet profile, performing at almost the same level as the standard IBR 686 sheet but offering approximately 5.1 % of material saved.

**Table 5.6: Comparison of profiles with varying rib-width and number of pans**

| Number of pans (n) | Rib-width (b) (mm) | Unfolded cover width (B') of the profile (mm) | Mid-span sheet deflections (Δ) (mm) | | Savings (+) or Excess (-) in material relative to the 925 mm standard input sheet coils (%) |
|---|---|---|---|---|---|
| | | | Finite Elements (mm) | Euler-Bernoulli's theory (mm) | |
| **3** | 20 | 836 | 15.4 | 15.8 | **+ 11** |
| | 33 | 915 | 12.6 | 12.8 | **+ 3** |
| | 48 | 975 | 10.6 | 10.7 | **- 4** |
| | 59.5 | 1 021 | 10.2 | 10.4 | **- 9** |
| **4** | 20 | 886 | 11.5 | 12.0 | **+ 6** |
| | 33 | 921 | 8.8 | 9.3 | **+ 2** |
| | 48 | 995 | 8.0 | 8.1 | **- 6** |
| | 59.5 | 1 053 | 7.5 | 8.0 | **- 12** |
| **6** | 20 | 1 022 | 8.2 | 8.1 | **- 9** |
| | 33 | 1 071 | 7.1 | 7.9 | **- 14** |
| | 48 | 1 176 | 5.1 | 5.4 | **- 25** |
| | 59.5 | 1 256 | 4.8 | 5.2 | **- 34** |
| **8** | 20 | 1 112 | 6.3 | 6.3 | **- 18** |
| | 33 | 1 175 | 6.2 | 6.2 | **- 20** |
| | 48 | 1 310 | 3.8 | 4.0 | **- 39** |
| | 59.5 | 1 414 | 3.5 | 3.9 | **- 50** |

In concluding the parametric study, the following dimensional parameters of IBR sheet profile were found to be optimum:

- ***Rib-height, h = 34 mm***
  A rib-height that equalled 34 mm produced the required strength. Choosing higher values might lead to buckling or yield failure.

- ***Rib-width, b = 23 mm***
  This was found to be the optimal parameter of the profile, because its variation had a minor influence on the stiffness yet affected material and cost substantially. Under the given loading conditions the profile with a rib-width of 23 mm had a deflection which was less than the allowable deflection by 2 %. The rib-width of 23 mm resulted in 5.1 % savings in material and cost.

- ***Number of pans***
  The number of pans affects the total cover width and the number of sheets required to cover the total roof area as well as the number of overlaps. The more pans there are in a sheet, the smaller the pan width and the cover width; resulting in higher labour costs due to many overlaps and increased material cost.

- ***Sheet thickness***
  The thickness of the 'optimal' IBR sheet depends on the purpose and use of the building on which it will be affixed.

## 5.10 Cost analysis

In this section the optimum parameters were used to simulate new and different profiles from the standard commercially available input sheet coils. The input sheet coil comes in different widths, which are: 925, 940, 1000, 1175, 1219, 1225, 1250 and 1320 mm (Arcelor Mittal, 2015). Figure 5.13 plots the width/thickness extras cost of the commercial input sheet coils versus the standard coil widths. The cost in Figure 5.13 was quoted by Arcelor Mittal based on the width of the galvanized coil, but the extras such as grading, thickness, zinc coating, surface finish and packaging were omitted (Arcelor Mittal, 2015).

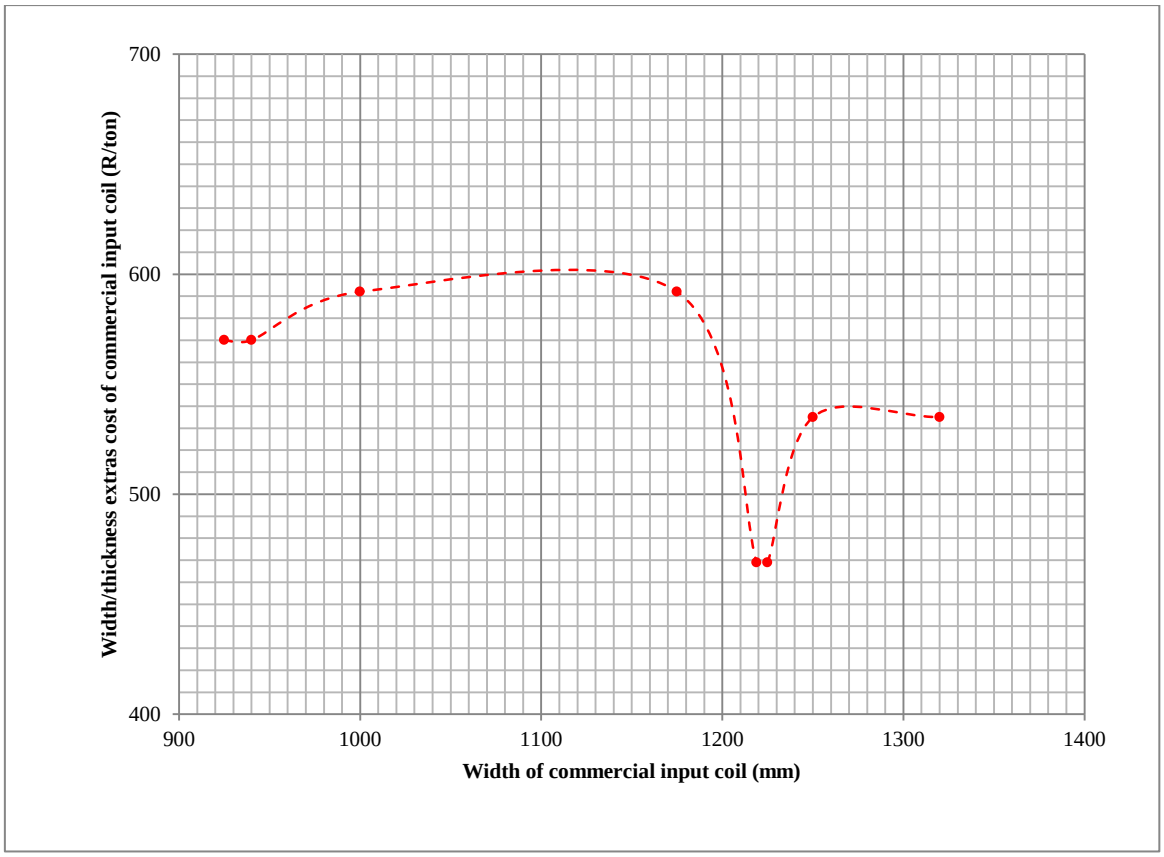


**Figure 5.13: Graph of width/thickness extras cost of the commercial input coil versus the width of the commercial input coil (Arcelor Mittal, 2015)[1]**

Table 5.7 presents the profiles which were formed from the Arcelor Mittal (2015) standard input sheet coils, using the optimum rib-height of 34 mm, rib-width of 23 mm and the number of pans was varied from three to eight.

Each profile in Table 5.7 is named with a capital letter P followed by two subscript digits. For example, profile $P_{43}$:

| | |
|---|---|
| P: | Stands for profile. |
| First digit: | Number of pans, n = 4 |
| Second digit: | The profile number in the rows of Table 5.7. |

[1]The costs shown in Figure 5.13 remained unchanged between 2015 and 01 January 2017 (Arcelor Mittal, 2017).

**Table 5.7: Profiles simulated from the optimum parameters**

| *Input coil width (mm)* | n = 3 | | | n = 4 | | | n = 5 | | | n = 6 | | | n = 7 | | | n = 8 | | |
|---|---|---|---|---|---|---|---|---|---|---|---|---|---|---|---|---|---|---|
| | Pro-file Name | Pan width (X') (mm) | Cover width (B) (mm) | Pro-file Name | Pan width (X') (mm) | Cover width (B) (mm) | Pro-file Name | Pan width (X') (mm) | Cover width (B) (mm) | Pro-file Name | Pan width (X') (mm) | Cover width (B) (mm) | Pro-file Name | Pan width (X') (mm) | Cover width (B) (mm) | Pro-file Name | Pan width (X') (mm) | Cover width (B) (mm) |
| *925* | $P_{31}$ | 190 | 779 | **$P_{41}$** | **116** | **743** | $P_{51}$ | 72 | 707 | $P_{61}$ | 42 | 671 | $P_{71}$ | 21 | 635 | $P_{81}$ | 5 | 599 |
| *940* | $P_{32}$ | 195 | 794 | **$P_{42}$** | **120** | **758** | $P_{52}$ | 75 | 722 | $P_{62}$ | 45 | 686 | $P_{72}$ | 23 | 650 | $P_{82}$ | 7 | 614 |
| *1 000* | $P_{33}$ | 215 | 854 | $P_{43}$ | 135 | 818 | **$P_{53}$** | **87** | **782** | $P_{63}$ | 55 | 746 | $P_{73}$ | 32 | 710 | $P_{83}$ | 15 | 675 |
| *1 175* | $P_{34}$ | 273 | 1 029 | $P_{44}$ | 179 | 993 | **$P_{54}$** | **122** | **957** | $P_{64}$ | 84 | 921 | $P_{74}$ | 57 | 885 | $P_{84}$ | 37 | 849 |
| *1 219* | $P_{35}$ | 288 | 1 073 | $P_{45}$ | 190 | 1 037 | $P_{55}$ | 131 | 1 001 | **$P_{65}$** | **91** | **965** | $P_{75}$ | 63 | 929 | $P_{85}$ | 42 | 893 |
| *1 225* | $P_{36}$ | 290 | 1 079 | $P_{46}$ | 191 | 1 043 | $P_{56}$ | 132 | 1 007 | **$P_{66}$** | **92** | **971** | $P_{76}$ | 64 | 935 | $P_{86}$ | 43 | 899 |
| *1 250* | $P_{37}$ | 298 | 1 104 | $P_{47}$ | 198 | 1 068 | $P_{57}$ | 137 | 1 032 | **$P_{67}$** | **97** | **996** | $P_{77}$ | 68 | 960 | $P_{87}$ | 46 | 924 |
| *1 320* | $P_{38}$ | 322 | 1 174 | $P_{48}$ | 215 | 1 138 | $P_{58}$ | 151 | 1 102 | **$P_{68}$** | **108** | **1 066** | $P_{78}$ | 78 | 1 030 | $P_{88}$ | 55 | 994 |

In Table 5.7 all profiles that are to the right of – and including the highlighted cells – meet the stiffness criterion. The profiles that are highlighted are economical. As mentioned before, the narrower sheet will lead to the requirement of many sheets and many overlaps. The pan width also decreases as the number of pans increases, and the disadvantage of a sheet with narrow pans is poor drainage that requires a steep roof and thus a greater sheeting length.

Figure 5.14 plots sheet deflection against the number of pans for all the profiles shown in Table 5.7. The sheet profiles which satisfy the stiffness criterion are those below the dashed line. The number of pans in each profile was restricted to a maximum of eight (n = 8) as indicated by the dotted line in Figure 5.14. Six profiles from each coil were simulated, giving a total of 48 profiles (listed in Table 5.7). From Figure 5.14, the profiles below and closest to the line of allowable deflection are the most economical and are highlighted in Table 5.7.

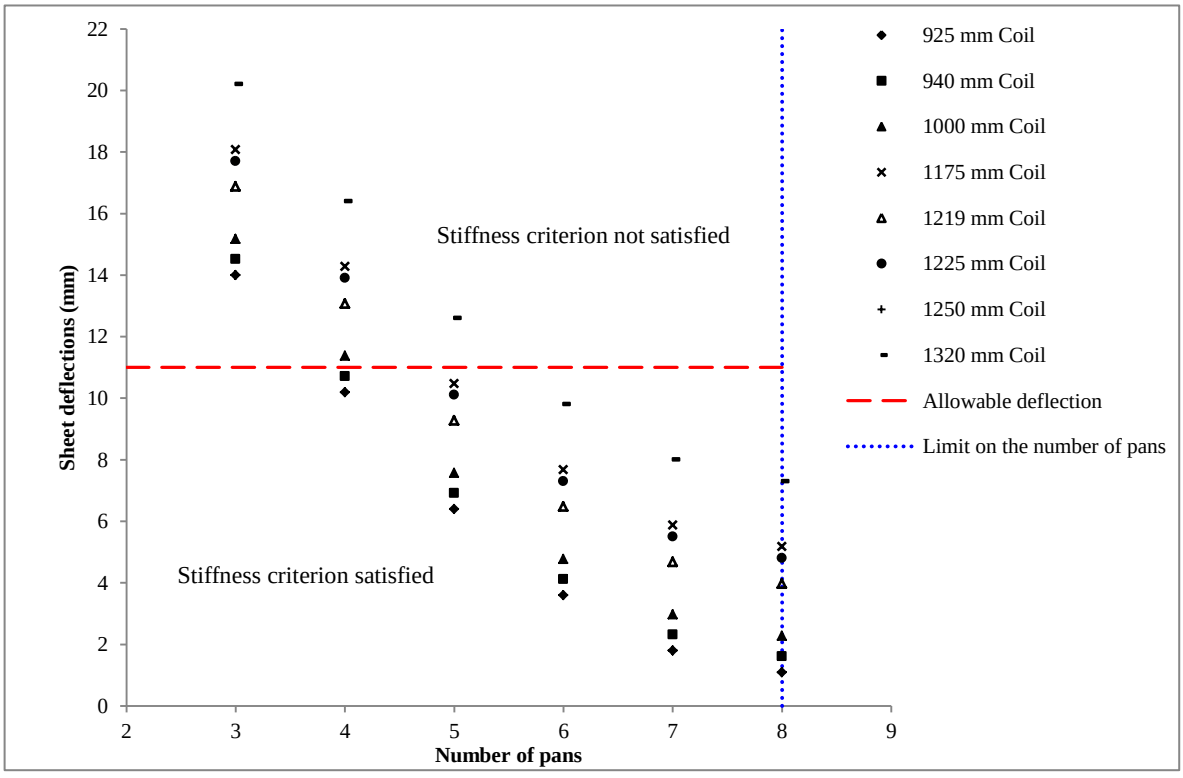


**Figure 5.14: Graph of sheet deflection versus number of pans, indicating the profiles which satisfy the strength criteria**

Figure 5.15 plots the cover width of the highlighted profiles in Table 5.7 against the cost of roof covering, using projections from Figure 5.13.

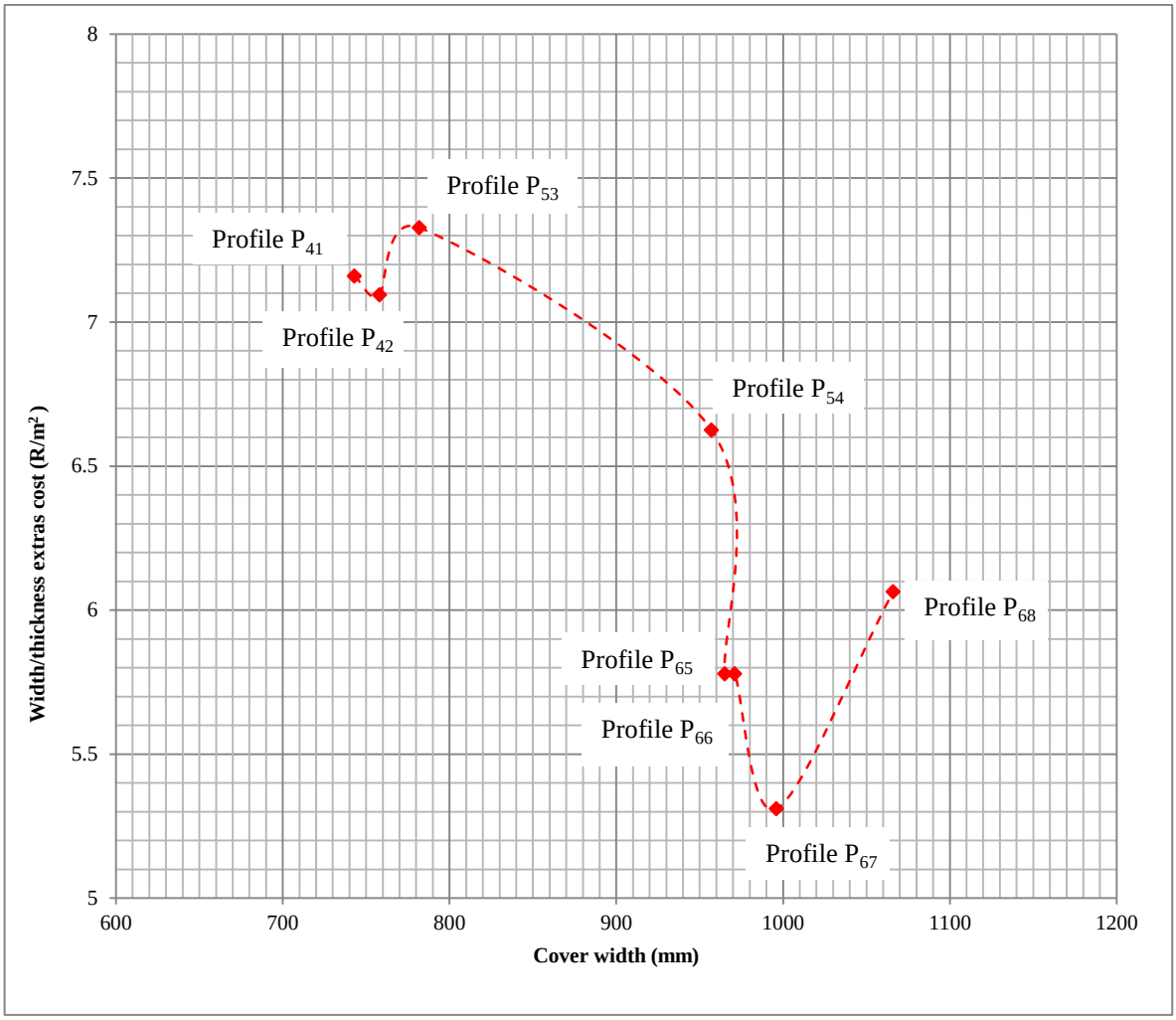


**Figure 5.15: Graph of cover width against cost**

In Figure 5.15 the most economical profile is $P_{67}$. It is made from a 1250 mm coil, and has six pans and a 97 mm pan width (Table 5.7) and offers a 996 mm cover width. The ribs are 34 mm high, 23 mm wide at the top and spaced at 166 mm centres. Figure 5.16 shows the fully dimensioned sketch of profile $P_{67}$.

With respect to cover width, profile $P_{67}$ is second best to $P_{68}$ by 7 %. A wider sheet leads to fewer sheets and fewer overlaps, and thus savings on labour cost. Profile $P_{67}$ also offers 80 % efficiency on production. Efficiency is the ratio of cover width to the width of the coil and it measures the amount of cover produced from the original coil width in order to

avoid waste and expenses. This means that 80 % of the original coil width is used up to produce cover and 20 % to produce ribs and thus stiffness.

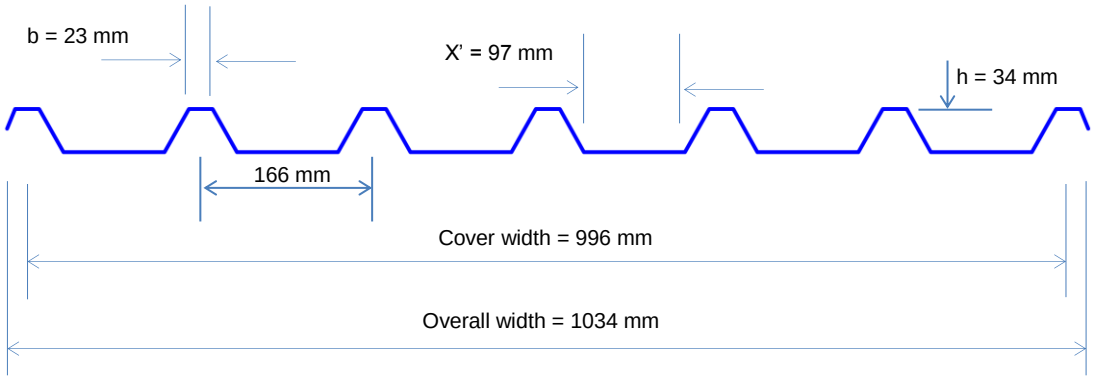


**Figure 5.16: Profile $P_{67}$ (not drawn to scale)**

Profile $P_{67}$ also offers good stiffness characteristics because it deflects 9.81 mm under the applied load.

Table 5.8 presents the recommended purlin spacing to support profile $P_{67}$ over a single, internal and end spans. The purlin spacing was obtained though iterative testing in Abaqus/CAE based on the computed uplift loading of 0.0016 N/mm$^2$ and a roof pitch of 5°. The purlin spacing was varied from 600 to 3000 mm in 300 mm increments and two sheet thicknesses were considered: 0.5 and 0.8 mm. For both sheet thicknesses, the single span controls the design and the thicker sheet can have a larger span.

**Table 5.8: Recommended purlin spacing to support profile $P_{67}$**

| **Maximum recommended purlin spacing (mm)** | | |
|---|---|---|
| **Type of span** | **Sheet thickness = 0.5 mm** | **Sheet thickness = 0.8 mm** |
| Single span | 1 510 | 2 130 |
| Internal span | 2 360 | 2 550 |
| End span | 2 095 | 2 290 |
| **Mass (kg/m$^2$)** | **3.93** | **6.28** |

# 6 CONCLUSIONS, LIMITATIONS AND RECOMMENDATIONS

## 6.1 Summary of the research

This dissertation presented a parametric study on IBR sheet profile supported by purlins and subject to wind uplift loading. This was done by using Finite Element Methods and Abaqus/CAE. The first objective of the study was to obtain the optimum dimension parameters that would be used to simulate new and different IBR profiles from standard sheet input coils whilst satisfying the stiffness criterion. The second objective was to perform a cost analysis in order to determine the most economical simulated profile.

The dimensional parameters were the rib-height (h), rib-width (b), number of pans (n) per 686 mm cover width and thickness (t) of the profile of the IBR sheet. Each parameter was varied within a specific range. The rib-height (h) was varied from 34 mm to 80 mm; the rib-width (b) from 20 mm to 59.5 mm; the number of pans (n) per 686 mm cover width from three to eight, and sheet thickness (t) was varied from 0.3 mm to 0.8 mm. Each of these parameters was varied whilst the others were kept constant, thus forming different IBR sheet profiles.

The results showed that increasing the rib-height (h) increases the depth of the cross-section of the profile, resulting in increased stiffness. Therefore, at large values of rib-height (h) (approximately 70 mm or more), the sheet deflection was relatively low, but the material required increased. No part of the sheet exceeded the yield stress even at smaller values of rib-height (approximately 34 mm). It was evident that the area around the bolts was the most stressed.

The rib-width (b) was found to be the deciding parameter of the profile because, although its variation had minor influence on the stiffness, it affected the material size required and thus the cost of the input coil. The ribs that are wider at the top might buckle under concentrated loads. Therefore, the rib-width (b) must be kept at a minimum, in order to avoid an unnecessary increase in the material needed with little or no increase in the stiffness of the profile. In contrast, increasing the sheet thickness (t) increased the stiffness, resulting in smaller deflections. Undoubtedly, thinner sheets will be more prone to local buckling and indentation compared with thicker sheets. The standard IBR 686 sheet has four pans, which offer sufficient stiffness and excellent drainage or water-carrying

capacity. Therefore, it makes sense to limit the number of pans (n) to the minimum number that will produce sufficient stiffness, because increasing the number of pans will result in an increase in cost.

The optimum parameters were found to be a rib-height (h) of 37 mm and a rib-width (b) of 23 mm. The optimum parameters were used to simulate new and different sheets from the standard commercially available sheet coil widths of 925, 940, 1000, 1175, 1219, 1225, 1250 and 1320 mm. The simulated profiles were assessed against the stiffness criterion and cost. The profile made from a 1250 mm wide sheet coil, with six 97 mm wide pans, ribs spaced at 166 mm centres and a 996 mm cover width was found to be the most economical. This profile has 80 % efficiency and is 10 % less expensive than the next best profile.

## 6.2 Limitations of the research

Limitations of this research originated in the study design:

- For each dimensional parameter that was varied there were few profiles formed and thus many profiles to model. Physical tests as recommended in SANS 10237 were not performed to verify the results.
- Many parameters affect the behaviour and failure modes of roof sheeting. Examples include: external parameters (such as types and magnitudes of loading; fixing and assembly of components); design parameters (such as connections, spacing and behaviour of purlins), material, and dimensional parameters of the profile (such as size and shape). Although all the above parameters affect or influence one another, it was not possible to incorporate all of them into the numerical experiments conducted.

Further, this research did not address the following:

- Mechanical contact between the sheet and the purlins, including slip or friction.
- The influence of other open, thin-walled often-used purlin sections, except the Z-section, on the behaviour and deflection of the IBR sheet.
- The deflections and behaviour of the purlin.

- The effects of gravity and other types of loadings on roof sheeting.

## 6.3 Recommendations for future research

It is recommended that the economical profiles presented in Table 5.7 be tested physically under different types of loading as recommended in SANS 10237. The findings will be useful in determining the purlin spacing and methods of sheet fixing.

A more accurate estimate of the critical buckling load of an IBR sheet influenced by its profile parameters could be obtained using non-linear buckling analysis methods such as Von Karman's theory (Landau and Lifshitz, 1970) or Winter's theory (Chajes and Winter, 1965), which incorporate geometric and mechanical non-linearities.

# REFERENCES


ArcelorMittal. (2015). *Extras List 140 Galvanised Sheet in Coil, 1-11*. Available: https://www.google.co.za/?gws_rd=ssl#q=ArcelorMittal.++++(2015).++++Extras+list+140+Galvanised+sheet+in+coil%2C+1+11
[Accessed: 29 November 2015.]

ArcelorMittal. (2017). *Extras List 140 Galvanised Sheet in Coil, 1-11*. Available: https://www.google.co.za/?gws_rd=ssl#q=ArcelorMittal.++++(2017).++++Extras+list+140+Galvanised+sheet+in+coil%2C+1+11
[Accessed: 13 January 2017.]

Balázs, I., Melcher, J. & Horáček, M. (2015). Stabilization of Beams by Trapezoidal Sheeting: Parametric Study. *Recent Advances in Engineering*.

Balázs, I., Melcher, J. & Horáček, M. (2012). Stabilization of Beams by Trapezoidal Sheeting: Parametric Study. In: *Proceedings of the 3rd European Conference of Civil Engineering (ECCIE '12). Advances in Mathematical and Computational Methods.* Paris, France.

Balex Metal. (2011). *Trapezoidal Sheets – Technical Catalogue*. Poland: Bolszewo. pp1-125.

Beer, F.P., Johnston Jr., E.R., De Wolf, J.T. & Mazurek, D.F. (2012). *Mechanics of Materials*. Sixth Edition. New York: McGraw-Hill Companies.

Bergfelt, A., Edlund, B. & Larsson H. (1975). Experiments on trapezoidal steel sheets in bending. *Third International Speciality Conference on Cold-Formed Steel Structures*. Paper 4. Missouri University of Science and Technology.

Bhatt, P. (1999) *Structures*. Fourth Edition. Harlow: Longman.

Case, J. & Chilver, A.H. (1964). *Strength of Materials – An Introduction to the Analysis of Stress and Strain*. London: Edward Arnold Publishers.

Case, J. Chilver, Lord A.H. & Ross, C.T.F. (1999). *Strength of Materials and Structures*. Fourth Edition. Butterworth Heinemann Publications.

Chajes, A. & Winter G. (1965). Torsional flexural buckling of thin-walled members, ASCE *J. Structural Division* 91(04):103-124.

Chaudhary, A.S. & Khan S.N. (2015). A parametric study on the effect of trapezoidal web profile on the angle of twist of steel I-beam for eccentric loading, *International Journal of Advanced Technology in Engineering and Science*, 3(01):273-279.

Cousins Steel International. (2015). *Product Brochure*.
Available: http://cousinssteel.co.za/686-ibr-profile
[Accessed: 17 January 2016.]

Dassault Systemes SIMULIA, Abaqus/CAE. (2014). Version 6.14-1. Available: https://www.google.co.za/?gws_rd=ssl#q=Dassault+Systemes+SIMULIA,+Abaqus/CAE+(2014)+Version+6.14-1&nfpr=1
[Accessed: 17 October 2015.]

Eurocode 3 – *Design of steel structures – Part 1-3: General rules – Supplementary rules for cold-formed members and sheeting*. (2005). Brussels: European Committee for Standardization.

Global Roofing Solutions. (2016). *Our Products*.
Available: http://www.globalroofs.co.za/portfolio/ibr-686-890/
[Accessed: 04 March 2016.]

Janushevskis, A., Melnikovs, A. & Auzins, J. (2015) Investigation of mechanical behaviour and shape optimization of roofing sheets using metamodels. *Journal of International Scientific Publications*, 9:216-226.

Jewett Jr, J.W. & Serway, R.A (2004). *Physics for Scientists and Engineers with Modern Physics*. Sixth Edition. Belmont CA: Thomson Learning Academic Centre.

Landau, L.D. , Pitaevskii, L.P., Kosevich, A.M. & Lifshitz E.M. (1970). *Theory of elasticity*. Second Edition. Moscow: Pergamon Press.

Lee, C.L., Mioduchowski, A. & Faulkner, M.G. (1995). Optimization of corrugated cladding, *Journal of Structural Engineering*, 121(8):1190-1196.

Liu, A.F., (2005). *Mechanics and mechanisms of fracture*. First Edition. Materials Park, Ohio: ASM International

Mahaarachchi, D. & Mahendran, M. (2009). Wind uplift strength of trapezoidal steel cladding with closely spaced ribs. *Journal of Wind Engineering and Industrial Aerodynamics*, 97(3):140-150.

Metsec. (2016). *Cold Rolled Steel Purlins: Purlin and Side Rail Systems*.
Available: http://www.metsec.com/purlins/
[Accessed: 01 March 2016.]

Mezzomo, G.P., Iturrioz, I., Grigoletti, G. & Gomes, H.M. (2010). Investigation of the mechanical behavior of trapezoidal roofing sheets using genetic algorithms. *Expert Systems with Applications*, 37(2):939-948.

Morgan, J. & Beck, V.R. (1976). Failure of sheet metal roofing under repeated wind loading. [Online]. *Proceedings of the Annual Engineering Conference (1976): Engineering 1976-2001. Townsville, Queensland*. Available: http://search.informit.com.au/documentSummary;dn=570969545478188;res=IELENG
[Accessed: 12 March 2015.]

Peng, L.X., Liew, K.M. & Kitipornchai, S. (2006). Analysis of stiffened corrugated plates based on the FSDT via the mesh-free method. *International Journal of Mechanical Sciences*, 49(3):364-378.

Robra, J. & Luza, G. (2008). Design of Z-purlins: Part 1 – Basics and cross-section values according to EN 1993-1-3; EUROSTEEL 2008. In: *Proceedings of the 5th European Conference on Steel and Composite Structures*. Graz, Austria: EUROSTEEL. Vol. A, pp129-134.

SAFINTRA (2012). *TUFDEK IBR Brochure*. Available: www.safintra.com [Accessed: 16 March 2015.]

SANS 10094. (2005) *The use of high-strength friction-grip bolts*. Edition 4. Pretoria: Standards South Africa.

SANS 10160-3. (2011) *Basis of Structural Design and Actions for Buildings and Industrial Structures*. Edition 1.1. Pretoria: Standards South Africa.

SANS 10162:-Part 1. (2011) *The Structural Use of Steel Part 1: Limit-States Design of Hot-Rolled Steelwork*. Edition 2.1. Pretoria: Standards South Africa.

SANS 10162:-Part 2. (2011). *The Structural Use of Steel Part 2: Cold-Formed Steel Structures*. Edition 2. Pretoria: Standards South Africa.

SANS 10237. (1991). *Roof and side cladding*. Edition 1. Pretoria: Standards South Africa.

SANS 1700:5-1. (2010). *Fasteners Part 5: General Requirements and Mechanical Properties Section 1: Mechanical Properties of Fasteners made of Carbon Steel and Alloy Steel – Bolts, Screws and Studs*. Edition 2. Pretoria: Standards South Africa.

Sharafi, P., Teh, L.H. & Muhammad N.S.H. (2013). Sizing optimization of trapezoidal corrugated roof sheeting supporting solar panels under wind loading. In: *Conference Proceedings of the Society for Experimental Mechanics Series*, 4:535-542.

Sharafi, P., Teh, L.H. & Muhammad N.S.H. (2014). Shape optimization of thin-walled steel sections using graph theory and ACO algorithms. *Journal of Construction Steel Research*, 101:331-341.

Sivachenko, E.W. & Broacha F.H. (1982). *Corrugated Plate having Variable Material Thickness and Method for Making Same*. U.S Patent No. 4, 317-350. Alexandria VA: United States Patent and Trademark Office.

SAISC (Southern African Institute of Steel Construction) (2013) *The Southern African Steel Construction Handbook*. Eighth edition. Johannesburg: Southern African Institute of Steel Construction.

Sun, H. & Spencer, J. (2005). Buckling strength of assessment of corrugated panels in offshore structure. *Marine Structures*, 18(7-8):548-565.

Timoshenko, T. (1953). *History of Strength of Materials*. New York: McGraw-Hill Books.

Vieira Jr, L.C.M., Malite, M. & Schafer, B.W. (2008). A numerical analysis of cold-formed steel purlin-sheeting systems. In: *Proceedings of the Fifth International Conference on Thin-Walled Structures*, Australia.

Vlasov, V.Z. (1959) *Thin-walled elastic beams*. Second edition (translated from Russian). Published for the National Science Foundation, Washington DC and the Department of Commerce, USA by the Israel Program for Scientific Translations, Jerusalem 1961.

Yu, W.W. & LaBoube, R.A. (2010). *Cold-Formed Steel Design*. Fourth Edition. Hoboken NJ: Wiley.

# APPENDIX A:
# DERIVATION OF THE APPLIED LOADS

There are a few common types of loading that metal roof sheeting experience, such as the self-weight of the roof, human and equipment loading during construction and maintenance, snow and rain, services or imposed loads and wind uplift. A number of researchers (Mahaarachchi & Mahendran, 2009; Vieira Jr, Malite & Schafer, 2008) have focused on the performance and design of roof-sheeting components subject to uplift loading only, since it has been considered the critical case.

In this research, the IBR sheet was subject to uplift loading in all model cases considered, except during the buckling assessment where a concentrated load was also applied.

## A.1 Estimation of the magnitude of the applied load (W)

### A.1.1 Specifications

- The roof is for a 48 m long warehouse with portal frames at 6 m centres.
- The building is situated in Johannesburg, on flat ground, and assumed to be surrounded by open terrain with negligible vegetation and no obstruction. The site altitude is 1800 m above mean sea level.
- Openings on all surfaces (including small windows and doors) are assumed to take approximately 5 % of the surface area. Two 8 x 3 m roller shutter doors will be installed on the long wall facing the wind direction.

Figure A.1 shows a typical section through an internal portal frame of the structure.

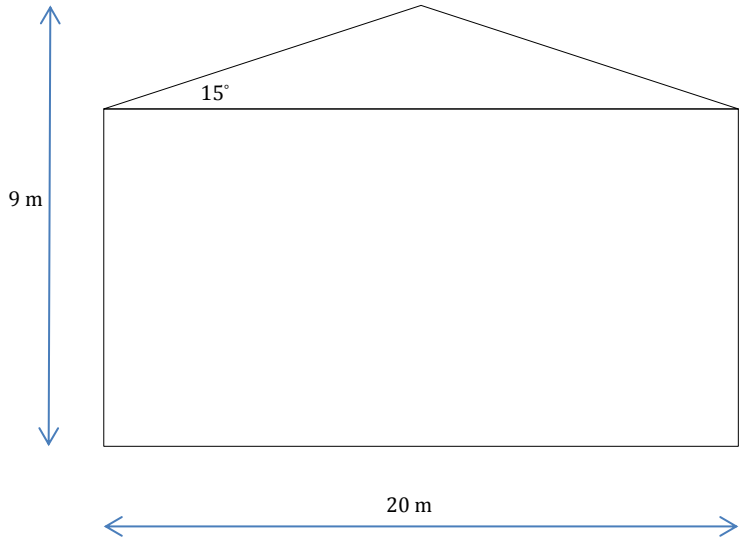


**Figure A.1: Cross-section through an internal portal frame of the structure**

SANS 10160-3 stipulates that the peak wind speed ($V_{b,\,peak}$) is given as:

$$V_{b,peak} = Fundamental\ wind\ speed\ (V_b) \times Probability\ factor \times Gust\ factor \times\ Roughness\ factor \times Topography\ factor \qquad A.1$$

### A.1.2 Fundamental wind speed

For most of South Africa, is assumed that:

$V_{b,0} = 28\ {}^{m}/_{s}$

### A.1.3 Probability factor

The probability factor is based on the design working life of the structure. In this case the structure was assumed to have normal consequences of failure, with a mean return period of 50 years.

$C_{prob} = 1.00$

### A.1.4 Peak gust wind speed

SANS 10160-3 allows the wind speed to be based on gust, which is 40 % greater than the basic wind speed.

$V_{b,peak} = 1.4V_b$

### A.1.5 Terrain roughness

For open terrain with negligible vegetation and no obstruction, Terrain Category A was assumed.

### A.1.6 Roughness factor

For Terrain Category A: Gradient height, $z_g$ = 250 m

Height of reference plane, $z_o$ = 0 m

Minimum height, $z_c$ = 1 m

Exponent, α = 0.07

Height above the ground, z = 9 m

$$Roughness\ factor, C_r(z) = 1.36\left(\frac{z-z_o}{z_g-z_c}\right)^{\alpha} = 1.08 \qquad A.2$$

### A.1.7 Topography factor

H is the height of the building

$L_u$ is the horizontal length of the upward wind slope and was assumed to be approximately 200 m

$$\emptyset = \frac{H}{L_u} = \frac{9}{200} = 0.045 < 0.05$$

Therefore, the wind funnelling effects can be ignored, and

$$Topography\ factor = C_o(z) = 1$$

Therefore, the peak wind speed,

$$V_{b,peak} = V_{b,o} \times C_{prob} \times C_r(z) \times C_o(z) \times 1.4 = 28 \times 1 \times 1.08 \times 1 \times 1.4 = 42.34\ {}^{m}/_{S}$$

The wind peak pressure is given as

$$q_p(z) = \frac{1}{2}\rho V_p(z)^2 \qquad A.3$$

By extrapolation from Table 4 of the code SANS 10160-3, air density, ρ = 0.96 at an altitude of 1800 m. Therefore,

$$q_p(z) = \frac{1}{2}\rho V_p(z)^2 = \frac{1}{2}(0.96)(42.34)^2 = 0.00086\ {}^{N}/_{mm^2}$$

The wind pressure acting on the internal surfaces of the structure is

$$W_i = q_p.z.C_{pi} \qquad A.4$$

And the wind pressure acting on the external surfaces of the structure is

$$W_e = q_p.z.C_{pe} \qquad A.5$$

Where

$z_e$ = reference height relevant to the internal pressure

$C_{pi}$ = Coefficient for the internal pressure

$C_{pe}$ = Coefficient for the external pressure

Clause 8.3 of SANS 10160-3 outlines the detailed procedure for calculating the external and internal pressure coefficients, which depend on the size of the loaded area, roof slope and the direction at which the wind strikes the building. The loading zones of the walls and roof are marked **A** to **J** when the wind acts normal to the long side of the building as shown in Figure A.2, and **A** to **I** when the wind acts normal to the gable wall as shown in Figure A.4. Figures A.3 (a) and (b) show the dimensions of the loading zones when the wind acts normal to the long side of the building. Figures A.5 (a) and (b) show the dimensions of the loading zones when the wind acts normal to the gable wall.

### A.1.8 External pressure coefficients

Roof slope = $15^{\circ}$

**For wind at 0° (normal to the long side of the building)**

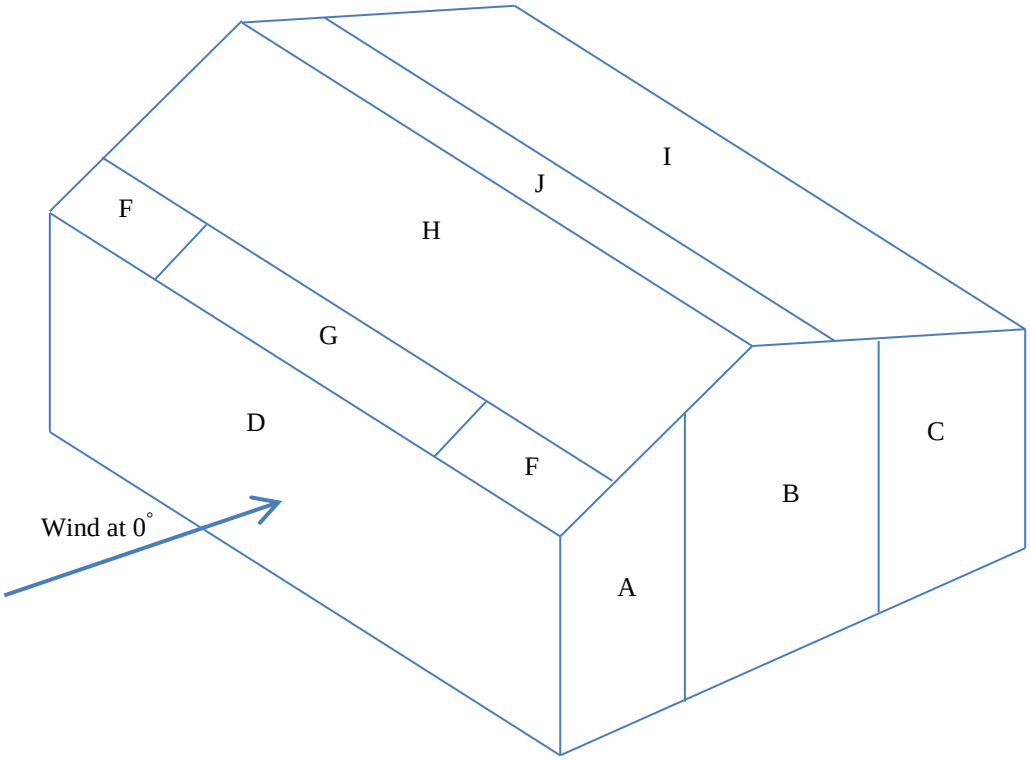


**Figure A.2: Loading zones of the walls and roof of the building when the wind acts normal to the long side of the building**

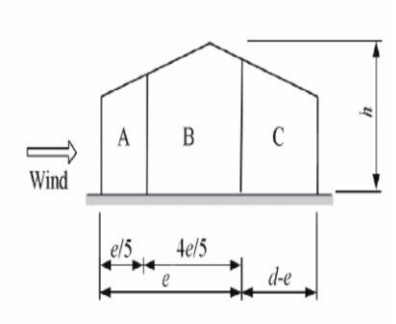


(a) Loading zones for the gable when the wall's wind acts normal to the long side of the building

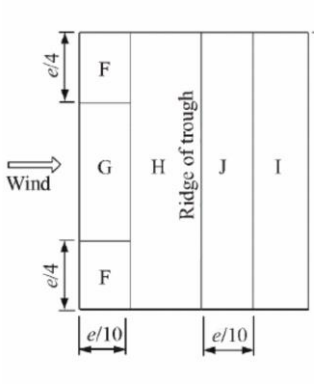


(b) Loading zones for the roof when the wind acts normal to the long side of the building

**Figure A.3: Dimensions of the loading zones of the gable wall when the wind acts normal to the long side (SANS 10160-3, 2011: 32, 40)**

## For wind at 90° (normal to gable wall):

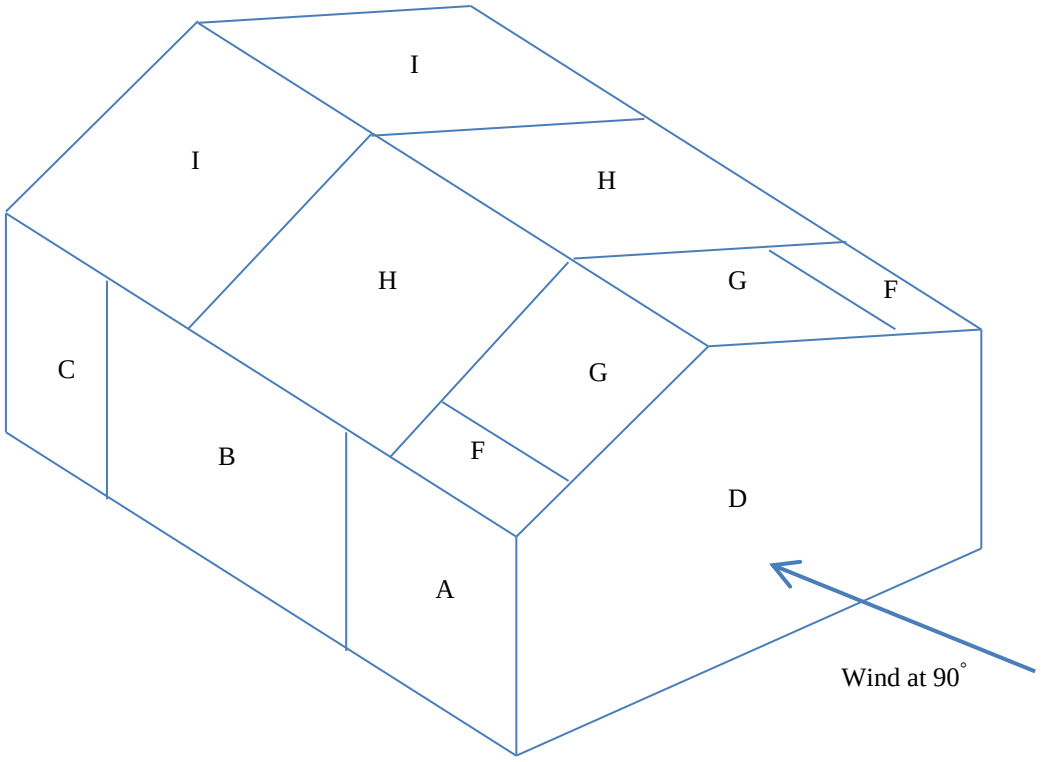


**Figure A.4: Loading zones of the walls and roof of the building when the wind acts normal to the gable wall**

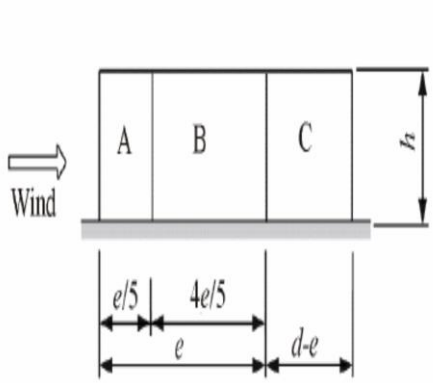


(c) Loading zones for the long side when the wind acts normal to the gable wall

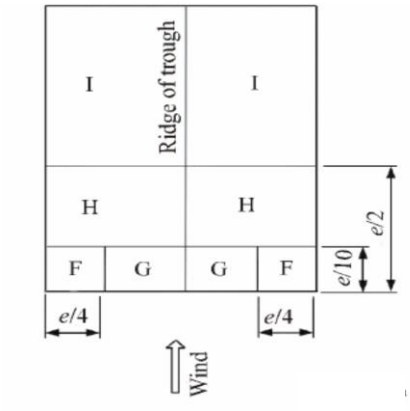


(d) Loading zones for roof when the wind acts normal to the gable wall

**Figure A.5: Dimensions of the loading zones of the long side and roof when the wind acts normal to the gable wall (SANS 10160-3, 2011: 32, 40)**

Tables A.1 and A.2 present the estimated external pressure coefficients based on SANS 10160-3 Tables 6, 10 and 11.

**Table A.1: Estimated external pressure coefficients when the wind acts normal to the long side**

| Wind acting at 0° (normal to the long side); Aspect ratio = H/d = 9/20 = 0.45 | | | | | |
|---|---|---|---|---|---|
| | **Loading zone** | **Length (m)** | **Width (m)** | **Area ($m^2$)** | **External Pressure Coefficient ($C_{pe}$)** |
| **Walls of the building** | **A** | 3.6 | 6.8 | 24.48 | -1.2 |
| | **B** | 14.4 | 8.25 | 118.8 | -0.8 |
| | **C** | 2 | 6.59 | 13.18 | -0.5 |
| | **D** | 48 | 6.32 | 303.36 | 0.8 |
| | **E** | 48 | 6.32 | 303.36 | -0.35 |
| **Roof of the building** | **F** | 4.5 | 1.74 | 7.83 | -2.5 |
| | **G** | 39 | 1.74 | 67.86 | -1.3 |
| | **H** | 48 | 9.41 | 451.68 | -0.13 |
| | **I** | 48 | 9.41 | 451.68 | -0.13 |
| | **J** | 48 | 1.74 | 83.52 | -0.7 |
| **Total area ($m^2$)** | | | | **1825.75** | |

**Table A.2: Estimated external pressure coefficients when the wind acts normal to the gable wall**

| Wind acting at 90° (normal to the gable wall); Aspect ratio = H/d = 9/48 = 0.19 | | | | | |
|---|---|---|---|---|---|
| | **Loading zone** | **Length (m)** | **Width (m)** | **Area ($m^2$)** | **External Pressure coefficient ($C_{pe}$)** |
| **Walls of the building** | **A** | 3.6 | 6.32 | 22.75 | -1.2 |
| | **B** | 14.4 | 6.32 | 91.01 | -0.8 |
| | **C** | 30 | 6.32 | 189.60 | -0.5 |
| | **D** | 20 | 7.66 | 153.20 | 0.8 |
| | **E** | 20 | 7.66 | 153.20 | -0.7 |
| **Roof of the building** | **F** | 1.8 | 4.1 | 7.38 | -1.9 |
| | **G** | 1.8 | 25.17 | 45.31 | -1.2 |
| | **H** | 7.2 | 25.18 | 181.30 | -0.8 |
| | **I** | 39 | 25.18 | 982.02 | -0.8 |
| **Total area ($m^2$)** | | | | **1825.76** | |

### A.1.9 Internal pressure coefficients

Clause 8.3 of SANS 10160-3 considers both the internal and external pressure to act simultaneously on the building. The calculation of the internal pressure coefficients incorporates any possible openings and leakages. It was specified in Section A.1.1 that there are two 8 x 3 m roller-shutter doors on the long side of the building facing the wind direction, and 5 % of the surface area has been allocated to other openings such as doors, windows and vents.

$Area\ of\ roller\text{-}shutter\ doors = 2(8\ m\ \times 3\ m) = 48\ m^2$

$Area\ of\ openings\ on\ the\ long\ side\ surface, A_1 = 48\ m^2 + 5\ \%(303 - 48) = 61\ m^2$

$Area\ of\ openings\ on\ other\ surfaces, A_2 = 5\ \%(1826\ m^2 - 303\ m^2) = 76\ m^2$

$A_1 < A_2\ \therefore The\ long\ side\ with\ roller\text{-}shutter\ doors\ is\ not\ dominanting\ the\ design.$

$The\ ratio\ of\ openings\ to\ surface\ area\ on\ the\ long\ side = \frac{61\ m^2}{303\ m^2} = 0.2\ or\ 20\ \% < 30\ \%;$

$Therefore, Clause\ 8.3.9\ of\ SANS\ 10160\text{-}3\ applies.$

**For the surface facing the wind, the opening ratio is given as:**

$$\mu = \frac{\sum Area\ of\ openings\ where\ C_{pe}\ is\ either\ negative\ or\ zero}{\sum Area\ of\ all\ openings} \qquad A.6$$

**For wind acting at 0$^o$ (normal to the long side):**

The positive pressure on the roof surface facing the wind direction:

$\mu = \frac{12.96}{144} = 0.09 \quad and \quad C_{pi} = 0.08$

The negative pressure on the roof surface facing the wind direction:

$\mu = \frac{61}{144} = 0.42 \quad and \quad C_{pi} = 0.38$

**For wind acting at 90$^o$ (normal to the gable wall):**

The positive pressure on the roof surface facing the wind direction:

$\mu = \frac{110.4}{144} = 0.77 \quad and \quad C_{pi} = 0.69$

In this research, only the worst combination of internal and external coefficients of the positive pressure were considered; such that:

Internally Pushing into the wall = Positive

Externally Pulling away from the wall = Positive

**For wind pressure at $0^0$ (normal to long side):**

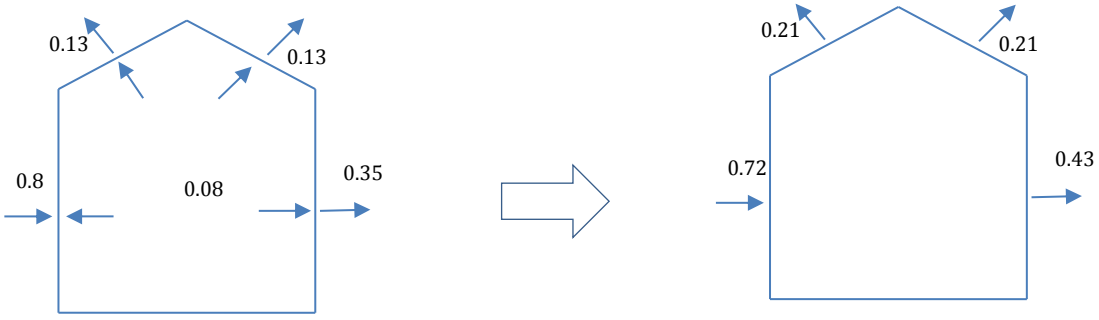


**For wind pressure at $90^0$ (normal to gable wall):**

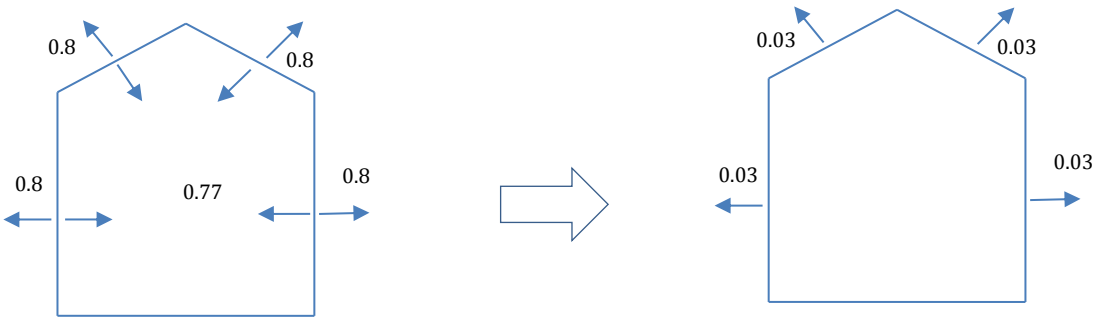


**Figure A.6: Coefficients for internal and external pressure**

The wind pressure acting at $0^{\circ}$ (normal to the long side of the building) is the critical case, and the pressure coefficients were substituted in Equation A.5 to obtain the nominal wind uplift used in this research:

$W_e = q_p(z_e)C_{pe} = 0.00086 \times 9000 \times 0.21 = 1.6\ kPa$

# APPENDIX B:
# DERIVATION OF EULER-BERNOULLI BEAM THEORY

## B.1 Terminology in Euler-Bernoulli beam theory

A beam is a structural member having one of its dimensions, often the length, much larger than the other two dimensions; designed to resist bending moments, transverse shears, axial tension or compression and, conceivably, torsion. Beams can deform axially, transversely and in rotation (Bhatt, 1999).

For a beam subject to transverse downward loading, the top surface fibre shortens whilst the bottom surface fibre elongates. Thus a neutral axis undergoing no change in length exists between the top and bottom surfaces. Refer to Figure B.1 (a) and (b).

A ***homogenous*** beam is one made from a material which has the same physical properties throughout. The neutral axis passes through the centroid of each cross-section of the beam (Case & Chilver, 1964).

## B.2 Assumptions in the Euler-Bernoulli beam theory

The Euler-Bernoulli beam theory was derived based on the following assumptions:

- Members can be represented by the neutral axis.
- The cross-section is either constant or varies smoothly.
- Plane sections originally normal to the neutral axis of the beam before bending remain plane and normal to the neutral axis of the beam after bending.
- Only bending deformations contribute to the internal strain energy. Contributions due to transverse shear and axial force are ignored.
- All deformations are small to ensure linearity.
- The material is elastic and isotropic.

## B.3 The Euler-Bernoulli beam theory

### B.3.1 Coordinate system

The Euler-Bernoulli beam theory models the beam in 2-dimensions, which refer to the length (x-axis) and the depth (y-axis); the effect of the third dimension (in the z-axis) which is the width of the cross-section is incorporated in the second moment of area of the section. Figure B.1 shows the x-axis, y-axis and z-axis of the simply supported beam carrying a distributed load.

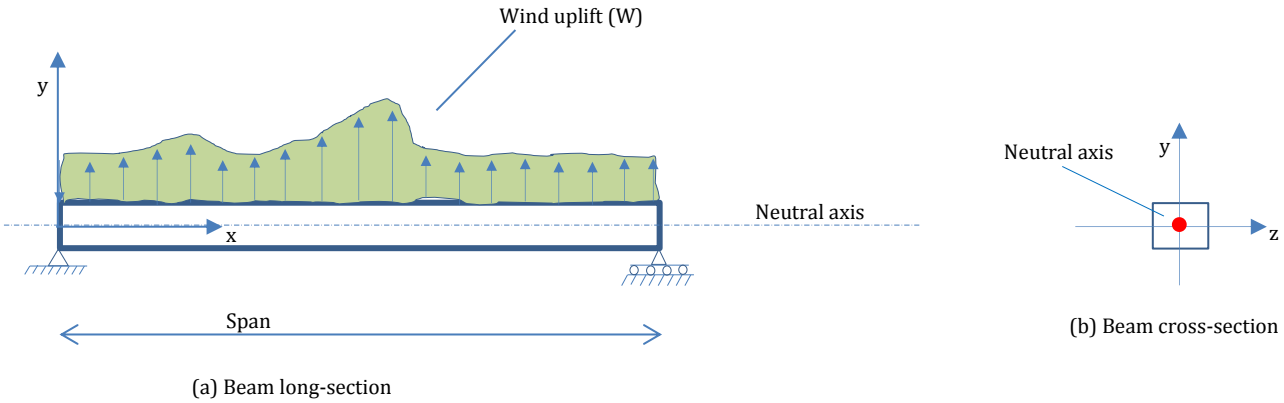


**Figure B.1: Beam long- and cross-section**

### B.3.2 Beam supports and boundary conditions

A simply supported beam is a beam supported by a roller and/or pin support at each end; with the ends being free to rotate and have no moment restraint. The beam deflection equation using Euler-Bernoulli theory was derived for the simply supported beam as shown in Figures B.2 (a) and (b).

### B.3.3 Stresses, strains and bending moments

The Euler-Bernoulli beam theory assumes that the stresses and strains due to bending are the only contributors to the internal energy of the beam. The direct stress and strain are denoted by the symbols σ and ε, respectively. The relationship between the strain and the longitudinal deflection is given by:

$$\varepsilon = \varepsilon_x = \frac{\partial u}{\partial x} = y\frac{d^2v}{dx^2} = v'' \qquad \text{B.1}$$

where the displacements under loading of a beam in the x-y plane are given by:

$u(x, y) =$ axial displacement and $v(x, y) =$ transverse displacement

The direct bending stress, σ in Figure B.2 (a) and (b) is linked to the strain through Hooke's law (Serway and Jewett, 2004) as:

$$\sigma = E\varepsilon = Ey\frac{d^2v}{dx^2} \qquad B.2$$

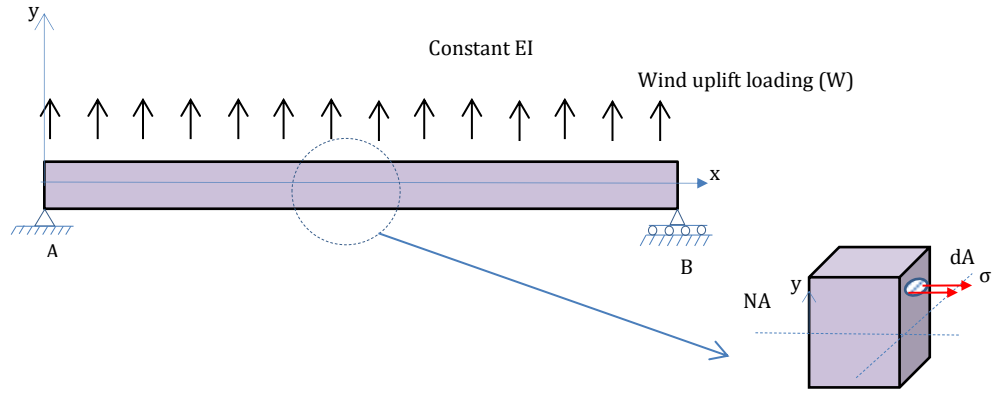


(a) A simply supported beam with wind uplift load acting on it

(b) Direct stress acting on a segment of area dA

**Figure B.2: Direct stress acting on the segment of area dA**

The bending moment ($M_z$) about the neutral axis, shown in Figure B.3 (b) is defined by the cross-section integral:

$$M_z = \int_A y\sigma dx = E\frac{d^2v}{dx^2}\int_A y^2 dA = EI_z\frac{d^2v}{dx^2} \qquad B.3$$

Where

$I_z$ is the second moment of area about the neutral axis

$EI_z$ is the bending stiffness with respect to the neutral axis, and the second moment of area is:

$$I_z = \int_A y^2 dA \qquad B.4$$

$A =$ area of the cross-section

### B.3.4 Beam deflections

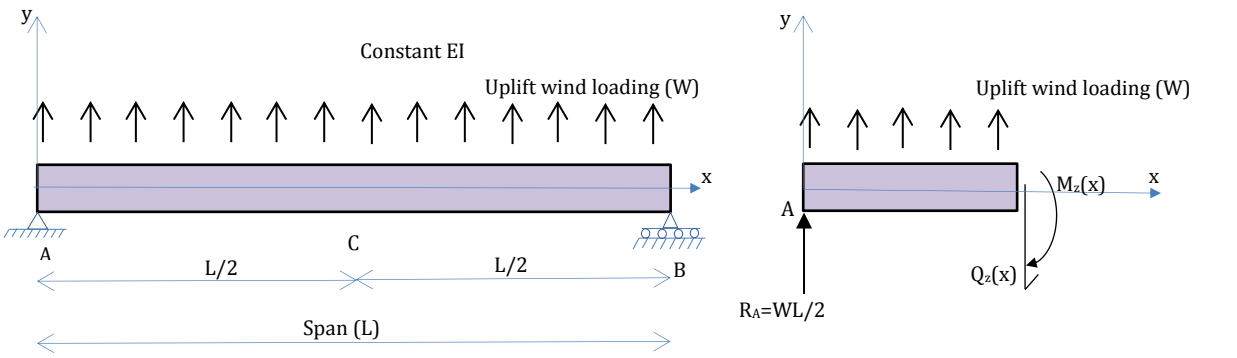


(a) Simply supported beam with a wind uplift loading acting on it

(b) Free-body diagram of a simply supported beam

**Figure B.3: A simply supported beam supporting an uplift wind loading**

Using Figures B.3 (a) and (b), the moment equilibrium equation with respect to x and assuming a positive clockwise moment:

$$M_z = R_A x - \frac{Wx^2}{2} = \frac{WL}{2}x - \frac{Wx^2}{2} = \frac{Wx}{2}(L - x) \qquad B.5$$

As before: $M_z(x) = EI_z \frac{d^2v}{dx^2}$

Integrating $M_z(x) = EI_z \frac{d^2v}{dx^2}$ twice with respect to x:

$$EI_z v(x) = \frac{WLx^3}{12} - \frac{Wx^4}{24} + C_1 x + C_2 = \frac{Wx^3}{24}(2L - x) + C_1 x + C_2 \qquad B.6$$

Where $C_1$ and $C_2$ are constants of integration.

For a simply supported beam, the boundary conditions are:

- The vertical deflection at x = 0 (at point A), $v_A(x = 0) = 0$
- The vertical deflection at x = L (at point B), $v_B(x = L) = 0$

Substituting the boundary conditions into Equation B.6 gives:

$$C_2 = 0 \quad \text{and} \quad C_1 = -\frac{WL^2}{24}$$

Substituting into Equation B.6 gives Equation B.7, which is the deflection equation in terms of x:

$$v(x) = -\frac{Wx}{24EI_z}(L - x)(L^2 + Lx - x^2) \qquad \text{B.7}$$

Equation B.7 gives the deflection curve that is symmetric about the mid-span point C in Figure B.3. The maximum deflection given by Equation B.8 occurs at mid-span or point C where x = L/2 in Figure B.3:

$$\text{Maximum deflection} = v_C\left(x = \frac{L}{2}\right) = \frac{5WL^4}{384EI} \qquad \text{B.8}$$

Since the IBR sheet is made up of ribs that are identical and equally spaced, the second moment of area, $I_z$ or $I_{NA}$, of one rib can be calculated and then multiplied by the total number of ribs in the sheet in order to get the total second moment of area of the sheet (Equation B.9). Each rib was further divided into three components, of which two pairs are identical as shown in Figure B.4.

$$I_z = I_{NA} \qquad \text{B.9}$$

where: $I_{NA}$ is the second moment of area of a single rib about the neutral axis

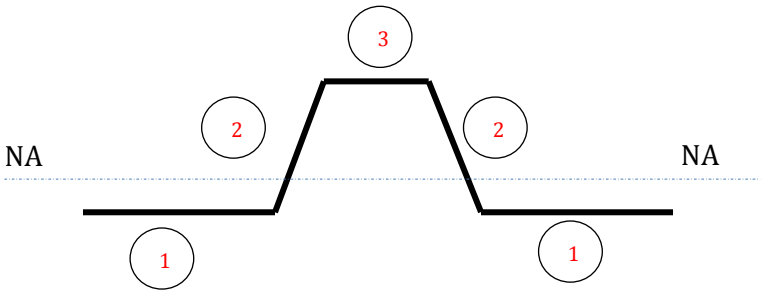


**Figure B.4: A rib taken from an IBR sheet and divided into elements**

$$I_{NA} = I_{NA(1)} + I_{NA(2)} + I_{NA(3)} = 2\left(\frac{b_1 d_1^3}{12}\right) + 2\left(\frac{b_2 d_2^3}{36}\right) + \left(\frac{b_3 d_3^3}{12}\right) \qquad \text{B.10}$$

$b_1, b_2$ and $b_3$ are the widths of elements 1, 2 and 3, respectively.

$d_1, d_2$ and $d_3$ are the depths of elements 1, 2 and 3, respectively.